Heat pump for industrial drying processes

Investigating zeotropic refrigerant mixtures for glide matching

ME55035: ME-EFPT MSc. Thesis

P.I. Widdows

Delft University of Technology

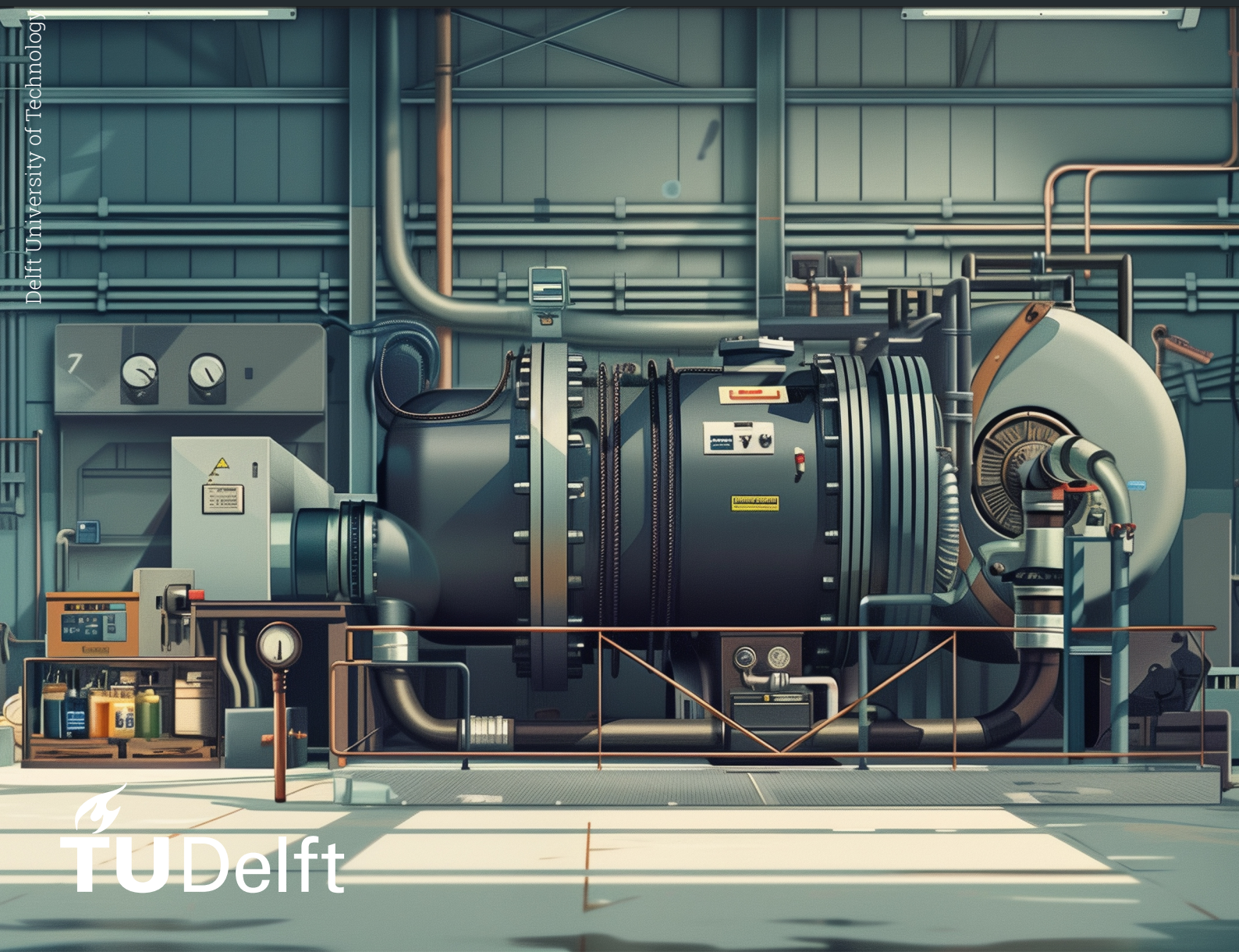

TU Delft

Heat pump for industrial drying processes

Investigating zeotropic refrigerant mixtures for glide matching

by

P.I. Widdows

to obtain the degree of Master of Science
at the Delft University of Technology,
to be defended publicly on Friday October 4, 2024 at 02:00 PM.

Student number:	4720318	
Project duration:	January 26, 2024 – September 27, 2024	
Thesis committee:	dr. ir. J.W.R. Peeters,	TU Delft, supervisor
	Prof. dr. ir. S.A. Klein,	TU Delft, supervisor
	Prof. dr. ir. R. Pecnik,	TU Delft, supervisor
	Prof. dr. ir. B.J. Boersma,	TU Delft

Cover:	AI art of an industrial heat pump by Ing. J.S. Beekman made using midjourney (Modified by J. Singh)
Style:	TU Delft Report Style, with modifications by Daan Zwaneveld

An electronic version of this thesis is available at `http://repository.tudelft.nl/`.

TU Delft

Preface

How do you even go to begin to wrap up a seven year academic journey? How would I begin to do justice to the people, the experiences, the highs and the lows? Perhaps I should start by thanking those without whom I would not have made it this far (Although admittedly that list is long).
I would, in that case, have to begin with thanking the two people without whom I would have been a high school dropout:

Jan Hein, I sincerely thank you for helping me as much as you did. You equipped me to handle everything this world can throw at person and then some. I thank you for my resilience, for protecting my optimism and for teaching me how to win an argument against myself.

Jeroen, the odds of you reading this are small. Nevertheless, if you had not bent the rules where you had to accommodate me, none of this would have been possible. You kept me in school and you managed to do it by changing school instead of trying to change me. I feel incredibly lucky to have had the right teacher at the right time. Thank you.

To Tunica, my first friends, my family, I love you all very dearly. You cannot go unmentioned in a list of people without whom I would not have made it out of high-school. I was alone, hurt and rude. You gave me friendship, you healed with me and reminded me of the kindness I wanted to give to the world as a child. As long as I live none of you will ever stand alone, you may always count on me.

My time at Delft University of Technology has been an incredible time. I was lucky to find a home at my study association and will forever regard ”Gezelschap Leeghwater” with an incredible fondness. I thank my many fellow committee members, association members and fellow couch potatoes for a place where personal development and laughter were present in equal measures.

Victor, you were a role-model from the day I met you. A kind-hearted and charismatic guy who’s only fault may be caring too much if not for the fact you also knew when to let go. You inspired me to keep hold of my interest in finance and continue to be a reference point of what I want to be for those that come after me, I hope to be for them what you were for me.

My dearest friends, LoCo 7, none better embody what Delft has given me more than you all. I am incredibly proud to call you my friends, I am so honoured by the time I’ve gotten to spend with all of you and I cannot imagine my time in Delft without you by my side at every turn, long night in the library or party. What an incredible blessing it has been to have met you all.

To the many teachers that inspired me along the way, I would not be the engineer I am without each and every one of you. Prof.dr.ir Goetheer, You fanned my spark into a flame and turned an interest in thermodynamics into my greatest passion. You are a testament to what an encouraging teacher can be for a young student finding their way.

Dr. L.L. Cutz, Luis, What an amazing time I’ve had working with you. In you I found a kindred soul, always looking for the opportunity in anything. I was lucky to meet a young professor like you who seeks to lift others up. I consider you more than a colleague or educator, you’re a true friend.

Prof.dr. Pecnik, Rene, It has been a pleasure to be your teaching assistant for many years of my time in Delft. I always felt heard and taken seriously by you, I do not know many teachers who are as open to you are to a young student’s perspective on education, examination and grading. I will also never forget your willingness to help me during my ambitious search for an internship and thesis topic and am grateful for what has always felt like the heartfelt support of an inspiring academic.

Prof.dr.ir. Klein, Sikke, as a student who above all wants to provide applied and practical work, you are an absolute inspiration. As you would always say after our meetings: ”nu ben ik weer helemaal enthousiast” and well, the feeling was always mutual. Thank you for teaching me how to combine theory with practice.

Dr.ir. J.W.R. Peeters, Jurriaan, I had the pleasure to perform two of my largest project under your supervision. Both the present work and the BTES modelling are two projects I am especially proud of. You were my most precise proof-reader ever and I will forever be impressed by how detailed you

managed to review my, at times long-winded, work. Additionally your continued encouragement and advice throughout my thesis was a gift I am very grateful for and specifically encouraging me to go to Birmingham to present my work was very special to me. I will also never forget when I failed your exam by one out of 90 points. I wanted to pass your course and move on, I did not want to fail on a single point. You told me not to focus on the points I did get but look at the points I did not. I was not trying to pass a course, I was trying to become an excellent engineer, you put that so succinctly and obviously and I carried that message through my entire master and will continue to do so far beyond.

My supervisors, I hope I have lived up to your expectations and have done you proud.

Sebastiaan, Jessie and of course my girlfriend Mariq, my graphics team, Thank you for helping this visual amateur do justice to my thesis. Mariq, thank you for your patience, support and love and trust you will receive the very same. Ezra, the one fellow EFPTer whom liked to argue as much as I did, thank you. It feels wonderful to have made a friend as obsessed with this field as I am and your practical insights made for the perfect addition to my theory. I hope you enjoyed my heavily commented drafts of your thesis.

To my Brother, I am very proud of what you've overcome and watch with immense happiness as you find your path day by day. To my mother, thank you for trying your best. To my father, my intelligence is a gift I thank you for as is my integrity and critical thinking.

And thank you reader for taking the time to read this, the very culmination of seven years of my life and every inch of my love for my field. Thank you for enduring my sentimental rant, you only graduate once and I took the opportunity in front of me.

To everyone who has gotten me to where I am, know that I have not forgotten and will forever strive to make your efforts worthwhile. I will not throw away my shot.

P.I. Widdows
Delft, September 2024

Abstract

This report analyses the improvement potential of zeotropic refrigerant mixtures on the performance of vapour compression heat pumps integrated into industrial dryers. The report reviews the scope of total global energy consumption and the percentage of this attributable to industry to demarcate application area. It proposes that by targeting industrial process heating, significant reductions to energy consumption and carbon emission by industry can be achieved. Heat pumps are introduced as the preferred system to accomplish this for temperatures up to 200 $^{\circ}$C. A performance limitation is identified in the form of heat transfer between process streams that reject and receive heat at non-constant temperatures. Zeotropic refrigerant mixtures are introduced in heat pumps to improve the interaction with non-isothermal heat sources and -sinks. The considered mixture compounds are limited to future-proof refrigerants and the mixtures are limited to binary ones.

Humid air encountered in industrial drying is targeted as one such non-isothermal process stream with a large potential for waste heat recovery. The most prominent industries that use dryers are identified and evaluated as to provide representative operating conditions at which a heat pump integrated dryer would have to work. Heat pump cycles are described both on a cycle scale as well as per component and the most important design aspects and considerations are presented. The methods used to allow heat pumps to interact favourably with temperature glides are presented namely zeotropic mixtures and trans-critical heat pump cycles.

A modeling strategy is proposed to simulate heat pump integrated dryers in large numbers in order to investigate the effects of dryer inlet and outlet conditions as well as refrigerant mixture composition both in terms of constituents and mixing ratio. The total process flow diagram is given and divided into definable thermodynamic states for both the (humid) air as well as the refrigerant. Governing equations for each component are presented and the calculation method for the thermodynamic states is discussed in terms of known state variables and used thermodynamic libraries. Finally a novel heat pump cycle is proposed, motivated by a desire to decouple the glide matching in the evaporator from that in the condenser, that attempts to use the fractionation risk present in zeotropic mixtures as an advantage instead. The criteria placed on refrigerant are presented both within the context of the future-proof limitation, legislative limitation as well as those introduced by the process requirements. The most promising refrigerant candidates from literature are presented for applications in the defined process conditions. Finally a selection is made of 13 refrigerants namely water, ammonia, (iso)butane, (iso)pentane, methane, ethane, propane, CO_2, propylene, ethylene and hexane. The thirteen refrigerants are combined into 78 refrigerant pairs and modelled using the described modeling strategy.

The modelling reveals that using zeotropic mixtures does improve the COP for many refrigerants when compared to their pure cycle performance. For drying at 180 $^{\circ}\mathrm{C}$ two heat pumps are proposed at different outlet temperatures. The cycles use 87.5%$_{mol}$ Isobutane mixed with Ethane and 87.5%$_{mol}$ NH_3 mixed with Propane for a high temperature and lower temperature outlet respectively. COPs of 3.38 and 3.44 were calculated with PRs of 16.53 and 6.84 for the Isobutane-based and NH_3-based cycles respectively. A lower drying temperature of 120 $^{\circ}\mathrm{C}$ was explored and here CO_2-based mixtures were identified as highly desirable refrigerants due to their non-toxic, non-flammable nature as well as low global warming and ozone depletion potential. The mixtures 87.5%$_{mol}$ CO_2-Isopentane and 90%$_{mol}$ CO_2-Isobutane were proposed, both feasible with single stage compression and possessing a COP of 3.96 and 4.02. Zeotropic mixtures improved the COP in at least 48 out of 78 possible refrigerant combinations when compared to the pure cycle COPs and allowed the dampening of flammability and toxicity where the pure refrigerant possesses those properties.

It is clearly demonstrated that future-proof binary zeotropic mixtures increase the performance of VCHP-integrated dryers across all relevant temperature ranges, by as much as 21.47%. The highest COPs are found when zeotropic refrigerant mixtures are used together with trans-critical operation. It is concluded that zeotropic mixtures improve the COP of vapour compression heat pump integrated dryers and should be utilised for non-isothermal processes like drying.

Contents

List of Figures

List of Tables

Nomenclature

Abbreviations

Abbreviation	Definition
ASHRAE	American Society of Heating, Refrigerating and Air-Conditioning Engineers
CapEx	Capital expenditure
COP	Conference of Parties
ECA	European Chemicals Agency
GWP	Global warming potential
HEX	Heat exchanger
HFE	Hydrofluoroethers
HFO	Hydrofluoroolefins
HTHP	High temperature heat pump
IEA	International Energy Agency
IPCC	Intergovernmental Panel on Climate Change
LMTD	Log mean temperature difference
NFPA	National Fire Protection Association
NIST	National Institute of Standards and Technology
ODP	Ozone depletion potential
ORC	Organic rankine cycle
PFAS	Per- or Polyfluoroalkyl substances
PFD	Process flow diagram
PPTD	Pinch point temperature difference
PR	Pressure ratio
VCHP	Vapour compression heat pump
WHR	Waste heat recovery

Symbols

Symbol	Definition	Unit
x	Quality	$\mathrm{kg_{vapour}\,kg_{total}^{-1}}$
m	Mass	kg
y	Mol fraction	-
M	Molar mass	$\mathrm{kg\,mol^{-1}}$
S	Entropy	$\mathrm{kJ\,K^{-1}}$
c_p	Heat capacity	$\mathrm{kJ\,kg^{-1}\,K^{-1}}$
ω	Absolute humidity	$\mathrm{kg_{water}\,kg_{air}^{-1}}$
φ	Relative humidity	-
r	Ratio	-
q	Specific heat	$\mathrm{kJ\,kg^{-1}}$
w	Specific work	$\mathrm{kJ\,kg^{-1}}$
T	Temperature	$\mathrm{°C}$
$\dot{Q}$	Heat flow	$\mathrm{kJ\,s^{-1}}$
$\dot{W}$	Work flow	$\mathrm{kJ\,s^{-1}}$
p	Pressure	bar
h	Specific enthalpy	$\mathrm{kJ\,kg^{-1}}$
H	Enthalpy	kJ
COP	Coefficient of performance	-
Ex_d	Exergy destruction	kJ
C	Flow thermal capacity	$\mathrm{kJ\,s^{-1}\,K^{-1}}$
A	Area	$\mathrm{m^2}$
U	Overall heat transfer coefficient	$\mathrm{kJ\,m^{-2}\,K^{-1}}$
N	Transfer units	-
Greek symbol	**Definition**	**unit**
σ	Entropy production	$\mathrm{kJ\,K^{-1}}$
ϵ	effectiveness	-
Δ	Difference	-
η	efficiency	-

Subscript	Definition
w	Water
w, sat	Water content if saturated
dp	dew point
db	dry bulb
wb	wet bulb
c	compressor
in	inlet
out	outlet
0	Deadstate
H	Hot stream
C	Cold stream
th	thermal
lm	logarithmic mean
min	Minimum
max	Maximum
sup	Superheat
vol	Volumetric
ref	Refrigerant
air	Air
mol	Molar
is	Isentropic
Ri	Refrigerant state i
Ai	Air state i
$total$	Total
sat_vap	Saturated vapour
sat_liq	Saturated liquid
Li	Saturated liquid loop state i
Vi	Saturated vapour loop state i
wt	Weight
$mass$	Mass
Fl	Flash tank

1 Introduction

In 2023 according to the International Energy Agency (IEA) the total global energy consumption was equal to nearly 440 EJ/a of which 38% is attributed to industry [31]. The need to transition to a carbon neutral energy mix, well documented by the Intergovernmental Panel on Climate Change (IPCC) and reaffirmed by policymakers at the 28th Conference of Parties (COP) thus requires a transition for industry as well [13]. The decarbonisation of industry requires a multifaceted approach of which one component is decarbonising the energy consumption related to process heating. As two-thirds of industrial energy use is attributed to heating, a significant reduction in greenhouse gas emissions can be achieved by targeting this part of the energy demand. Electrification is an important strategy to achieve this and electric-driven heat pumps are considered the preferred technology for temperatures up to 200°C [50].

A typical heat pump, illustrated in figure 1.1, works by using electricity to power a compressor to circulate a fluid, typically referred to as the refrigerant. The compressor brings the refrigerant to a high pressure level at which it can reject heat at elevated temperatures. After supplying heat, the pressure is reduced in the expansion valve which allows the refrigerant to absorb heat at lower temperatures.

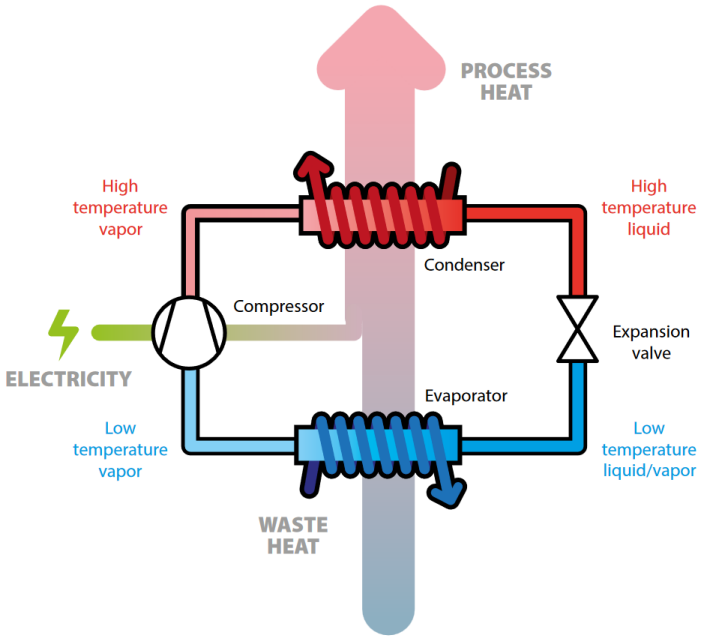

Figure 1.1: Schematic depiction of a simple heat pump cycle [7]

The fact that a heat pump can supply multitudes of heat compared to the amount of consumed electricity makes it a very efficient power-to-heat solution. The ability to supply heat at higher temperatures than at which it absorbs is relevant for industrial decarbonisation as 89% of industrial heat is required above 100°C [76] while 51% of industrial waste heat is available below 100°C [6]. By use of a heat pump, low-grade heat sources can be upgraded to usable temperatures for industry at high energy efficiencies. A large source of such low-grade heat is produced by industry itself as an estimated 49% of industrial energy consumption is lost to the environment [6]. The use of heat that would otherwise be lost is referred to as waste heat recovery (WHR). Bianchi et al. (2019) estimated that 20.1% of industrial energy is suitable for WHR using heat pumps. This means approximately a third of industrial heat demand could theoretically be supplied from its own waste heat using heat pumps, electrifying this portion in the process.

While heat pumps are becoming cost-effective technologies compared to fossil fuel powered alternatives there remains a gap between theoretically possible and economically feasible WHR, specifically when large temperature lifts are targeted [33]. Improving the performance of heat pump technologies would allow for better cost-efficiencies, increasing the adoption rate and making a larger segment of the theoretically possible WHR economically viable. One area of heat pump performance improvement is the exergy loss that occurs in the heat exchangers of the system. The most significant contributor to these losses is the exergy destruction associated with stream to stream heat transfer to and from the refrigerant [55, 78]. The heat transfer associated exergy destruction is highest when the process stream is at a non-constant temperature. When the process stream has this non-isothermal behaviour the heat exchange occurs at a temperature glide as illustrated in the left image of figure 1.2.

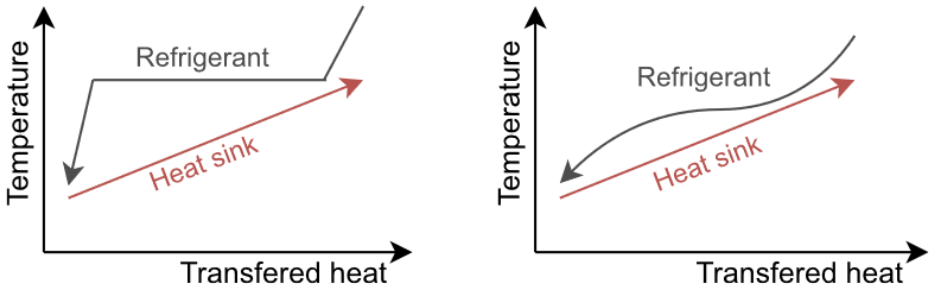

Figure 1.2: Illustration of temperature glide phenomenon without (left) and with (right) glide matching [70]

The left image in figure 1.2 shows a typical temperature profile for a refrigerant depicted alongside that of a heat sink to which the refrigerant is supplying heat. The refrigerant goes through a phase change characterised by a constant temperature (isothermal). Because the heat sink does not have this isothermal behaviour the temperature difference between the two streams grows larger. As exergy losses scale with the temperature difference, these are also larger. By reducing the temperature difference between the streams during heat transfer, exergy losses are reduced and performance is increased. This concept, referred to as glide matching is depicted in the right image of figure 1.2.

An example where significant waste heat potential is available, use of which is currently limited by the presence of temperature glides, is the drying operation used in many industrial processes. Drying is defined as a thermal process by which water is removed to produce a solid product. Industrial dryers commonly use convective heat transfer to extract the moisture from the product with hot air as the medium [56]. The exhaust of this process is a mixture of the air and the evaporated water, referred to as humid air. All thermal energy, neglecting losses to the environment, ends up in this waste stream presenting a large potential for WHR. Additionally, the dominant current method for producing the hot air stream is by use of a gas fired boiler [56]. Significant carbon reduction can be realised if gas fired boilers are replaced with heat pumps.

Methods to accomplish glide matching in heat pumps are an area of active research. One method to achieve glide matching is to replace the refrigerant of the heat pump with a zeotropic refrigerant mixture. A zeotropic mixture is defined as mixture of which the components have different boiling points. The resulting mixture posses a temperature glide in its two phase region [24]. This temperature glide can be altered by changing the choice of mixed refrigerants and their fractions thus allowing the glide to be matched to that of a waste heat source.

Use of zeotropic refrigerant mixtures is being explored both in the context of organic Rankine cycles (ORCs) [3, 44, 73] and heat pumps [1, 20, 24, 61, 72, 78]. In spite of this being a field of active research, a matching of heat pumps using zeotropic mixtures to typical drying processes has not been performed. Furthermore, this work limits the considered mixture compounds to refrigerants that are considered future proof. Future proof means minimal contributions to climate change, measured in global warming potential (GWP) as well as no damaging effects on the ozone layer, measured in ozone depletion potential (ODP). Additionally, toxic compounds such as Per- or Polyfluoroalkyl substances (PFAS) are excluded as well. This demarcates the research focus of the present work to the use of zeotropic future proof refrigerant mixtures to achieve glide matching in heat pump cycles applied to industrial dryers. Specifically, the research question to be answered is formulated as

"How can future-proof binary zeotropic refrigerant mixtures be used to increase the performance of heat pumps applied to the waste heat recovery of industrial drying processes"

The report is structured into 8 chapters that present the theory required to answer the research question, the methodology used to investigate zeotropic mixture effects in heat pumps and the results and following conclusions on the use of these mixtures to increase heat pump integrated dryer performance.

Chapter 2 provides an overview of drying operations in industry. The chapter provides the definitions of common properties used to describe humid air as encountered in drying operations and the underlying theory. The concept of a Mollier diagram is introduced to show the inter-dependency of these properties and how the diagram can be used to describe a generic drying process. The latter half of the chapter is used to describe the industrial sectors which employ dryers and which dryer types they use. The chapter concludes with an identification of the in- and outlet conditions of the most relevant industries for the purposes of designing heat pump cycles operating between these streams.

Chapter 3 describes the basic heat pump cycle and then two ways it is altered to achieve glide matching. An overview of the thermodynamic cycle as a whole is given followed by an analysis of the specific components found in this cycle. Important design aspects of each component are given such as the relevant types of compressors, the design methodology for a heat exchanger and classical and more novel pressure reduction components.

Chapter 4 introduces the research methodology that is used to design and optimise heat pump integrated dryers using zeotropic mixtures. First is a description of the process and a full process flow diagram of the integrated dryer. Several thermodynamic states are defined at which the refrigerant and air are to be calculated followed by the equations and relations used to perform these calculations. A heat pump model implemented in python is introduced and integrated into a larger mixture analysis model that analyses all possible zeotropic mixtures proposed and identifies the best performing cycles. The concept of a novel cycle is proposed and motivated and any additional relations required for this cycle are given. The chapter concludes with the selection of the refrigerants to be studied.

Chapter 5 presents the modelling results for drying conditions taken from industry. The modelling output is classified and the 20 best performing mixtures are presented. The heat pump with the highest performance is extensively analysed and compared to the pure cycle to demonstrate the effects of the zeotropic mixture. The chapter goes on to present another high performance cycle with a more desirable compression ratio and concludes by extrapolating the insights from specific cycles into general insights on the effects of zeotropic mixtures

Chapter 6 build on the preceding chapter by investigating whether the optimal mixtures and their performance change when the drying conditions are changed. The inlet temperature of the dryer is lowered to represent other industrial drying sectors and uses. The outlet temperature is changed to investigate whether the angle of the glide impacts the effect of zeotropic mixture use.

Chapter 7 presents a proof of concept design of the previously introduced novel cycle. Given the cycle was not calculated using the modelling strategy, the design procedure that led to the result is presented first. The resulting cycle is then given and evaluated based on its performance. Given the novelty of the cycle, the concept is then investigated in order to identify the underlying thermodynamics that define its performance.

Chapter 8 concludes the report by reiterating the best performing cycles found in chapters 5 and 6 and the general insights on the use of zeotropic mixtures. It contrasts the improved performance with increased operational complexity and discusses which aspects of zeotropic mixture heat pumps require further study. The novel cycle is discussed and the potential of the cycle is compared to the optimal basic cycle. The novel cycle's areas of future study are also presented.

2

Overview of industrial drying

This chapter presents a characterisation of a generic industrial drying process and its underlying physics, a field referred to as psychrometrics. The chapter proceeds to estimate the amount of industrial energy use attributable to drying activity per sector. The two industries with the largest usage of dryers are described in more detail. The current dominant drying technologies used by these industries are discussed as well as the most relevant alternative technologies. The chapter concludes with a selection of drying conditions representative of the industry for which heat pump cycles will be designed.

2.1. Fundamentals of Industrial Drying

Drying is commonly defined as the removal of water via a thermal process to produce a solid product. During drying, two processes are occurring simultaneously, the first being the transfer of heat from the drying environment to surface moisture to evaporate it. The second process occurring is the internal mass transfer of moisture to the surface. Drying is thus a complex operation involving transient transfer of heat and mass and often involves physical and chemical transformations of the product. Over 85% of industrial dryers use convective heat transfer to supply heat to the wet feed-stock. Typically, the heat drying medium is air or, when possible, direct combustion gasses are used [56]. The heating of the drying medium is typically done in a gas-fired heater and a generic drying process based on this is depicted in figure 2.1.

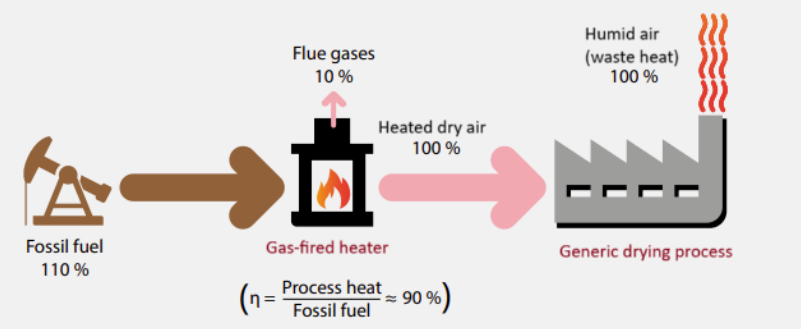

Figure 2.1: A schematic depiction of the energy streams in a generic gas-fired drying process [7]

The waste stream of a drying process is a mixture of dry air and water vapour which is referred to as moist or humid air. The study of systems involving humid air is referred to as psychrometrics [5, 55]. In describing humid air, several properties can be distinguished of which one is the absolute humidity given as

$$\omega = \frac{m_W}{m_G} \tag{2.1}$$

in terms of the mass of water vapour (m_W) and the mass of dry air (m_G) in the humid air. The absolute humidity numerically expresses the added mass of water vapour in terms of the original (dry) air mass.

In addition to the absolute humidity one can also define the relative humidity, given as

$$\varphi = \frac{m_W}{m_{W,sat}} \tag{2.2}$$

which expresses the fractional saturation with water vapour of a humid air sample in terms of the mass of water vapour (m_W) and the mass that would be present in a saturated sample at the same temperature and pressure ($m_{W,sat}$). This property ranges between 0 and 1 as supersaturated humid air is not typically encountered in drying applications.

Several important temperature values can also be distinguished in describing humid air. First is the temperature of the humid air as measured by a thermometer which is referred to as the dry bulb temperature (T_{db}) and is the actual mixture temperature. Additionally there is the wet bulb temperature (T_{wb}) which is the adiabatic saturation temperature. T_{wb} is equivalent to the temperature the mixture would have if at equal enthalpy the relative humidity was set to 1. The wet bulb temperature is measured using a thermometer of which the bulb is fully encompassed in wet cloth. The final temperature property is the dew point temperature (T_{dp}) which is the temperature at which a humid air sample begins condensing water. This value is always below T_{wb} and is reached when the relative humidity is set to 1 at constant absolute humidity. It is common practice to depict the relative- and absolute humidity as well as the aforementioned temperatures and their inter-dependencies graphically in a Mollier chart. An example of a Mollier chart is given in figure 2.3 on the following page.

Shown in figure 2.3 is a generic drying process, depicted in dark blue, is included to illustrate the use of this chart in the context of drying applications. Ambient air with a relative humidity of 0.8 and a T_{db} of 10°C is defined as state 1. The air is heated to state 2 with a T_{db} of 35°C having constant absolute humidity but changing the relative humidity as $m_{W,sat}$ is now higher. Note that the lowering of relative humidity as temperature increases is the fundamental principle which enables drying using hot air. Finally a drying operation brings the air to state 3, saturating the humid air (φ equal to 1) and increasing the absolute humidity as water is extracted from the dryed product. This drying operation is represented by a constant enthalpy process [56]. Marked in light blue are the T_{db}, T_{wb} and T_{dp} for state 2 being approximately 35, 18 and 7°C respectively. The amount of latent heat stored in the water vapour is typically much greater than the sensible heat of the humid air. To illustrate the order of magnitude of this difference one can look at the change in enthalpy required for water to be heated from 0 to 100°C versus the enthalpy of evaporation to go from saturated liquid to vapour at 100°C. The latent heat is more than 5 times greater than the sensible heat and thus is a far more significant contribution to the total heat of the sample.

An illustration of the difference between a typical gas-fired drying process versus a hypothetical heat pump drying system is given in figure 2.2.

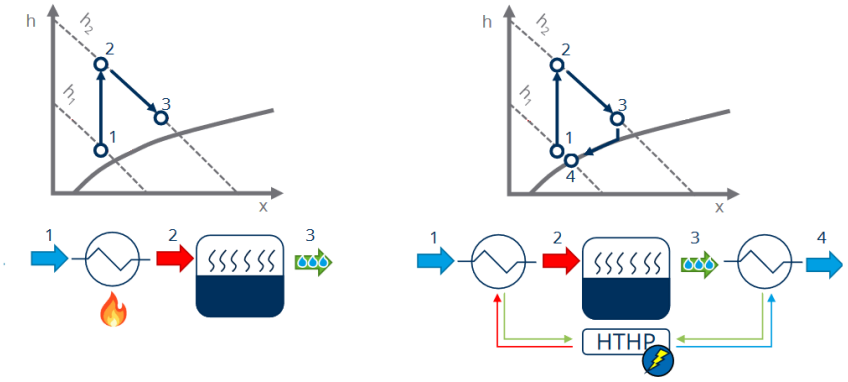

Figure 2.2: Gas-fired (left) and heat pump driven (right) drying processes with simplified Mollier diagrams

The left cycle is a generic drying process with a simplified version of the associated Mollier chart presented in figure 2.3. The right cycle depicts the proposed dryer, now electrified by use of a (high temperature) heat pump represented by HTHP in the figure. The waste heat source utilisation is depicted in the simplified Mollier chart by the process from state 3 to 4. Note that this is predominantly done along the saturation line ($\omega = 1$) and is thus accessing the latent heat of the water vapour present in the humid air.

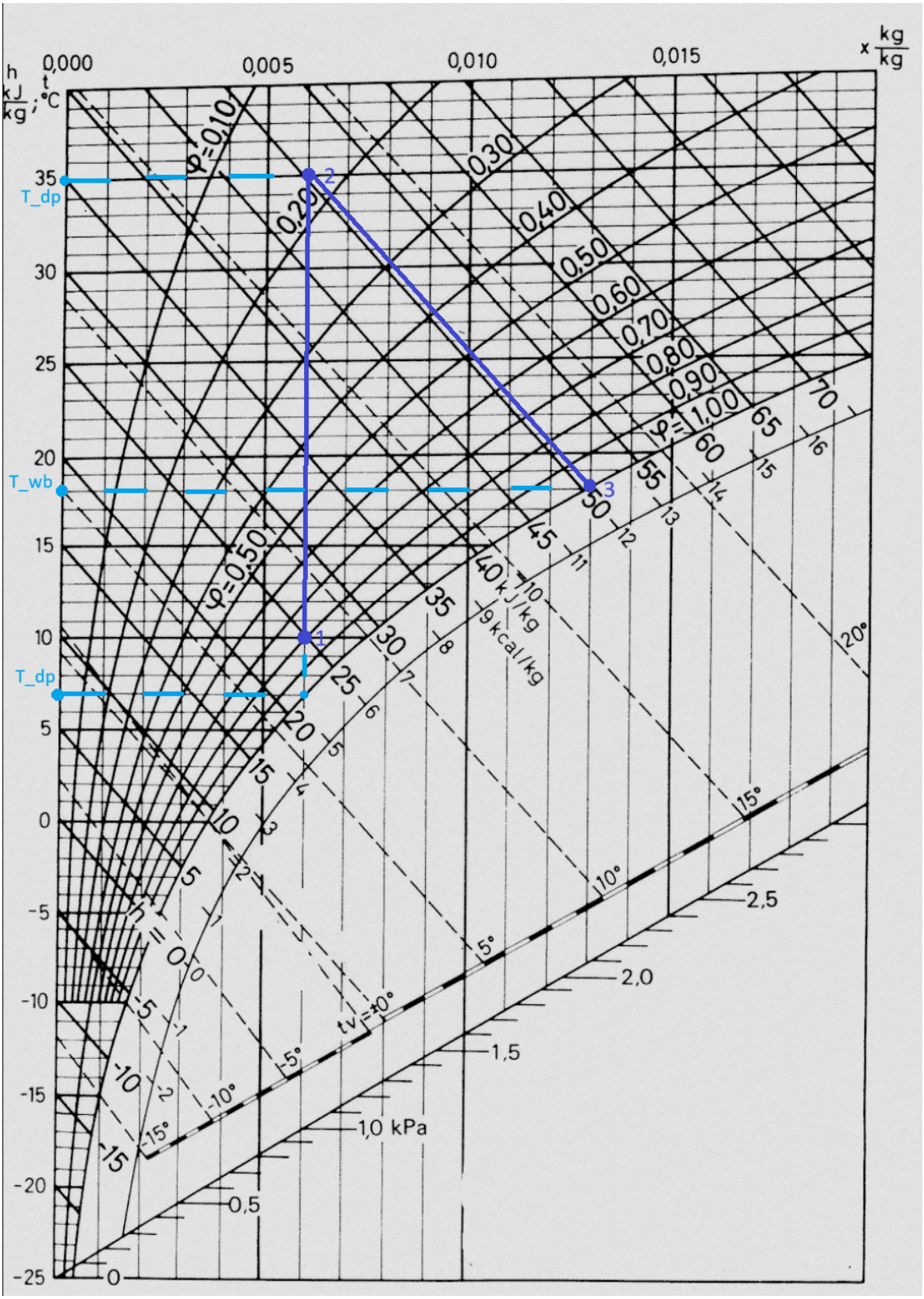

Figure 2.3: Mollier chart depicting a generic drying process (dark blue) and examples of T_{db}, T_{wb} and T_{dp} (light blue) for humid air in terms of dry bulb temperature (t), specific enthalpy (h), absolute humidity (x) and relative humidity (φ). [18]

2.2. Industrial drying applications

Drying applied on an industrial scale occurs in a variety of sectors such as the paper, food, chemicals, metal, textiles and wood industry and has been estimated to account for approximately 20% of all industrial energy use [36, 56]. This estimate is indicative of the WHR potential of drying but a more detailed analysis of process conditions is required for the purposes of designing integrated heat pump systems. A breakdown of several industrial sectors, their contribution to total industrial energy consumption and the portion attributable to drying is given in table 2.1.

Table 2.1: Sector-wise breakdown of industrial energy use and portion attributed to drying process

Industry sector	Percentage of total industrial energy use [21]	Portion caused by drying
Paper & Pulp	13.55%	50-55% [10, 16, 32, 42]
Food	11.62%	20 - 25% [35]
Textiles	1.28%	50% [39]
Wood	3.87%	70% [39]
(petro)Chemical	21.48%	7.4% [39]
Mining	1.54 %	15.5% [39]

The two largest industries in terms of total energy use is the paper and pulp industry and the food industry. These account for approximately a quarter of all industrial energy use. Just the drying processes in these two industries account for 9.1% of all industrial energy use. From these values it is clear that the paper and pulp industry and the food industry present themselves as large sectors in which drying constitutes a significant part of the energy use. It is estimated that these two industries account for 45% of all industrial drying energy consumption [17]. Due to the dominance of these two industries in the use of industrial dryers they are deemed the most practical examples to describe industrial drying in greater detail and provide representative operating conditions for proposed heat pump cycles.

2.2.1. Paper industry

The paper industry is the third largest industrial consumer of energy [21] and the largest user of industrial dryers [17]. The drying section of a paper mill can employ a variety of technologies as its working principle. The dominant technology used to dry paper and pulp is the multi-cylinder dryer [16, 43]. As visible in table 2.2 the multi-cylinder dryer accounts for nearly 90% of the industry's dryers. Its working principle is that consecutive spinning cylinders are heated internally using steam while the paper web is fed between the rollers as shown in figure 2.4.

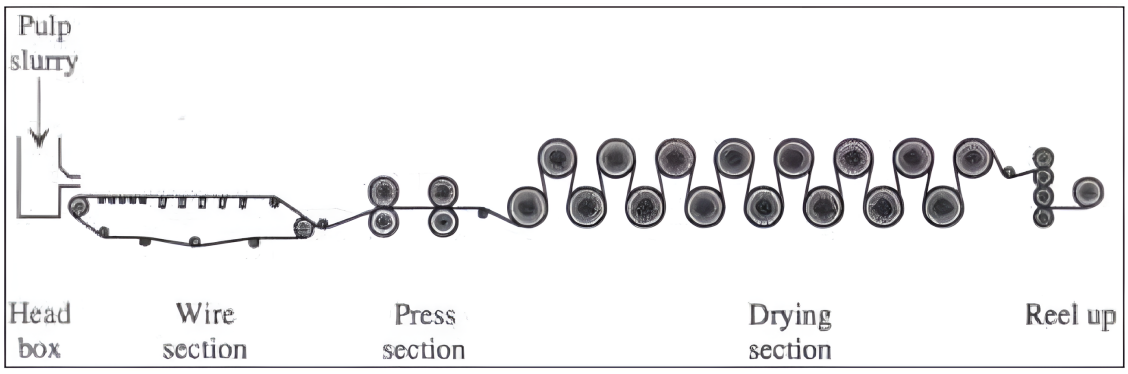

Figure 2.4: Schematic depiction of the dominant paper drying technology; multi-cylinder drying [25]

The steam allows the exterior of the cylinder to be heated and this is the part in contact with the paper. The feed temperature of steam varies over the cylinders with the last ones being fed the hottest steam. Buysse (2021) reported a maximum steam temperature of 138°C in the multi-cylinder dryer [10].

A maximum steam temperature of 138°C is corroborated by Ghosh (2011) for fine paper but steam as hot as 180°C is encountered for different paper types [16, 25]. While the cylinders are heated using steam the drying chamber itself still uses heated air at approximately 100°C to carry the evaporated water to the exhaust thus for this dryer type the waste stream is also humid air.

Alternative technologies for drying take up a much smaller segment of the industry. Yankee dryers and impingement dryers are the two most common alternatives to the multi-cylinder dryer. Both technologies use gas at high temperatures and velocities blown perpendicular onto the surface of the paper instead of using parallel convection. Yankee dryers use air as the drying medium while impingement dryers use superheated steam and thus do not fall under the field of psychrometrics. A Yankee dryer is typically used in high temperatures dryers to achieve large moisture capacities for the air. A typical Yankee dryer is reported to use air heated to 300°C [16]. Impingement drying requires superheated steam typically at temperatures between 250 and 300°C. Both Yankee and impingement dryers thus require temperatures above the realistic supply range of a heat pump cycle. While the waste heat could be utilised for other purposes it is not suitable for the dryer concept considered in this work.

The representative drying conditions for the purpose of designing a heat pump driven paper mill are thus defined as those used in multi-cylinder dryers. By excluding the Yankee and impingement dryers from this definition only a small amount of the industry is placed out of scope. Additionally Yankee and impingement dryers are typically applied to niche paper types, Yankee dryers for tissue grade paper and impingement for coating paper. The limited use of alternative technologies in the paper industry further strengthens the use of multi-cylinder as the selected source for conditions representative of the sector. Specifically the heating of the air used to carry the evaporated water out is targeted.

Table 2.2: Drying technologies used in the paper & pulp industry with their total industry share, industry share per grade, energy use, drying rate and quality [56]

Dryer; *application*	Industry share (%)[a]	Grades	Distribution (%)	Energy use (MJ/kg H_2O)	Drying rate (kg H_2O/hm^2)	Paper quality (+, ~,–)[b]
Multi-cylinder; *Printing, base papers & boards*	85–90	Tissue	5	2.8–4.0	20	~
		Paper	95	2.8–4.0	20	+
		Board	95	2.8–4.0	15	+
		Coating	35	3.0–4.5	5–10	~
Yankee; *Soft tissues & boards*	4–5	Tissue	84	4.0–5.0	200	+
		Paper	0			
		Board	3	2.8–3.5	30–50	+
		Coating	0			
Infrared; *Sizing & coating*	3–4	Tissue	0			
		Paper	1	5.0–8.0	10–30	~
		Board	1	5.0–8.0	10–30	~
		Coating	15	5.0–8.0	70–120	~
Impingement; *Increased capacity*	2–3	Tissue	0			
		Paper	4	2.8–3.5	50–120	~
		Board	0			
		Coating	50	3.0–5.0	40–140	~
Through; *Soft tissues, filter fabrics*	1–2	Tissue	11	3.4–4.5	170–550	+
		Paper	0			
		Board	0			
		Coating	0			
Condebelt; *In production scale*		Tissue				
		Paper				
		Board	1	2.6–3.6	200	+,–
		Coating				
Impulse; *Pilot stage*		Tissue				
		Paper	0	0.55–1.4	500–8000	+,–
		Board	0	0.55–1.4	500–8000	+,–
		Coating				

[a] Pulp dryers excluded.
[b] ~ indicates that quality might improve or worsen depending on paper grade.

2.2.2. Food industry

The food industry accounts for 11.62% of industrial energy use making it the fourth largest industry. It is also the second-largest user of industrial dryers, accounting for about 12% of dryers in industry. This industry is incredibly diverse in scale, drying conditions and type of feedstock. Because of this it is important to review this sector as well as more varied operating conditions might be identified. This industry is thus a valuable addition to the paper industry in representing drying technology. Approximately 85% of dryers in the food industry use heated air convection as the drying principle [38, 56, 62, 71]. This portion of food dryers will have a humid air waste stream, potentially suitable for WHR of its waste heat. An overview of the most suitable type of dryer used for a given feedstock is given in table 2.3.

Table 2.3: Most suitable dryer type per food product [56]

Products	Dryer type
Vegetables, confectionery, fruits	Compartment and tunnel
Grass, grain, vegetables, fruits, nuts, breakfast cereals	Conveyor band
Grass, grain, apple, lactose, poultry manure, peat, starch	Rotary
Coffee, milk, tea, fruit purees	Spray
Milk, starch, predigested infant foods, soups, brewery, and distillery by-products	Film drum
Cereal grains	Moving or stationary packed beds
Starch, fruit pulp, distillery waste products, crops	Pneumatic
Coffee, essences, meat extracts, fruits, vegetables	Freeze and vacuum
Vegetables	Fluidized bed
Juices	Foam mat
Apples and some vegetables	Kiln

Shown in table 2.3 and according to Mujumdar (2007), food drying technologies can be classified into 14 types. Several of these technologies such as the cabinet, tunnel, belt and conveyor dryer are essentially variations of the same concept. These work by moving the product through the drying chamber with hot air flowing in the opposite direction to perform convective drying. An illustration of a typical tunnel and a typical conveyor dryer, to graphically demonstrate the similarities, is given in figure 2.5.

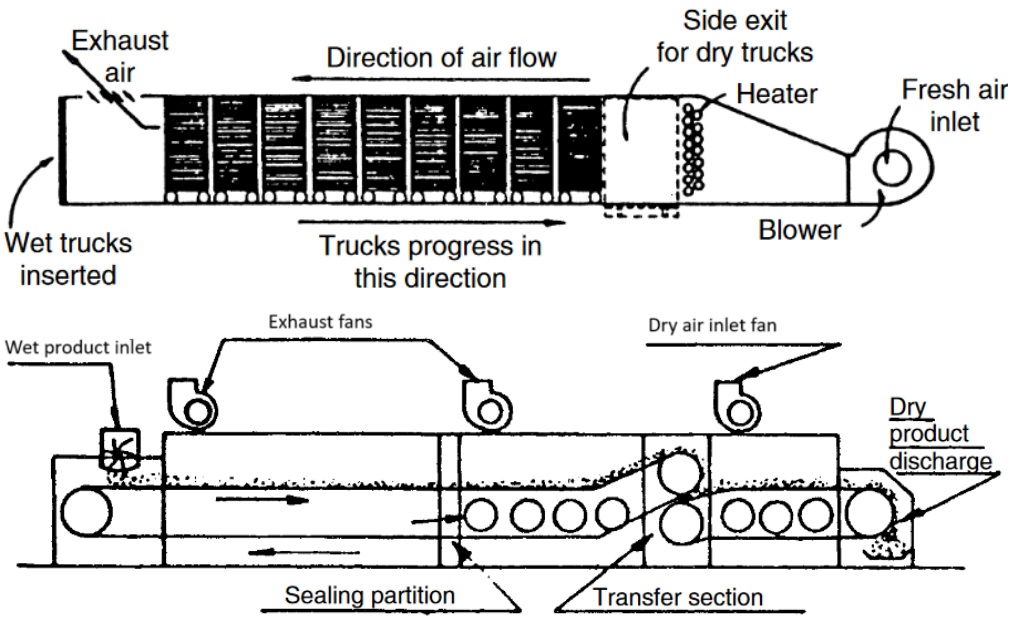

Figure 2.5: Illustration of a tunnel (top) and a conveyor (bottom) dryer illustrating their comparable operating principle [56]

Here the drying feedstock in both types of dryers enters on the left side and moves through the dryer. The heated air enters on the opposite side, thus the hottest air dries the driest product, extracting the final moisture. The different variations have evolved due to various differences between products such as their geometries, shrinking rates and drying rate. Spray drying is specifically singled out by Mujumdar (2007) as the dominant drying technology for liquid food feedstocks.

While spray drying technology also brings the air and the feedstock into the drying chamber at opposite directions and is shown in figure 2.6. The difference between spray drying and the technologies used for solid feedstock is the need to disperse the liquid product to increase the contact area. Liquid feedstock dispersal can be done in a variety of ways and in the illustrated examples an atomizer wheel and a spray nozzle are used to accomplish this. Note that the variant using a spray nozzle uses an added air stream at high velocity, also atomising the feedstock as done with the atomizer wheel and thus being conceptually the same.

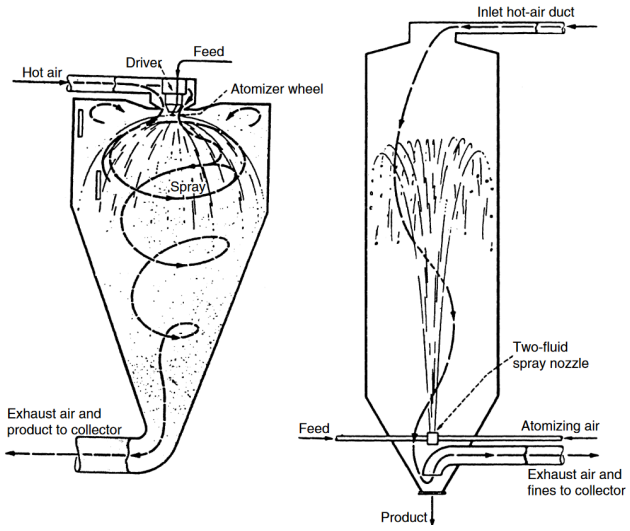

Figure 2.6: Two illustrations of spray dryers used for liquid food feedstock using an atomizer wheel (left) and a spray nozzle (right) to increase contact area between the hot air and the feedstock [56]

Besides the actual drying process several additional product quality considerations are present for food when compared to other industries. Processes that involve food products are subject to hygiene standards and the retention of nutritional value and vitamins is also important. The sanitation aspect of drying requires at least 60°C for short duration ($\sim$ 5 min) and 48°C for long duration (> 24h) disinfestation [56]. The work performed by Loembda et al. (2023) concludes that when heat pumps are substituted into a food dryer nutritional content is maintained while the colour of the product is improved [47]. The nutrition and colour results of Loembda et al. (2023) are based on their performed meta-study of 31 heat pump dryers applied to a variety of products and dryer conditions. The lowest temperature reported is 40°C for wolfberry drying and the highest temperature was reported to be 105°C for adzuki bean seeds. The temperatures reported for the feedstocks studied by Mujumbar (2007) mostly fall in this temperature range as well with the largest divergence being corn which is dried at 110°C. For spray drying higher temperatures are encountered. For example a spray drying plant operated by Friesland Campina uses an air temperature of 180°C [23].

Thus for the purposes of identifying representative drying conditions for the food industry several categories can be identified. Low temperature drying is here defined as any food drying process performed using air with a T_{db} lower than 100°C. High temperature drying is defined as processes using air with a T_{db} between 100 and 150°C. The final category is very high temperature drying for air temperatures beyond 150°C. All these categories fall in temperature ranges for which heat pumps are the preferred electrification method. The entire food drying sector should thus be targetable for heat pump integration.

3

Heat pump technologies

This chapter presents the basic heat pump cycle in terms of its components, operating principle and performance indicator. It then presents how this cycle is modified to achieve temperature glide matching. First the zeotropic mixture cycle is discussed and then the most commonly encountered alternative, trans-critical heat pump operation, is presented. The chapter concludes with three sections on component-wise design considerations. First on heat exchanger design, then on compressor selection and finally on pressure reduction. The pressure reduction component typically used in heat pump cycles, the expansion valve, is presented. In addition to the expansion valve a more novel pressure reduction component called an ejector is presented.

3.1. Basic heat pump cycle

Heat pumps are thermodynamic systems that use an amount of (electrical) work ($\dot{W}_c$) to transport or "pump" thermal energy from a cold reservoir to a hot reservoir. As defined in annex 58 of the IEA, when a heat pump supplies heat at a temperature exceeding 100°C it is classified as a high temperature heat pump (HTHP) [77].

A basic vapour compression heat pump (VCHP) cycle is shown in figure 3.1. Depicted are the typical components of this cycle namely the compressor, condenser, expansion valve and the evaporator. Figure 3.1 also shows the associated pressure (p) - specific enthalpy (h) diagram of the basic cycle illustrating the high pressure level (points 2 and 3) and low pressure level (points 4 and 1) that the system works between. Note that point 2 illustrates the actual compressor outlet while point 2s is included to demonstrate the compressor outlet if it was operating isentropically. The difference between point 2 and 2s is used to graphically illustrate the non-ideality of the compressor.

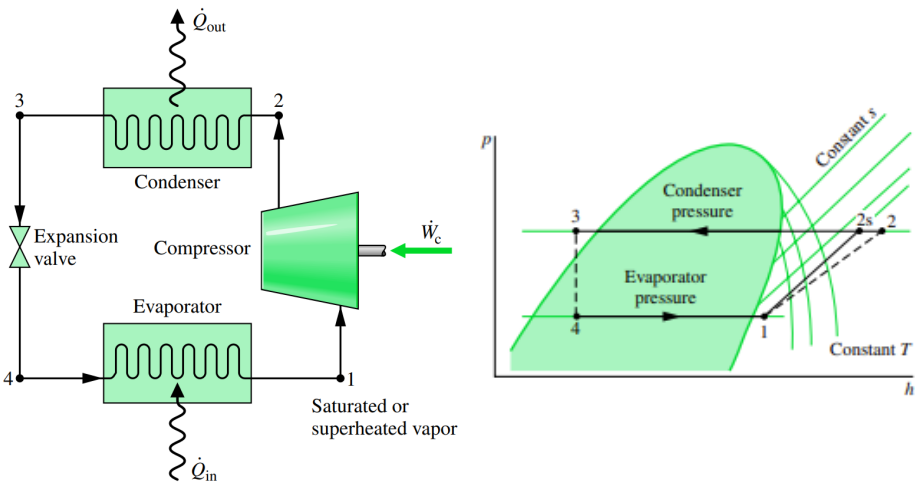

Figure 3.1: A basic vapour compression heat pump cycle with associated pressure (P)-specific enthalpy (h) diagram [55]

The change in enthalpy between points 2 and 3 is caused by the heat rejection ($\dot{Q}_{out}$) in the condenser and the change between points 4 and 1 is caused by the heat absorption ($\dot{Q}_{in}$) in the evaporator. Also depicted in the p-h diagram of figure 3.1 is the two-phase region of the refrigerant in green. A typical heat pump cycle operates within this area, referred to as sub-critical operation. By operating through the two-phase region large amounts of enthalpy can be stored and released in the evaporation and the condensation respectively. This also introduces the need to increase the pressure level as the isotherms depicted show that for a constant temperature condensation can be caused simply by increasing the pressure sufficiently. Thus by de- and re-compressing the refrigerant heat can be stored and extracted from the phase changes of the refrigerant.

The effectiveness of a heat pump cycle is typically expressed in terms of a coefficient of performance (COP) defined as

$$COP = \frac{\dot{Q}_{out}}{\dot{W}_c} = \frac{h_2 - h_3}{h_2 - h_1} \tag{3.1}$$

in terms of the delivered heat ($\dot{Q}_{out}$) and the electric power used by the compressor ($\dot{W}_c$). These values can be expressed as the change in enthalpy of the refrigerant in the corresponding component, here numbered in accordance with figure 3.1. It is important to note that different from an efficiency, a COP can be, and typically is, greater than unity.

Exergy is defined as the maximum theoretical work obtainable from a system as it comes into equilibrium with the environment and thus can be conceptualised as the useful part of energy. Just as for energy, an exergy balance can be made for a given thermodynamic system. As opposed to energy, exergy can be destroyed trough irreversibilities. The exergy destruction is defined as

$$Ex_d = T_0 \sigma \tag{3.2}$$

Where σ is the entropy production of the system and T_0 is the temperature of the environment which is typically referred to as the dead state. The exergy destruction is important to quantify per heat pump component as to indicate where useful energy is lost. As discussed in chapter 1 the exergy destroyed during heat exchange without glide matching is the dominant factor. The exergy destroyed during heat exchange is defined as

$$Ex_d = H_{H,in} - H_{H,out} - T_0(S_{H,in} - S_{H,out}) + H_{C,in} - H_{C,out} - T_0(S_{C,in} - S_{C,out}) \tag{3.3}$$

Where $H_{n,i}$ and $S_{n,i}$ give the enthalpy and entropy of stream n, being either the hot (H) or cold (C) stream, where i designates whether the value is taken at the in- our outlet [52, 55]. Eq. The expression given in (3.2) can be used to calculate the exergy destruction in the compressor and the expansion valve using the entropy increase for σ. The expression given in Eq. (3.3) is used in the condenser and evaporator where in the former the refrigerant is the hot stream and in the latter the cold stream.

3.2. Glide matching heat pumps

A basic heat pump cycle uses sub-critical operation to store and release heat using latent heat which typically occurs at a constant temperature. When the interacting streams are also isothermal this is an advantage but for glide matching purposes this property of the phase change needs to be circumvented. There are two dominant strategies that are typically proposed in literature. The first method for enabling glide matching is changing the refrigerant behaviour in the two-phase region by introducing a zeotropic mixture. The alternative strategy is to avoid the two-phase region by bringing the refrigerant above its critical temperature, referred to as trans-critical operation.

3.2.1. Zeotropic mixture cycle

Zeotropic mixture cycles aim to modify a typical sub-critical VCHP cycle with a mixture of multiple refrigerants with different boiling points. The difference in boiling points mean that the refrigerant mixture will have a temperature glide in the two-phase region. An illustration of the glide matching refrigerant compared to a basic VCHP interacting with an isothermal heat source and heat sink is shown in figure 3.2.

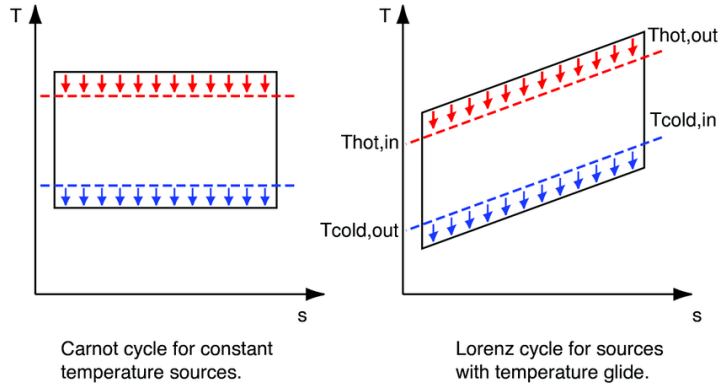

Figure 3.2: Deviation from theoretically perfect cycle of a basic VCHP (Carnot cycle) for glide-matching VCHP (Lorenz cycle) [75]

The left image depicts the theoretically optimal normal VCHP cycle called the Carnot cycle. The right image shows the theoretically optimal cycle for a zeotropic mixture cycle called the Lorenz cycle. Note the perfect matching of the mixture's glide to that of the heat source and -sink. The present work limits itself to refrigerant mixtures of two compounds referred to as binary mixtures. One advantage of zeotropic mixtures is that they do not always require changes to a cycle's components or operating conditions. An example of this is the work by Bell et al. (2019) where they sought to create a drop-in replacement for R-134a using a refrigerant mixture [4]. Because a refrigerant mixture's properties can be customized by adjusting its constituents and their proportions it can be used for a wide range of applications and matched to pre-existing equipment if present.

3.2.2. Trans-critical cycle

A trans-critical VCHP cycle aims to elevate the refrigerant past its critical point such that instead of a condensation the refrigerant delivers heat as a supercritical fluid. A trans-critical cycle can still be described using the process flow diagram (PFD) introduced in figure 3.1 but the term condenser is typically replaced with gas cooler as the former is referring to a phase change no longer occurring. In trans-critical operation there is still a variation in material properties during the heat transfer in the critical region. This variation occurs when crossing the Widom line, is referred to as pseudo-condensation and should be accounted for in the design [76]. The original idea of operating a VCHP cycle above the critical point was patented in 1990 by Lorentzen [49]. Lorentzen did not stop their work on the topic as four years later they published a work demonstrating that CO_2 possesses "near ideal" properties for trans-critical operation [48]. A generic temperature (T) specific entropy (s) diagram demonstrating the glide matching of such a trans-critical CO_2 cycle is given in figure 3.3. Here two additional processes are shown when compared to figure 3.1 found in VHCP cycles namely process 1-2 and 4-5, showing super-heating and sub-cooling respectively.

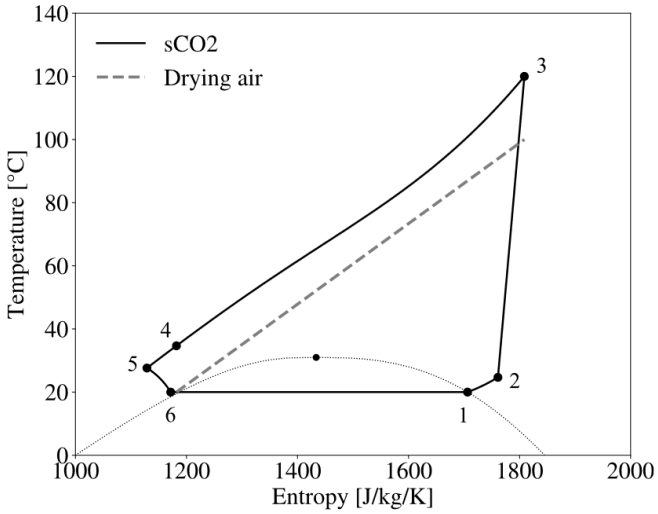

Figure 3.3: Generic glide matching demonstration of a trans-critical CO_2 cycle with air: 1 Outlet of the evaporator; 2 Inlet of the compressor; 3 Outlet of the compressor; 4 Outlet of the gas cooler; 5 Inlet of the expansion valve; 6 Outlet of the expansion valve [76]

Since Lorentzen's work CO_2 has been extensively studied by both academia and industry. Yang et al. (2021) published an overview paper on trans-critical CO_2 cycles discussing the research progress on the topic. They showed that the technology is relatively mature and ready for deployment. They went on to discuss that academic work should focus on novel cycle components and intelligent control schemes [74]. The conclusion that academia should focus on novel cycle components for trans-critical cycles is not new as this was already suggested in the work by Chua et al. (2010) a decade before [12]. Illustrations of the maturity of the trans-critical CO_2 cycle are given by industry, for example the successful commissioning of a 65 MW_{th} trans-critical heat pump station in Esbjerg in 2023 by MAN energy solutions [27].

The challenge CO_2 introduces is the requirement for high pressures to operate above the critical point. Because of these high pressures, work is being done to explore alternative refrigerants in trans-critical cycles. Zhao et al. (2024) proposed trans-critical operation of R1233zd(E),R1336mzz(Z), n-Butane and Ammonia for the purpose of heating air from 80 to 200°C [76]. Of these refrigerants n-butane is repeatedly reported as an interesting candidate for trans-critical operation [34, 53, 57]. In similar work performed by Vieren et al. (2023) R1336mzz(Z) and R1233zd(E) are also indicated to have recurring high performances for HTHP cycles. When specifically looking at natural refrigerants they propose cyclobutene, cis-2-butene, isopentane and pentane as effective refrigerants in trans-critical operation [70].

3.3. Heat exchangers

Heat exchangers (HEXs) are used to facilitate heat transfer between two fluids at different temperatures. HEXs can be indirect-contact or direct-contact but the former is most commonly used as this type keeps the two streams separate from one another. A direct-contact HEX mixes the two streams such that they equalise at an intermediate temperature. Direct-contact HEX are most commonly applied when simultaneous mass and heat transfer is desired or when the interacting fluids are immiscible liquids but in the latter case separation of the two streams at the outlet remains an issue [54]. Rarely is mixing of the two streams desired and, depending on the temperature difference, large amounts of exergy can be lost in this way hence the prevalence of indirect-contact HEXs. In all types of HEXs The temperature difference between the streams is the driving force of the heat transfer. The total heat transfer in a HEX can be expressed as

$$Q = UA\Delta T_{lm} \tag{3.4}$$

in terms of the heat transfer area (A), the overall heat transfer coefficient (U) and an appropriate mean temperature difference between the hot and cold streams(ΔT_{lm}) [54]. Equation (3.4) is a generalized expression which makes use of tabulated values and correlations to determine U instead of manually calculating the thermal resistances present in the system [65]. The logarithmic mean temperature difference (LMTD) can be used to determine ΔT_{lm} which results in the following expression for parallel-flow and counterflow HEXs:

$$LMTD = \frac{(T_H - T_c)_{out} - (T_H - T_c)_{in}}{\ln(T_H - T_c)_{out} - \ln(T_H - T_c)_{in}} \tag{3.5}$$

Where $(T_H - T_c)_{out}$ is the temperature difference between the hot and cold stream at the outlet and $(T_H - T_c)_{in}$ at the inlet of the HEX [54]. According to Mills and Coimbra (2015) the LMTD method is widely used in engineering practice due to its simplicity but is useful only when inlet and outlet temperatures are known. If the inlet and outlet conditions are not known the LMTD method can still be be applied using iterative solutions or specially constructed charts but a simpler solution is to use the $\epsilon - N_{tu}$ formulation.

By expressing the HEX performance in terms of effectiveness (ϵ) and number of transfer units (N_{tu}) a method can be formulated that does not require iteration for unknown outlet conditions [54]. Here ϵ quantifies the ratio of actual heat transfer achieved in a HEX in terms of the theoretically possible heat transfer. In practice the value of ϵ for a given HEX will be between 0.6 and 0.9 [54]. N_{tu} can be interpreted as the amount of heat transfer the HEX is capable of. Both ϵ and N_{tu} are dimensionless numbers and their mathematical formulations depend on the type and configuration of the heat exchanger being designed and are available in References [54, 65]. It is important to note that both $\epsilon - N_{tu}$ and $N_{tu} - \epsilon$ relations are available and depending on what aspect of the to be designed HEX is unknown the appropriate relation can be selected. For a counterflow HEX, the most relevant HEX for VCHP cycles, the $\epsilon - N_{tu}$ and corresponding $N_{tu} - \epsilon$ relation is given as

$$\epsilon = \frac{1 - \exp(-N_{tu}(1 - R_c))}{1 - R_c \exp\{-N_{tu}(1 - R_c)\})} \iff N_{tu} = \frac{1}{1 - R_c} \ln \frac{1 - \epsilon R_c}{1 - \epsilon} \tag{3.6}$$

with R_c being the heat capacity ratio of the two streams defined as

$$R_c = \frac{C_{min}}{C_{max}} \tag{3.7}$$

where C is the flow thermal capacity of the stream being the sum of the specific heat capacity and the mass flow of the stream. C_{min} is the smallest of the two flow thermal capacities in the HEX and C_{max} the largest.

It should be understood that the effectiveness and LMTD formulations are mathematically equivalent and thus either can be used for the design of a HEX. Current practice favours the effectiveness method for HEX design. This preference is because of the physical significance of both dimensionless numbers involved. Additional advantages are the suitability for computer-aided design and the aforementioned availability of non-iterative solutions for unknown outlet conditions [54].

The condensers and evaporators in a VCHP cycle are usually indirect-contact HEXs as the process stream and the refrigerant should not be mixed. The most commonly used indirect contact HEX type is the shell-and-tube heat exchanger consisting of a tube bundle in a shell as shown in figure 3.4. One fluid stream passes through the tubes, while the other flows in the shell around the tubes. Typically baffles are included in the shell-side to elongate the flow path of the associated stream as well as to hold the tube bundle in place. The tube side fluid can have very high pressures and the tubes are easily cleaned [63]. In the design of shell-and-tube HEXs as well as others commercial software tools like ”ASPEN v12 exchanger design and rating” are available to facilitate in-depth design, as employed by Zhao et al. (2024) for example [76]. During heat exchange in both the evaporator and condenser

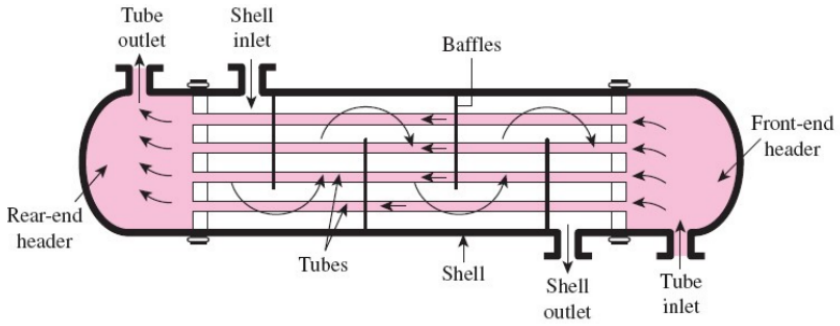

Figure 3.4: Schematic depiction of a typical shell-and-tube heat exchanger including baffles to elongate shell-side flow path and front and rear headers [29]

pressure drops can be expected. Nevertheless the flow work associated with the pressures encountered is neglected as it is assumed the enthalpy of the refrigerant is the dominant energy contribution. Neglecting pressure drops also has the effect of skewing a comparison between VCHP cycles as was argued by Bell et al. (2019) based on the work of Mclinden et al. (2017) and Domanski et al. (1992) [4, 15, 51]. Mclinden et al. (2017) demonstrated that models that incorporate the pressure drop show a smaller impact on the COP for high pressure fluids than low pressure ones. As was done in the work by Mclinden et al. (2017) initial modeling of ideal cycles will be performed but the resilience of high pressure cycles to pressure drop accounting must be taken into account when comparing the performance of cycles.

A final important consideration in designing the heat exchangers is the pinch point analysis. Pinch point analysis revolves around the identification of the smallest encountered temperature difference during the heat transfer. As process streams rarely have perfectly matched heating behaviours it is important to ensure that the temperature difference remains large enough such that heat transfer remains feasible. The mismatch in heating behaviour can be the consequence of different flow thermal capacities as well as differences in phase change behaviour. Thus, given the same $\dot{Q}$, it is expected that a different temperature change will occur in the two streams. This introduces a trade-off as the larger the temperature difference between the streams, the greater the heat exchanged which allows for a smaller heat exchanger at the cost of exergy destruction.

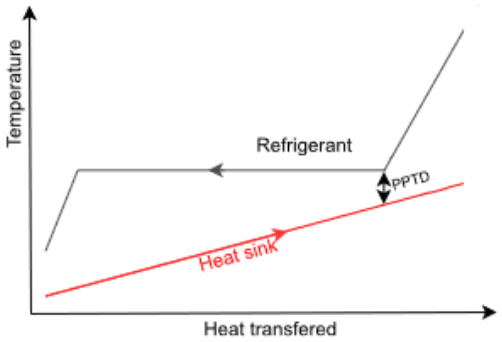

Figure 3.5: illustration of a pinch point analysis and defintion of the PPTD [70]

The common strategy, as graphically depicted in figure 3.5, is to define the minimum pinch point temperature difference (PPTD). At this point during the heat transfer the ΔT is at its minimum. By predefining the temperature difference at this minimum distance one can ensure feasible heat transfer over the entire process. In the context of calculating thermodynamic cycles for heat pumps several PPTDs can be found in literature such as $3^{\circ}\mathrm{C}$ used by Zhao et al. (2024), $5^{\circ}\mathrm{C}$ used by Zuhlsdorf et al (2018) and $5^{\circ}\mathrm{C}$ used by Vieren et al. (2023) for all condensers and evaporators in their respective heat pump models [70, 76, 78]. In general PPTD's range between 5 and $15^{\circ}\mathrm{C}$ for heat exchanger design and are typically a cost optimisation problem seeking an optimum between capital expenditures (CapEx) of the HEX versus the costs of energy [14].

3.4. Compressor

The compressor stage serves to increase the pressure, priming the refrigerant for condensation. Compressors can be classified as positive displacement or dynamic compressors, the latter is frequently referred to as turbocompressors. Positive displacement compressors draw gas into a chamber and then reduce the volume of this chamber. As this process is performed at constant speed it follows that the resulting volumetric flow rate is also constant. turbocompressors transfer kinetic energy to the gas which is converted into pressure by reducing the velocity of the refrigerant using diffusers. Compressors can be further classified as reciprocating or rotating. Reciprocating compressors are exclusively positive displacement compressors while rotating compressors can be dynamic or positive displacement. Rotating compressors have several advantages such as their smaller size, more silent operation, low vibration and better control and modulation capability [26]. An overview of commercially available compressors is given in figure 3.6. Kiss and Ferreira (2017) identifies scroll, piston and screw as compressor types typically employed in heat pump cycles [37]. according to the IEA (2014) and Liang et al. (2022) as well as industrial parties such as MAN energy solutions turbo-machinery is also well suited for use in a HP cycle with compressor power ratings above 100 kW [27, 41, 46].

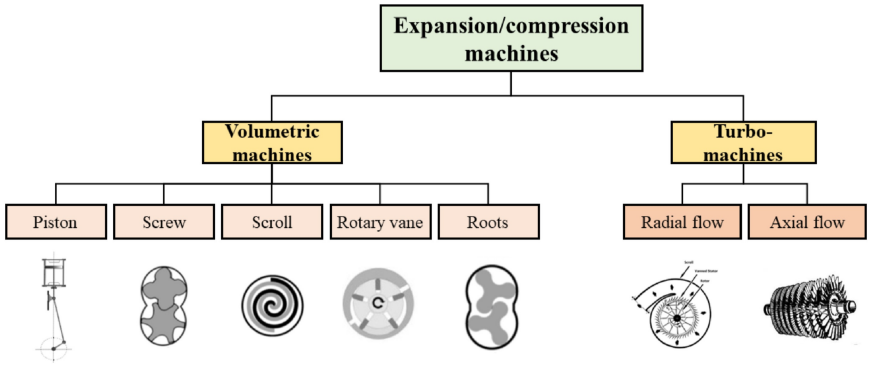

Figure 3.6: Categories of commercially available compressors [46]

Of these four compressor types the scroll and piston compressor technologies are not commercially available for industrial scale heat pumps such as the ones required for large drying processes [37, 41] Thus the focus is on screw compressors and turbo compressors.

Screw compressors consist of one or two rotating screw(s) which trap a pocket of fluid and progressively force it to the discharge and are therefore of the positive-displacement type. They can achieve moderate pressure ratios (PRs) of 2.5 to 5.5 but posses low volume flow rates limited to approximately $650\mathrm{m}^3\,\mathrm{h}^{-1}$[37]. Oil is not needed for lubrication, however, it is often employed as a seal between the screw and the housing, and between the screws in the case of a twin screw.

Recent work has shown that these compressors can also be used in wet compression scenarios [8]. Brancaccio (2023) performed interesting work arguing for the potential of wet compression screw compressors where the liquid fraction of the refrigerant effectively performs the part of the oil but without contaminating the refrigerant. While this work is valuable it is unknown how this operating principle interacts with refrigerant mixtures and is thus an active field of research of its own which falls outside the current scope of this work. Thus it is assumed that the compressor must be operated in a dry compression regime. It is typical in industry that when a compressor requires no droplets be present that a degree of superheat (ΔT_{sup}) is introduced.

Turbo-compressors use fast spinning blades called rotors to impart velocity to the refrigerant which is subsequently turned into pressure through the stators. Given the high velocity at which the blades spin, these compressors are highly sensitive to droplets and should thus be operated in strictly dry compression regimes [55]. They can be used for high total pressures and provide good volumetric flow rate [27]. Oil free variants exist and are preferred for HTHPs as lubricating oil can become thermally unstable above 150°C [8, 19, 53].For compressors the non-ideality of performance is typically represented in terms of the volumetric (η_{Vol}) and isentropic (η_c) efficiencies. The values of these are dependent on the pressure ratio and the type of compressor. For a screw compressor η_c has an optimum of 70% for PRs between 3 and 4 [37] with η_{Vol} between 90 and 100 %. For a turbo-compressor these are typically higher but under conservative estimation can also be assumed to be in this range [76].

3.5. Pressure reduction component

A typical heat pump uses an expansion valve to reduce the pressure back to the level of the evaporator. It is common to assume isenthalpic behaviour for this component [55]. the expansion valve is not a component of significant innovation but the associated entropy production has led to work investigating potential novel components that can take the place of an expansion valve. One such concept that is specifically valuable for high temperatures and more specifically the associated high pressures is the ejector. The high pressures found in cycles such as a trans-critical CO_2 cycle show the most promising use case for ejectors [70].

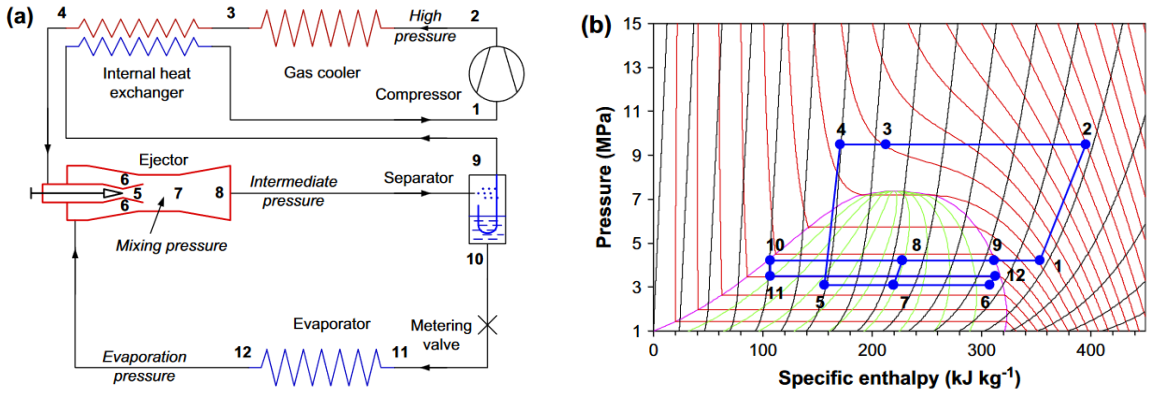

Figure 3.7: Trans-critical R744 ejector system. (a) Component layout. (b) Corresponding pressure–specific enthalpy diagram [19]

Shown in figure 3.7 is a trans-critical CO_2 cycle using such an ejector with its associated pressure-specific enthalpy diagram. The difference with a basic VCHP cycle is most clear when evaluating the cycle at the separator. Instead of evaporating the multi-phase refrigerant it is instead split and the two saturated phases are heated separately. This corresponds to state 10 for the liquid phase which is heated to state 12 and state 9 for the saturated gas which is heated to state 1. The ejector mixes the outlet of the gas cooler, taking the place of the condenser, and mixes it with the evaporated liquid. Use of an ejector was modeled by Elbel et al. (2008) using a constant pressure model and Li et al. (2005) using a constant volume model. A VCHP cycle modified with an ejector, when done right, allows for an isentropic conversion of pressure related flow work into kinetic energy [19, 45]. While this technology is potentially very important in further heightening the effectiveness of applicable HTHP cycles it is difficult to implement. It's nature as a concept, taking into account the separator step, will be difficult to integrate with a zeotropic refrigerant mixture. As mixtures are the focus of the present work ejectors are thus left outside the scope of this work at this stage.

4

Methodology

This chapter discusses the methodology used to investigate zeotropic mixtures in VCHP-integrated dryers. The chapter begins with a process flow diagram depicting the entire system of the basic heat pump integrated dryer. The process flow diagram is then used to define the thermodynamic states of the (humid) air and of the refrigerant mixture. The interactions between the refrigerant and the air streams is explicitly elaborated upon. The system is then discussed per component, where the governing equations and assumptions of each component are specified. The methodology used to calculate the air and refrigerant mixture thermodynamic states is given in terms of the models and thermodynamic libraries used and their validity ranges. The modelling strategy and procedure is given which were implemented in python to perform the calculations. The chapter concludes with the proposal of a different type of heat pump cycle. The novel cycle is motivated using the heating profile of humid air and the process flow diagram is given for an integrated dryer with this type of heat pump as well.

4.1. Basic heat pump cycle: Process definition

The large variety of drying process types and conditions presented in chapter 2 will be represented by a generic adiabatic drying operation. For the purposes of glide-matching and VCHP design it is not essential to model the inner workings of the dryer. The drying process is thus chosen to be represented by a black-box operation adiabatically humidifying incoming hot air. Integrating a heat pump into this generalized drying process is accomplished by connecting the in- and outflow of the dryer to the heat exchangers of the VCHP cycle as shown in Figure 4.1.

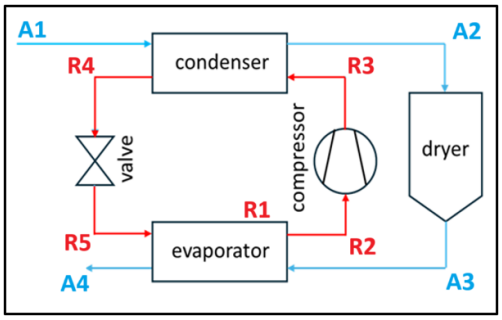

Figure 4.1: Process flow diagram of a vapour compression heat pump integrated into a drying unit with defined states of air (blue), defined states of the refrigerant mixture (red) and their flow directions

Shown is the air stream in blue and the refrigerant mixture stream in red as well as four thermodynamic states for air and five for the refrigerant mixture of which the definitions follow. Starting with the air states, the input air is assumed to be taken from the environment (denoted by A1) and is thus at ambient pressure, temperature and relative humidity which are taken to be 1 atm, 10 $^{\circ}\mathrm{C}$ and 80% respectively [11, 43]. This air is heated by the heat pump within the condenser to the required inlet conditions of the dryer (A2). The humid air outflow of the dryer (A3) is the heat source utilised in the evaporator of the heat pump. The humid air exiting the evaporator (A4) is returned to the environment.

The thermodynamic states of the refrigerant mixture stream are also defined at several points within the process flow diagram. The refrigerant mixture will absorb heat in the evaporator and reach a saturated vapour state (R1). The saturated vapour will be at the evaporator's operating pressure. As a common safety measure to prevent wet compression a degree of superheat, ΔT_{sup}, is designed to be present at the exit of the evaporator. The superheated vapour state (R2) is thus at a temperature ΔT_{sup} higher than R1 but also present in the evaporator and thus at its operating pressure. R2 is fed to the compressor such that the refrigerant mixture reaches elevated pressure and temperature (R3). The goal of this compression is to bring the refrigerant mixture to an appropriate isobar such that subsequent heat release to the dry air in the condenser is feasible. Feasibility here means that, upon heat release, the refrigerant mixture's temperature remains sufficiently higher than the temperature of the dry air being heated. The refrigerant mixture exiting the condenser (R4) will be at reduced specific enthalpy but remains at the condenser pressure. This stream is fed through the expansion valve (R5) to bring the refrigerant mixture back to the evaporator pressure and lies in the two-phase region of the mixture.

an addition to this simple cycle can be made motivated by the first law of thermodynamics. The energy balance of the heat pump can be defined as

$$\dot{Q}_{out} = \dot{Q}_{in} + \dot{W}_c \tag{4.1}$$

Where $\dot{Q}_i$ is the heat transferred, denoted by subscript "out" when heating dry air and denoted by subscript "in" when heat is being extracted from the humid air. $\dot{W}_c$ is the work done by the compressor. This equation shows that for any cycle where the compressor performs work ($\dot{W}_c > 0$), $\dot{Q}_{out}$ will be higher than $\dot{Q}_{in}$. Given that $\dot{Q}_{out} > \dot{Q}_{in}$ and that drying is adiabatic, there will be more heat added between A1 and A2 than subtracted from A3 to A4 and thus some waste heat is present in the air outlet state A4. A heat exchanger is proposed between air states A1 and A4 to pre-heat the ambient air and utilise the VCHP cycle's waste heat. The modified cycle's process flow diagram is shown in Figure 4.2.

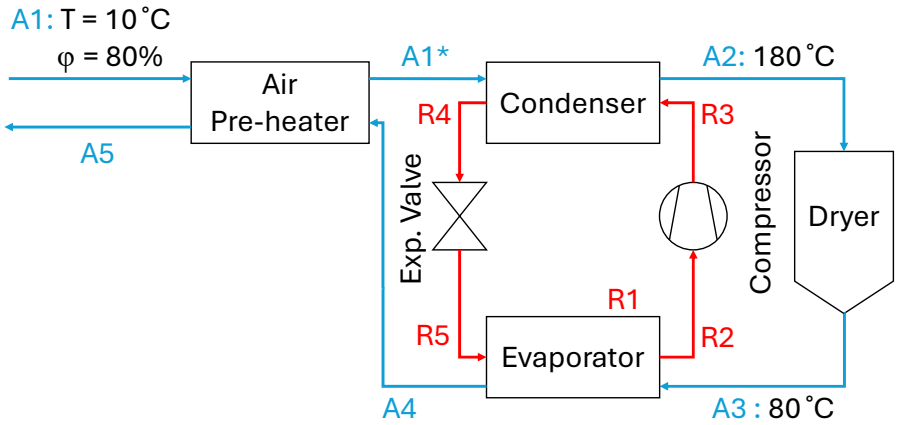

Figure 4.2: Process flow diagram of a VCHP and air-to-air heat exchanger integrated into a drying unit with defined states of air (blue), defined states of the refrigerant mixture (red) and their flow directions

Shown is the originally proposed VCHP cycle with one new component and two new defined states for the air. The new component is a heat exchanger operating between two air streams and thus falls under the same governing equations and assumptions that apply to the condenser and evaporator. State $A1^*$ is introduced to define the preheated air at equal pressure and absolute humidity as A1 but at an elevated temperature. State A5 is introduced as the new exhaust condition of the system to the environment. The proposed cycle reduces the total temperature lift required by the heat pump section and targets the lowest quality waste heat to perform the lowest temperature heating. The PPTD used in the air-to-air HEX is set to be the same for the VCHP HEXs.

4.2. governing equations

The following section presents a component-wise analysis of how to describe the VCHP cycle both with and without pre-heater. Key global assumptions made throughout this section are pre-emptively summarised in Table 4.1 with the components to which they apply and section within which they are justified given.

Table 4.1: Overview of global modelling assumptions

Assumption	relevant component	Justifying section
Minimum pinch point temperature difference = 5.0 $^{\circ}\mathrm{C}$	Heat exchanger	section 3.3
Degree of superheat = 7.5 $^{\circ}\mathrm{C}$	Compressor and Evaporator	Section 3.4
Pressure losses are neglected	Heat exchangers	Section 3.3
η_c = 70%	Compressor	Section 3.4

4.2.1. Heat exchangers

Both the evaporator and the condenser are assumed to be well-insulated such that any heat removed from one stream is gained by the other. This assumption translates to a coupling of heat fluxes using the first law of thermodynamics given by

$$\dot{Q}_{air} = \dot{Q}_{ref} \rightarrow \dot{m}_{air}(h_{in,air} - h_{out,air}) = \dot{m}_{ref}(h_{out,ref} - h_{in,ref}) \tag{4.2}$$

where $\dot{Q}_i$ is the heat exchanged by process stream i, $\dot{m}_i$ is the mass flow rate of process stream i and $h_{d,i}$ is the specific enthalpy of a process stream i in direction d. It is important to note here that the temperature difference is, at every point within the heat exchanger, greater than or equal to the pinch point temperature difference. The global PPTD, thus being applied to the air-to-air HEX, the evaporator and the condenser, is chosen to be 5 $^{\circ}\mathrm{C}$. A PPTD of 5 $^{\circ}\mathrm{C}$ is an intermediate value within the encountered values in literature as presented in section 3.3.

The target temperature of the air entering the dryer T_{A2} is set to be 180 $^{\circ}\mathrm{C}$ which was categorised as very high temperature drying in chapter 2 and is, for example, used in the drying of liquid food products. The exit temperature of the dryer T_{A3} is set to be 80 $^{\circ}\mathrm{C}$ in accordance with data from both paper and food drying with the humidity defined by the enthalpy of the dryer inlet, following the adiabatic drying definition.

4.2.2. Compressor & expansion valve

The compressor is modelled using an isentropic efficiency defined as

$$\eta_c = \frac{h_{3,is} - h_2}{h_3 - h_2} \tag{4.3}$$

where h_i denotes the refrigerant mixture's specific enthalpy at thermodynamic state i and $h_{i,is}$ denotes the specific enthalpy at thermodynamic state i if the compression was performed isentropically. The determination of the compressor outlet is done by solving for the outlet and the isentropic outlet simultaneously using the scalar minimisation function available in the python library SciPy [9, 22]. The isentropic compression point has equal entropy as the inlet and a given pressure p. The actual outlet has the same pressure p and a specified enthalpy following Eq. (4.3). The "bounded" method is then applied above the pressure of the compressor inlet to determine the value for p if an appropriate isobar exists. The isentropic efficiency is assumed to be 70%, a conservative value in line with the data presented in chapter 3.4 and explicitly recommended as a good approximation of real compressor efficiency by Kiss and Ferreira. (2017) [37].

The expansion valve is modelled as an isenthalpic expansion, a common definition for the component. The expansion valve operates between the condenser pressure p_{R4} and the evaporator pressure p_{R1}. The determination of the pressure levels the expansion valve operates between is the consequence of the calculation of other refrigerant mixture states and is presented in section 4.4.2.

4.3. Modelling strategy

In order to determine the effects of different refrigerant mixture constituents, mixture ratios and operating conditions a model programmed in python was constructed. The goal of the model is to calculate the performance of heat pumps operating between the same heat source and -sink namely the dryer outlet and inlet respectively. The heat pumps must be compared at the same operating point which is chosen to be defined using the pinch point in the condenser and evaporator. The goal of the code is to optimise the COP without violating the PPTD or requiring wet compression for VCHP cycles using a wide range of different refrigerant mixtures. Shown in Figure 4.3 is a flow chart of the heat pump calculation and optimisation implemented in python.

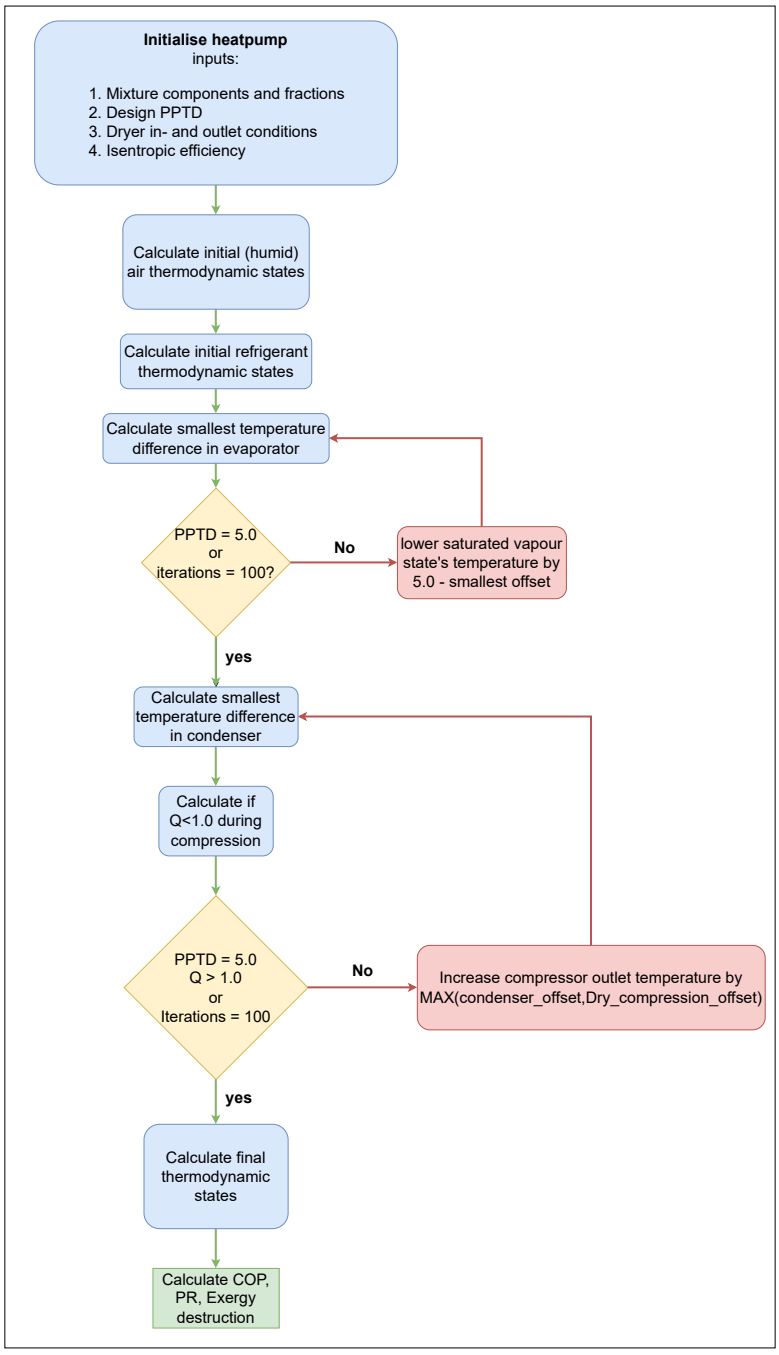

Figure 4.3: Flow chart depicting the calculation procedure of pinch-point optimised heat pumps with calculation steps in blue, conditions in yellow, iteration loops in red and outputs in green

An initial calculation is made of the heat pump using definitions which will be presented in detail in subsections 4.4.1 and 4.4.2 for the air and refrigerant respectively. The pinch point in the evaporator is calculated and, if unequal to the specified minimum PPTD, the refrigerant's temperature (R1) is modified accordingly. If the evaporator's PPTD is larger than the minimum PPTD then T_{R1} is increased, if the PPTD is smaller than the minimum it is decreased instead. The same method is applied to the condenser to determine the PPTD and bring it to the minimum PPTD value.

The inlet of the condenser is the outlet of the compressor (R3) which is defined to require dry compression. As the superheat is kept equal between heat pumps the only modifiable aspect of compression is the exit temperature of the compressor. A second check is performed to ensure no wet compression occurs, expressed as the quality being equal to or lower than 1.0. Both the pinch point analysis of the condenser and the wet compression check report by how much T_{R3} must be changed to meet their respective condition. The most severe of the two temperature changes is used. For example, if the PPTD analysis returns that T_{R3} must be 10 $^{\circ}\mathrm{C}$ larger as to not violate the minimum PPTD but the wet compression check reports a 15 $^{\circ}\mathrm{C}$ increase is required then the latter value, being the larger, is used. The implementation of the PPTD and wet compression checks is given in Appendix A.2

The heat pump calculation procedure specified in Figure 4.3 is implemented in python as part of a larger model capable of calculating and comparing heat pumps for all possible refrigerant pairs. The model is comprised of three main modules that work together as shown in Figure 4.4.

The top-level module is Optimiser.py, which contains two main classes: Divider and MixtureSweep. The Divider class creates pairs of all considered refrigerants and divides them into steps of 5 $\%_{mol}$. The MixtureSweep class is responsible for calling heatpump.py, comparing the outputted heat pump cycles based on their performance, and then reporting the best performing mixtures and their composition. Each binary pair is modelled in a VCHP dryer by calling heatpump.py. The MixtureSweep class stores the data of each pair's highest COP, providing a dataset of the best performing composition of each binary pair. This allows for easy identification of the best matching of a VCHP to a dryer's operating conditions. Additionally, the MixtureSweep class records the COP of each binary pair for every calculated mixture composition, showing the effect of each refrigerant mixture over the full range of possible compositions. The implementation of MixtureSweep is given in Appendix A.3.

The second module, heatpump.py, contains the Heatpump class, which operates at the middle level and is responsible for calculating a heat pump cycle as shown in Figure 4.3. The output is a heat pump definition with no wet compression and minimal pinch point temperature differences.

The inner module, defined as states.py, is responsible for defining the thermodynamic state of a compound or mixture thereof based on two state variables. It includes two classes: ThermoState and ThermoStateHumid. The ThermoState class handles the calculations for refrigerants using the REFPROP library, while the ThermoStateHumid class handles the calculations for humid air using the CoolProp library. The states.py module is called by heatpump.py to calculate the necessary thermodynamic states used in the heat pump cycle.

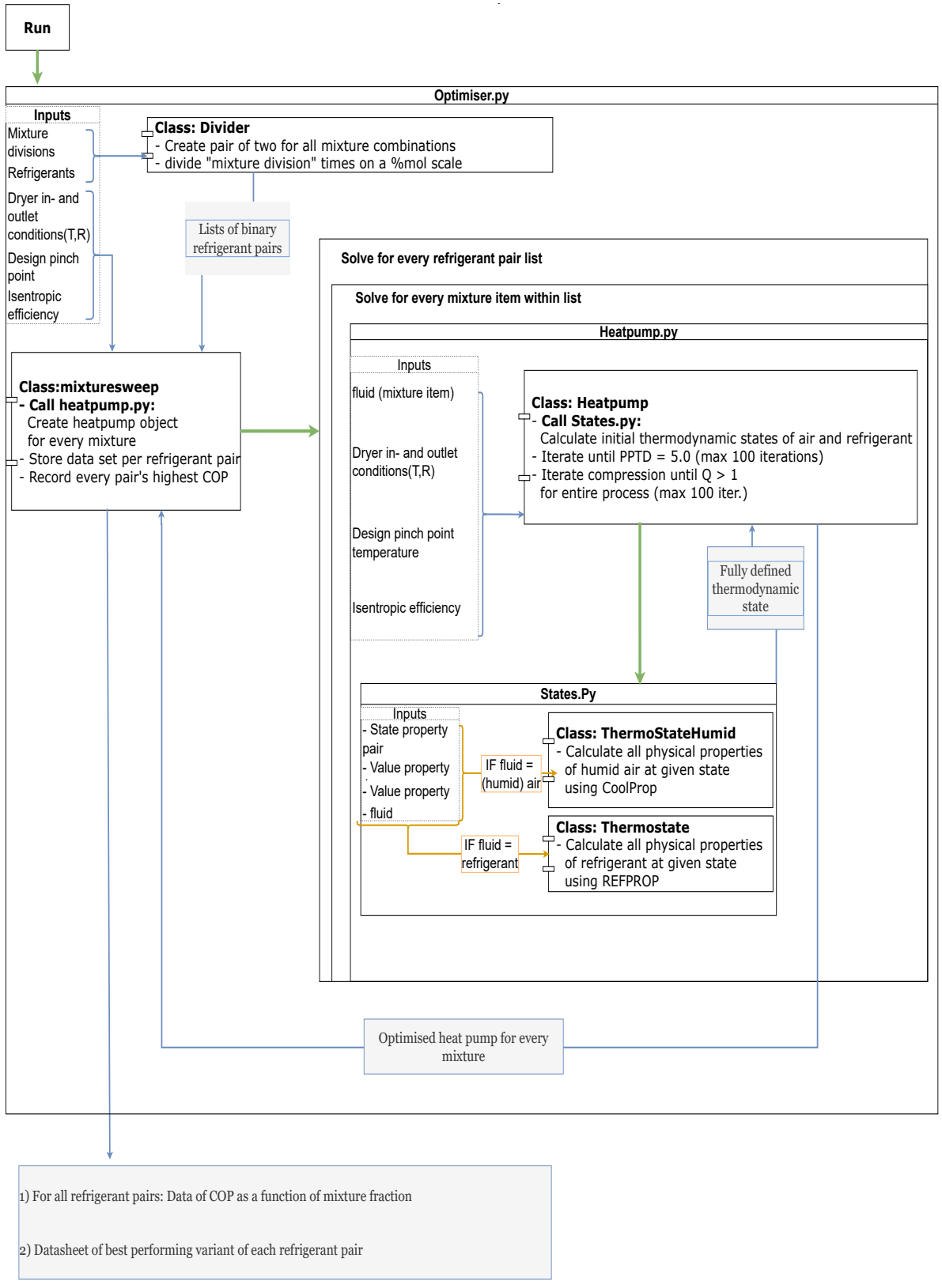

Figure 4.4: Code hierarchy of the model showing initialisations in green, data exchange in blue and conditional calls in yellow

4.4. Thermodynamic state calculations

Given the definition of the process, its governing equations, its thermodynamic states and the modelling strategy, implementation can now be proposed. In order to calculate the defined thermodynamic states of refrigerants and their mixtures appropriate models and values need to be used. It was chosen to rely on the REFPROP V10.0 thermodynamic state library developed by The National Institute of Standards and Technology (NIST) as this is considered an industry standard [5, 30]. This database consists of 147 pure fluids, 5 pseudo-pure fluids and mixtures with up to 20 components. For considered carbohydrate refrigerant mixtures such as those comprised of pentane or CO_2 the GERG-2008 model is used as this demonstrated a better stability during modelling. The GERG-2008 model describes 21 natural gas components of which the most relevant are carbon dioxide, n-butane, n-pentane, isopentane and isobutane [40]. The GERG-2008 model has a validity range of 90 to 450 $^\circ\,\mathrm{K}$ and pressure up to 35 MPa with an extended validity range up to 700 $^\circ\,\mathrm{K}$ and 70 MPa [40]. The model is report to have relative uncertainties of 0.03 to 0.1% for thermodynamic state calculation, 1 to 2% for the heat capacities and 1 to 3% for vapour-liquid equilibrium calculations within the validity range.

Humid air can be described at various levels of complexity. The simplest method to describe the air-water vapour mixture is by assuming it behaves as an ideal gas mixture. An ideal gas mixture can be described using the related Dalton model which assumes that each component behaves as an ideal gas as if it were alone at the given temperature and volume [55]. This simple analysis fails to account for the interactions between air and water molecules that must be accounted for. While more complex equations of state and mixture models that use interaction parameters can be applied, the most reliable data will always be based on experimental data. Implemented within the CoolProp open-source thermophysical library is a humid air property library called HAPropsSI based on the findings of The American Society of Heating, Refrigerating and Air-Conditioning Engineers (ASHRAE) as part of the research project ASHRAE-RP1485 [28]. The CoolProp library is reported to reproduce the humid air experimental data with very high accuracy between pressures between 0.01 kPa and 10 MPa and temperatures between 130 and 623.15 $^\circ\,\mathrm{K}$ [5].

4.4.1. Air Thermodynamic state calculations

Using the HAPropsSI function provided in CoolProp the properties of all air states can be calculated given 3 state properties. State $A1$ is the input from ambient and thus any 3 ambient condition properties can be taken to define it. The average annual ambient temperature and relative humidity were taken in combination with atmospheric pressure to define this state. state $A1^*$ is defined by the introduction of the air-to-air HEX. The HEX's pressure drop is neglected so the pressure is still 1 atm, the absolute humidity is constant as well and the temperature is taken to be the PPTD below the exit condition of the evaporator T_{A4} such that the maximal amount of waste heat is captured. This introduces an iteration requirement as the state $A4$ is defined by the heat pump but the heat pump is affected by the incoming temperature $A1^*$ as included in the modelling hierarchy given in figure 4.4. State $A2$ is defined similarly to $A1^*$ by assuming constant absolute humidity and pressure through the condenser and using the dryer inlet temperature of 180 $^\circ\mathrm{C}$. State $A3$ is defined by the adiabatic drying process meaning h_{A3} is equal to H_{A2}, atmospheric pressure and the dryer outlet temperature of 80 $^\circ\mathrm{C}$. State $A4$ is defined using the using Eq. (4.2) to specify the specific enthalpy. Additionally, the relative humidity is taken as 1 as it is assumed the latent heat of the evaporated water is accessed successfully. Finally, following the assumption of neglected pressure losses, the pressure is taken to be 1 atm. The exit condition $A5$ is specified using the same three assumptions but applying Eq. (4.2) to the air-to-air HEX instead. The values used to determine the defined air states are summarised in Table 4.2 below.

Table 4.2: All values used to define the initial thermodynamic state of air at 6 points using the CoolProp function HaPropsSI

Air state	state property 1	state property 2	state property 3
A1	$T = 10\ ^\circ\mathrm{C}$	$\varphi = 0.8$	$p = 1\ \mathrm{atm}$
A1*	$T = T_{A4} - \Delta T_{PP}$	$\omega = \omega_{A1}$	$p = 1\ \mathrm{atm}$
A2	$T = 180\ ^\circ\mathrm{C}$	$\omega = \omega_{A1}$	$p = 1\ \mathrm{atm}$
A3	$T = 80\ ^\circ\mathrm{C}$	$h = h_{A2}$	$p = 1\ \mathrm{atm}$
A4	$H = H_{A3} - \Delta H_{R2\rightarrow R5}$	$\varphi = 1.0$	$p = 1\ \mathrm{atm}$
A5	$H = H_{A4} - \Delta H_{A1^*\rightarrow A1}$	$\varphi = 1.0$	$p = 1\ \mathrm{atm}$

4.4.2. Refrigerant thermodynamic state calculations

Using the REFPROP thermodynamic library to define the states of the refrigerant requires the specification of two state properties. R1 can be defined using the knowledge that it is in the saturated vapour state meaning the quality (x_{R1}) is equal to one. Additionally the temperature is chosen to be the minimum PPTD below the dew point temperature of the humid air stream $T_{dp,A3}$. This initial guess is to be iterated upon to bring the refrigerant as close as allowed to the air's temperature as depicted in Figure 4.3. The dew point provides a good starting point as this indicates the start of the latent heat release and thus the most relevant glide to match. State R2 is also in the evaporator meaning that, assuming pressure loss are neglected, the pressure is equal to that of R1. R2's temperature is ΔT_{sup} higher than T_{R1}.

The refrigerant states R3 and R3$_{is}$ are defined together given their interdependence. R3 and R3$_{is}$ have an unknown but equal pressure p$_{max}$. The enthalpy of R3 and R3$_{is}$ is coupled through the isentropic efficiency given in Eq. (4.3) chosen to be 70%. The temperature of state R3 is defined in relation to the required temperature of the air (T_{A2}). The temperature at R3 must be at least the PPTD above T_{A2} unless defined to be higher following the pinch analysis. The entropy of R3$_{is}$ is equal to that of R2 following the definition of R3$_{is}$. p$_{max}$ is then determined using the SciPy "minimise scalar" function using the "bounded" method and the constraints placed on the entropy of R3$_{is}$, the temperature of R3 and the enthalpy relation given by η_c.

State R4 is defined using the no loss assumption meaning that the pressure is still equal to the compressor outlet p_{R3}. The second property is the specific enthalpy which can be defined using Eq. (4.2) applied to the dry air stream and the refrigerant leaving the compressor. State R5 is defined by the enthalpic expansion assumption meaning that the specific enthalpy does not change and thus remains equal to h_{R4}. The pressure must be the same as the pressure of the other evaporator states p_{R1} and p_{R2}. The values used to determine the defined refrigerant states are summarised in Table 4.3 below.

Table 4.3: All values used to define the initial thermodynamic state of the refrigerant mixture at 5 points using the CoolProp function PropsSI

Refrigerant state	state property 1	state property 2
R1	$T = T_{dp,A3} - PPTD$	$x = 1$
R2	$T = T_{R1} + \Delta T_{sup}$	$p = p_{R1}$
R3$_{is}$	$p = p_{max}$	$s = s_{R2}$
R3	$T = T_{A2} + PPTD$	$p = p_{max}$
R4	$H = H_{R3} - \Delta H_{A1^* \rightarrow A2}$	$p = p_{R3}$
R5	$h = h_{R4}$	$p = p_{R1}$

the implementation of the state definitions given in Table 4.2 and 4.3 and the use of SciPy to determine the value of p$_{max}$ is available in Appendix A.1

4.5. Novel heat pump cycle: Process definition

One problem encountered when applying zeotropic mixture VCHP to the glides of a dryer is that it encounters two different glides in the evaporator and the condenser. The heating profile of dry air is a linear relation between temperature and specific enthalpy for temperatures relevant to drying processes. Investigating the humid air profile yields Figure 4.5.

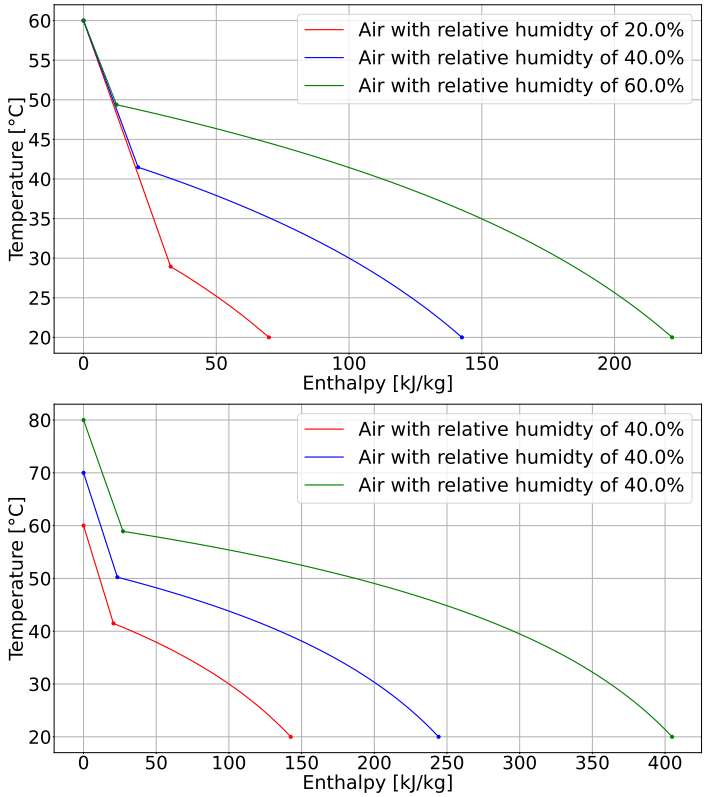

Figure 4.5: Graphs showing the heating profile of humid air both at different relative humidities (top) and at different starting temperatures (bottom)

These graphs show the variety both in amount of heat released and the profile of that release depending on the relative humidity. It is clear that for temperature variations the shape at a given relative humidity stays similar but stretched over the x-axis, releasing more heat along a similar profile. The relative humidity effects the amount of heat released but also the temperature at which heat can be supplied. For example in the top graph, the 60% relative humidity humid air at 60 $^{\circ}\mathrm{C}$ shown in green releases more than 200 $\mathrm{kJ/kg_{air}}$ where at the same temperature but 40% relative humidity not even 150 $\mathrm{kJ/kg_{air}}$ has been released. The glides of dry air heating and humid air cooling are not the same both in terms of magnitude and shape.

Matching both the linear glide of the dry air and the complex glide of humid air is theoretically possible using a VCHP cycle but cannot actively be designed for as both glides are defined by the mixture and so the perfect glide in both HEXs can only be a matter of fortuitous refrigerant behaviour. Classic VCHP cycles thus present with a limitation as there are two different glides that the refrigerant must match but only one degree of freedom. A modification to the classic heat pump cycle is proposed to allow for different glide matching the evaporator and the condenser. The novel cycle proposal separates the liquid and vapour phase from one-another using a flash tank which, by nature of zeotropic mixtures, will posses different compositions allowing decoupled glide matching in the HEXs. A zeotropic refrigerant is by definition comprised of constituents with different boiling points. A difference in boiling points means that during a phase change the liquid and vapour phases have different compositions. By introducing a flash tank to separate the liquid and vapour phases two different refrigerant loops are created, a top loop rejecting heat in the condenser and a bottom loop absorbing heat in the evaporator. The T-s cycle of the ideal proposed novel cycle is given in Figure 4.6 in contrast to the ideal simple cycle. Provided as well is a PFD of the novel cycle given in Figure 4.7.

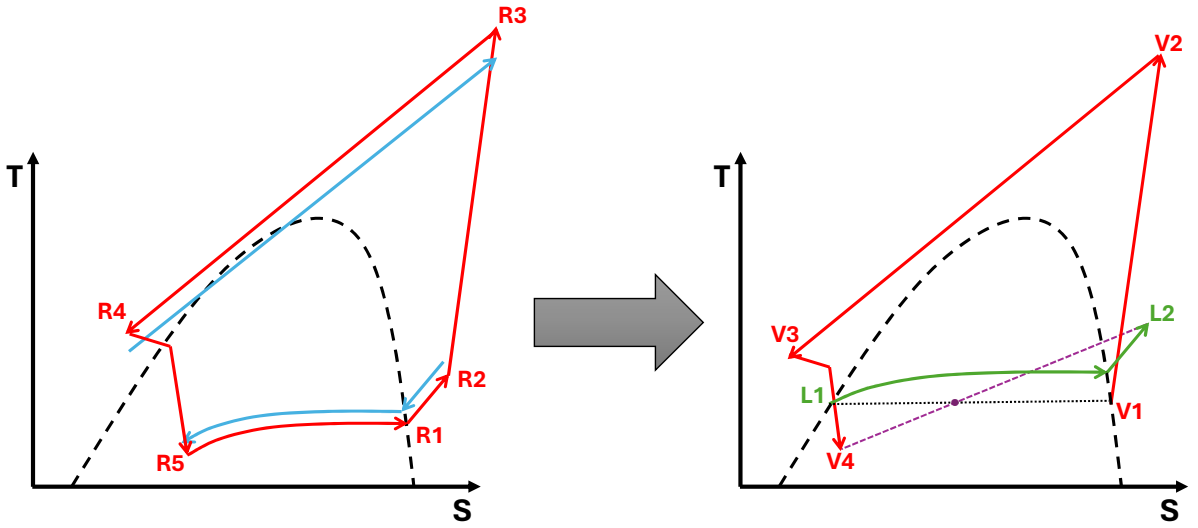

Figure 4.6: Optimal cycle of classic (left) and novel (right) heat pump cycles interacting with (humid) air given in blue, the refrigerant in red and in the novel cycle the saturated liquid loop in green and the mixing in the flash tank in purple

Shown in Figure 4.6 in the left T-s diagram in blue are schematic depictions of the temperature glides of (humid) air and what a perfectly matched basic VCHP cycle would present as. The perfect simple VCHP cycle is translated into the perfect novel cycle, shown in the right T-s diagram which is comprised of two loops. The first loop starts from the saturated liquid given in green and flows through the evaporator to absorb heat. The second loop starts from the saturated vapour given in red and rejects heat in a condenser at elevated pressures realised by a compressor. The two loops start and end in the flash tank which is assumed to be well-mixed and adiabatic and the resulting equilibrium state shown in purple.

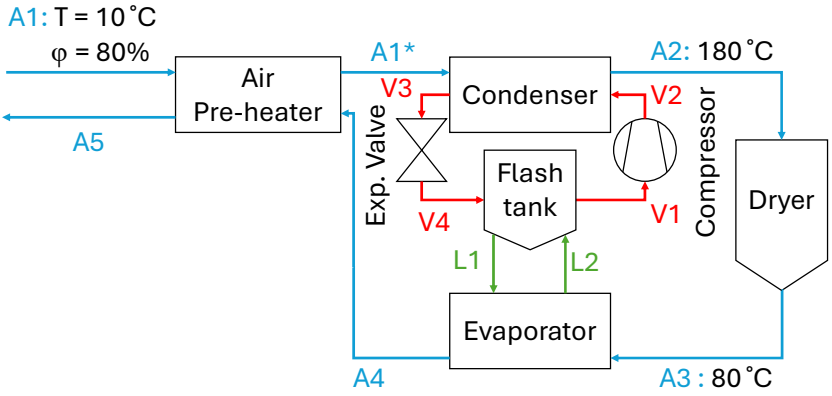

Figure 4.7: Process flow diagram of novel heat pump cycle integrated into a dryer with defined states and directions of (humid) air (blue) and refrigerant separated into a bottom (green) and top (red) loop

The bottom loop is defined by two states namely the saturated liquid phase (L1) at the flash tank temperature and pressure. This liquid phase then flows through the evaporator to absorb the waste heat. The exit condition of the evaporator is either a saturated or superheated vapour state (L2). The top cycle employs the exact same operations as the previous cycle. The flash tank is a thus far unused type of component. It is assumed that the mixing of the return streams happens adiabatically and that the result is well-mixed. Adiabatic mixing means the energy balance in the flash tank is defined as

$$m_{total} * h_{total} = m_{sat\_vap} * h_{sat\_vap} + m_{sat\_liq} * h_{sat\_liq} \tag{4.4}$$

Where h_i is the specific enthalpy of the refrigerant with the subscript denoting either the two phase mixture in the flash tank, the saturated vapour leaving towards the compressor or the saturated liquid flowing down to the evaporator.

The mass of each stream is given by m_i. The mass balance over the flash tank is given as

$$m_{total} = m_{sat\_vap} + m_{sat\_liq} \tag{4.5}$$

Where each massflow can be subdivided as

$$m_i = y_{1,i} * M_1 + y_{2,i} * M_2 \tag{4.6}$$

stated in terms of the mol fraction y of stream i of either compound 1 or 2 comprising the binary refrigerant mixture. The molar mass given by M of compound 1 or 2.

4.5.1. Advanced heat pump cycle: Thermodynamic state calculations

In the alternative heat pump cycle that splits the liquid and vapour loops alternative expressions are defined. The top loop of the cycle uses similar thermodynamic state definitions as stated in Table 4.3 with an omission of the superheat state. For the bottom loop new definitions are introduced. Thermodynamic state L1 is defined using its definition as a saturated liquid meaning the quality (x_{L1}) is equal to 0. The pressure and temperature are equal to the flash tank conditions so either can be used to define the second state property. The outlet state of the evaporator L2 is defined using an equal pressure as L1 following the no pressure loss assumption. The temperature is defined as the humid air temperature T_{A3} minus the PPTD. This targets minimum temperature difference during heat exchange but may be set lower upon iteration if the PPTD is violated somewhere else in the heat exchange. The definitions for the top and bottom loop are summarized in Table 4.4 below.

Table 4.4: All values used to define the initial thermodynamic state of the Liquid refrigerant loop at 2 points and the vapour refrigerant loop at 4 points using PropsSI

Refrigerant state	State property 1	State property 2
L1	$T = T_{Fl\_T}$	$x = 0$
L2	$T = T_{A1} - \Delta T_{PP}$	$p = p_{L1}$
V1	$T = T_{Fl\_T}$	$x = 1$
$V2_{is}$	$T = \eta_c * (T_{V2} - T_{V1}) + T_{V1}$	$s = s_{V1}$
V2	$T = T_{A2} + \Delta T_{PP}$	$h = h_{V1} + \frac{h_{V2,is} - h_{V1}}{\eta_c}$
V3	$H = H_{V2} - \Delta H_{A1^* \rightarrow A2}$	$p = p_{V2}$
V4	$h = h_{V3}$	$p = p_{FL\_T}$

4.6. Refrigerant selection

Refrigerant selection is an immensely important design step for VCHP cycles. The material and thermal properties of the refrigerant need to be matched to the process requirements of the system and specifically the heat source and heat sink the cycle is applied to. When operating sub-critically the phase change behaviour of the refrigerant is an additional property to take into account. When operating trans-critically the critical pressure and temperature are important parameters.

As discussed in chapter 1 the present work only considers refrigerants that are classifiable as future-proof. This term is defined using hard constraints for GWP and ODP as well as soft constraints for toxicity and flammability. Refrigerant mixtures that do not meet the defined hard constraints are excluded from consideration altogether. Violating soft constraints does not disqualify a mixture outright but these are disfavoured in proposed mixtures.

The hard constraints placed on the refrigerants are a GWP of less than 150 and an ODP of approximately 0. This also in line with the most recent legislation on the topic namely the Kigali amendment to the Montreal protocol[64]. The values for the GWP and ODP of refrigerants are procured from REFPROP. An additional hard constraint on refrigerant selection is made in the form of an exclusion of synthetic refrigerants such as hydrofluoroolefins (HFOs) and hydrofluoroethers (HFEs) as well as any others that are classified as PFAS. This final hard constraint is made in acknowledgement of the health risks posed by PFAS and in anticipation of proposed restriction of their use by the European Chemicals Agency (ECA)[59, 60].

Soft constraints are placed on the toxicity and flammability of the considered refrigerants. Two systems of classifying flammability and health risk are encountered in literature discussing refrigerant safety. The first is the NFPA-704 grading system defined by the National Fire Protection Association (NFPA) to classify the flammability, reactivity and health risk posed by a material in three respective colour groups [58]. The second system is the ASHRAE 34 standard for classifying refrigerants as defined by ASHRAE [2]. As both these systems are used in literature the soft constraints will be expressed using both terminologies. Refrigerants are preferred that have a NFPA-704 grade in flammability and health of 2 or less. Alternatively, refrigerants must be classifiable as A2L or safer under the ASHRAE 34 standard. The resulting preferred refrigerant are mildly flammable at worst with health risks only under intense or chronic exposure.

It is important to note that a binary mixture of which one constituent violates a constraint does not by always result in a mixture that violates that constraint. This phenomenon was demonstrated by Fernandez et al. (2022) who expressed the flammability of a mixture in terms of the mixing ratio and demonstrated that an A3 (highly flammable) refrigerant can produce an A2L(mildly flammable) mixture if blended with the right additions[20]. They specifically showed that a mixture of the natural and flammable (A2/A3 class) refrigerants butane and pentane will, when blended with 60$\%_{mol}$ non-flammable (A1) r-125, be classified as A2L. This effect does not only apply to flammability and thus for all defined constraints the mixture's properties should be considered, not those of the constitutes. An example of this is the work by Bell at el. (2019) who investigated mixtures to replace r-134a for military applications [4]. An emphasis was placed on non- or lightly flammable refrigerant mixtures and it was demonstrated that a diverse selection of binary and tertiary mixtures, some using A2 refrigerants, can closely reproduce the performance of r-134a while being estimated as A1 class.

4.6.1. Refrigerant candidates

Refrigerants that are suitable for zeotropic VCHP cycles require high critical conditions to match the temperatures needed for drying as presented in chapter 2. Mixtures of CO_2 with n-butane and pentane were explored by Ganesan et al. (2023) and showed both mixtures had a maximum temperature glide when the CO_2 fraction was 30$\%_{mol}$ [24]. Pentane specifically shows great promise at achieving good COPs under large temperature lifts in sub-critical operation due to its high critical temperature [20, 24, 78]. Sanchez et al. (2024) explored CO_2 based mixtures with R32, R1234yf and R1270 to reduce the otherwise high pressures characteristic of pure CO_2 cycles. The results showed the largest increase to the COP (15.3%) for a 19.3$\%_{wt}$ addition of R32 [61]. Work done by Abedini et al. (2023) exploring binary refrigerant mixtures for various use-cases showed the potential of water based refrigerant mixtures for heating applications up to 200 $^{\circ}\mathrm{C}$ [1]. For one application Abedini et al. (2023) reported that the introduction of a binary zeotropic mixtures caused a 10% increase to the COP when compared to pure fluids.

One other conclusion by Abedini et al. (2023) was that most of the best performing mixtures were comprised of highly flammable hydrocarbons [1]. This finding corroborated by Fernandez et al. (2022) who reported their five best performing tertiary mixtures for each ASHRAE 34 flammability class. In class A3 the best performing mixture was a binary blend of predominantly pentane (74 $\%_{mol}$) with R1234ze(Z). In class A2L the four best performing mixtures all possessed as much pentane as possible while being classifiable as A2L [20]. These findings reaffirm the importance to apply the refrigerant constraints on the resulting mixture and not the components as otherwise such results will be overlooked. The recurring presence of pentane [1, 20, 24] in these works indicates this compound as a promising mixture component.

Given the above described works the refrigerants CO_2, Butane, Propane, Pentane and water are selected for refrigerant pair candidates. Additionally NH_3 is included as it is a refrigerant with an ODP and GWP of 0 it is within the hard constraints presented in subsection 4.6. Ammonia is additionally classified as B2L meaning it is less flammable than several hydrocarbons commonly used but does present toxicity concerns. The isomers of butane and pentane are also included as they are comparable but can present different mixing behaviour as will be demonstrated in section 5.1. other order hydrocarbons (Methane, Ethane and hexane) are also selected to be modelled as these also do not posses a GWP or ODP higher than the defined limits. The final two additions are Ethylene and Propylene to investigate the effect of a double bond in the performance of a hydrocarbon refrigerant.

5

Simple cycle modelling

This chapter presents the results of the modelling of 13 refrigerants and their mixtures in a VCHP-integrated dryer, with an inlet temperature of 180 °C and an outlet of 80 °C. The chapter first presents the modelling results, starting with the success rate of the code to contextualize the resulting proposed refrigerant mixtures. The analysis then focuses on the twenty mixtures that yielded the highest COP. The temperature-specific entropy diagram of the highest COP cycle is presented as well as the temperature-exchanged heat diagram, to demonstrate the successful glide matching. This best COP cycle is then compared to other high performance cycles on the basis of PR, P_{max} and refrigerant properties such as flammability, as specified in the preceding discussion on refrigerant selection presented in section 4.6.

5.1. Simple cycle results

The thirteen considered refrigerants presented in subsection 4.6.1 were combined into 78 refrigerant pairs. Each refrigerant pair was divided into possible compositions in steps of 2.5 $\%_{mol}$. 78 refrigerant pairs each divided into 41 possible compositions means a total of 3198 refrigerant mixtures were proposed. Every mixture was modelled within a VCHP-integrated dryer with assumptions as defined in Table 4.1 and drying conditions selected in subsection 4.2.1. The known values and applied assumptions are summarized visually in Figure 5.1.

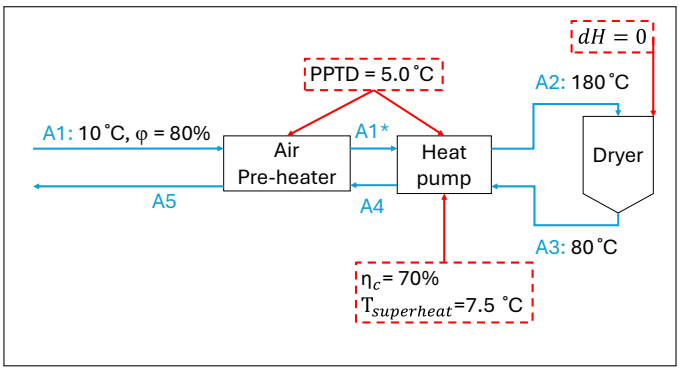

Figure 5.1: Simplified process flow diagram of a integrated heat pump dryer highlighting design assumptions using red and (humid) air state values using blue

Shown is a simplified PFD using the same air states defined in section 4.1 with known design values marked using red and (humid) air state properties marked using blue. As shown, the integrated heat pump cycle must heat ambient air at 10 °C and a φ of 80% to a temperature of 180 °C. The heat source is the humid air exiting the dryer which is defined to be at 80 °C in accordance with data from food and paper dryers [23, 42]. The model successfully calculated 1415 mixtures for a success rate of approximately 44.25%. The modelling output is categorized in a Sankey diagram given in Figure 5.2 and is available in Appendix B.1.

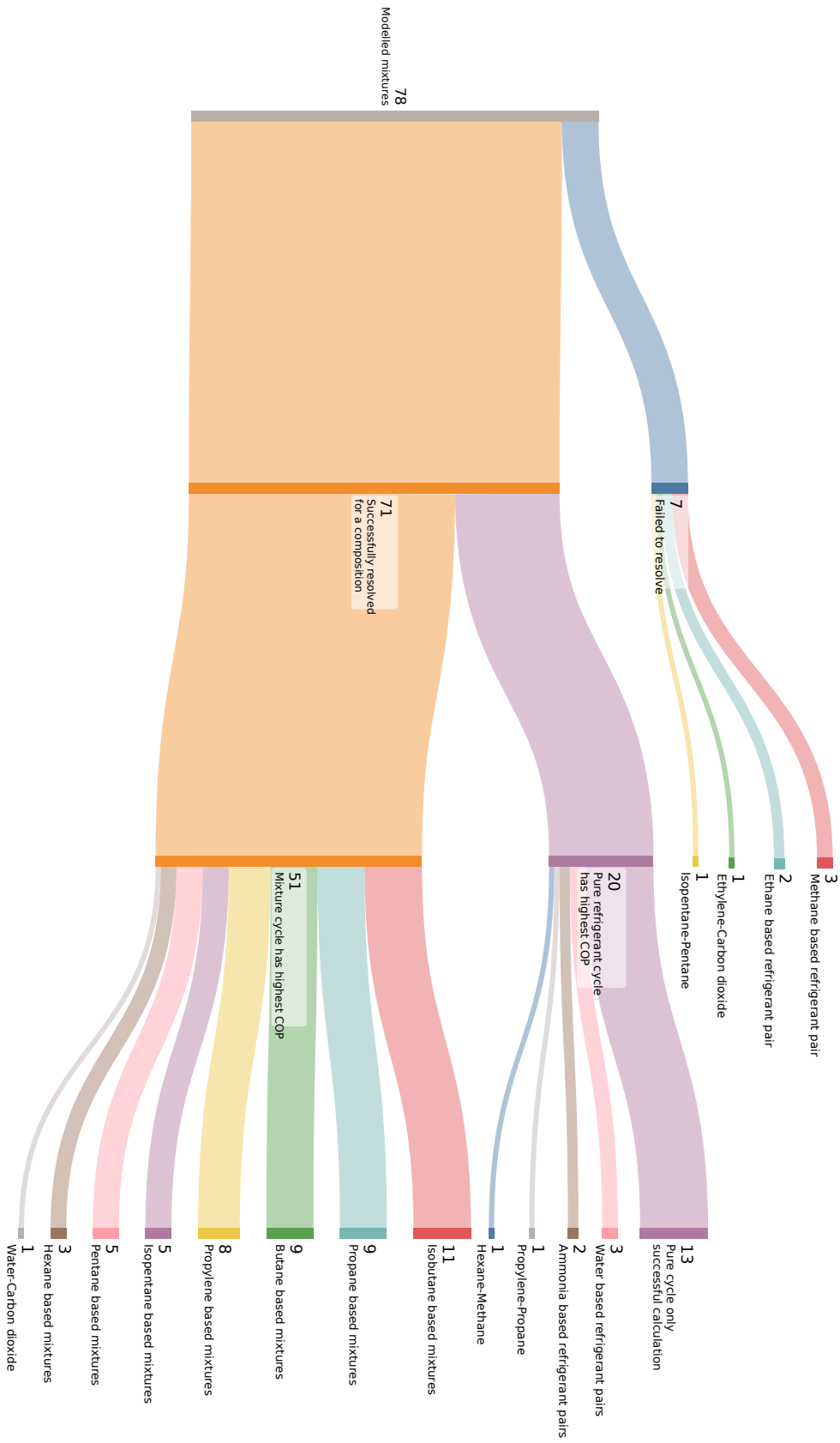

Figure 5.2: Sankey diagram classifying the modelling outputs in terms of successes and failures and further specifying primary compounds per category

Of the 78 pairs, 7 failed to resolve for any composition. The 7 unresolved pairs were mostly comprised of at least one lower-order hydrocarbon with the exception of the Pentane-Isopentane mixture. The reason Pentane-Isopentane fails to resolve is explored in section 5.2. Of the 71 refrigerant pairs modelled successfully, 20 reported no COP improvement for mixtures. Of the 20 pairs for which mixtures did not improve the COP, 13 were only successfully modelled for the pure refrigerants thus the pure refrigerant has the highest COP only by default. Of the 51 refrigerant pairs for which mixtures improved the COP, Isobutane is most often encountered as the constituent with the largest fraction in the mixture.

5.1.1. Highest COP cycle

Out of the 1415 mixtures that were successfully calculated the twenty results with the highest COP are shown in Figure 5.3.

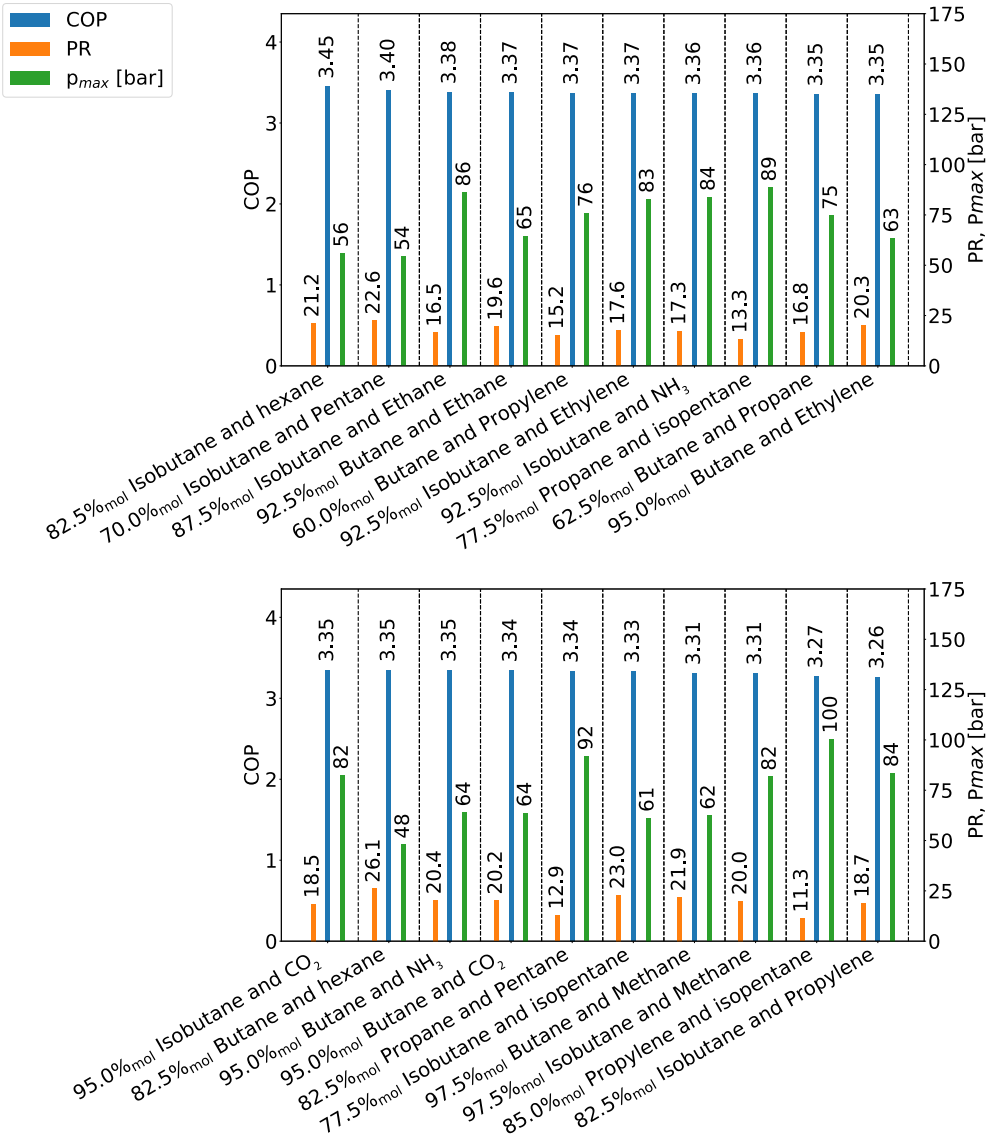

Figure 5.3: 20 mixtures with the highest calculated COP in a VCHP-integrated dryer operating between 180 and 80 °C with COP (blue), highest encountered pressure (green)and PR (orange) shown

The 20 highest calculated COPs were between 3.45 and 3.26 with the highest encountered pressures (p_{max}) between 48 and 100 bar and pressure ratio's between 11.3 and 26.1. The greatest COP was achieved by an 82.5$\%_{mol}$ Isobutane-Hexane mixture with a pressure ratio of 21.2 and a top pressure of 56 bar. The T-s and T-Q diagrams of the optimal Butane-Hexane heat pump cycle are given in Fig-

ure 5.4 and 5.5 respectively. Visible is that out of the 20 highest COP mixtures, 17 are either mostly N-Butane or Isobutane with 60$\%_{mol}$ Butane being the lowest fraction encountered for these two constituents. Given the dominant presence of the Butane isomers in the top twenty presented in Figure 5.3 as well as the total modelling output presented in Figure 5.2, there appears to be a correlation between modelling stability and mixture performance suggesting that mixtures constituents that resolve well tend to perform better.

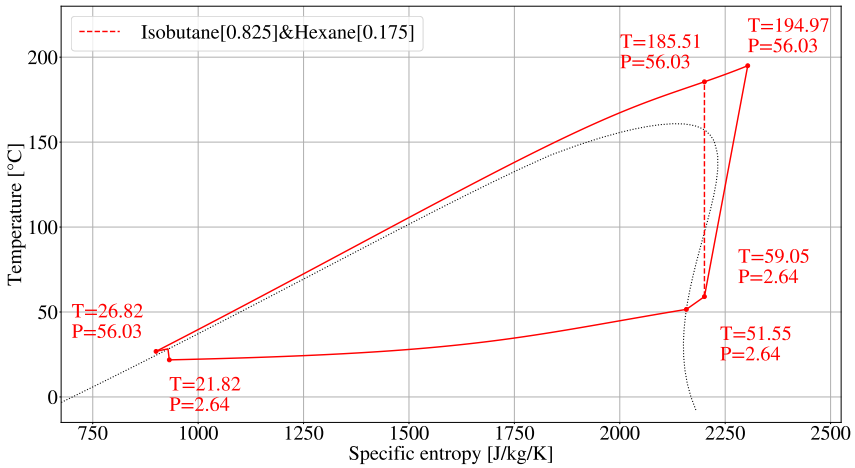

Figure 5.4: Temperature (T)-specific entropy (s) diagram showing the dryer integrated heat pump with the highest COP with states marked and interconnected in solid red and the isentropic compression marked in dashed red

Figure 5.4 shows the thermodynamic cycle of the heat pump using the same state definitions introduced in Chapter 4.4.2. Given are the five thermodynamic states, interconnected by solid red lines, as well as the isentropic compression line given by the dashed red line. This cycle is a trans-critical cycle, clearly visible by the top isobar at 56.03 bar not passing through the two-phase region. The expansion valve reduces the pressure from the condenser's operating pressure of 56.03 bar to the operating pressure of the evaporator being 2.64 bar. The glide matching introduced by the zeotropic mixture is clearly visible here as the refrigerant begins at 21.82 $^{\circ}\mathrm{C}$ in the two-phase region and ends as saturated vapour at 51.55 $^{\circ}\mathrm{C}$ at the same pressure. The superheating of the refrigerant vapour then brings the refrigerant to a temperature of 59.05 $^{\circ}\mathrm{C}$ which is the inlet condition of the compressor. Investigating the TQ-plot given in Figure 5.5 shows the heat transfer in the condenser as well as the evaporator where red depicts the refrigerant and blue the (humid) air.

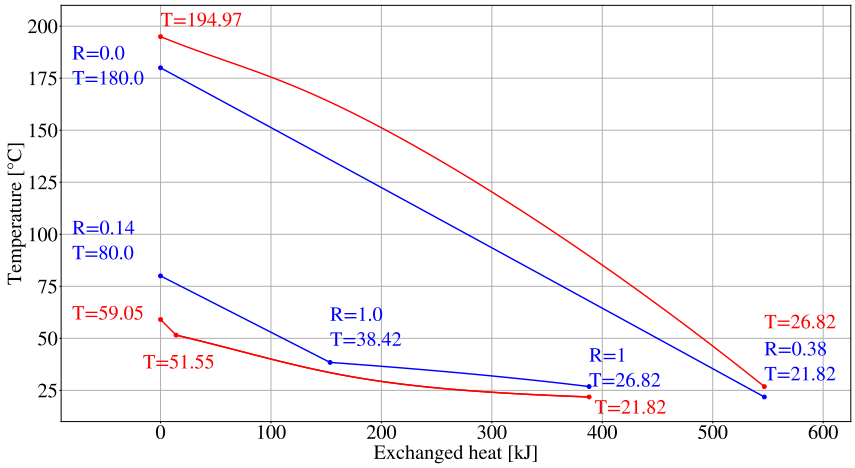

Figure 5.5: Temperature (T)-heat (Q) diagram showing the heat transfer within the evaporator and the condenser where red is the refrigerant and blue the air within the dryer integrated heat pump with the highest COP

Within the evaporator the glide matching is also visible, the red refrigerant line curving around the knee of the humid air located at the dew point. By curving around the dew point of the humid air the temperature difference can be kept much smaller than if the refrigerant had an isothermal phase transition. It is also visible that the temperature at the compressor outlet is not 185 $^{\circ}\mathrm{C}$, the minimum required value defined by the PPTD, but instead 194.97 $^{\circ}\mathrm{C}$. The additional temperature was calculated by the code and is a consequence of the refrigerant's steepening glide as it cools down causing the pinch point to be at the air's inlet with an air temperature of 21.82 $^{\circ}\mathrm{C}$ with a refrigerant temperature of 26.82 $^{\circ}\mathrm{C}$, exactly the design PPTD apart. The PPTD in the evaporator is encountered around 150 kJ of heat exchanged and is located around the knee of the humid air's heat release present at its dew point with T_{dp} equal to 38.42 $^{\circ}\mathrm{C}$. The refrigerant's glide curves around the dew point such that the temperature when exiting the two-phase region is as close to the humid air temperature as possible. Investigating the optimisation of the mixture ratio can be done by comparing the COP and exergy destruction versus the mixture ratio as is done in Figure 5.6.

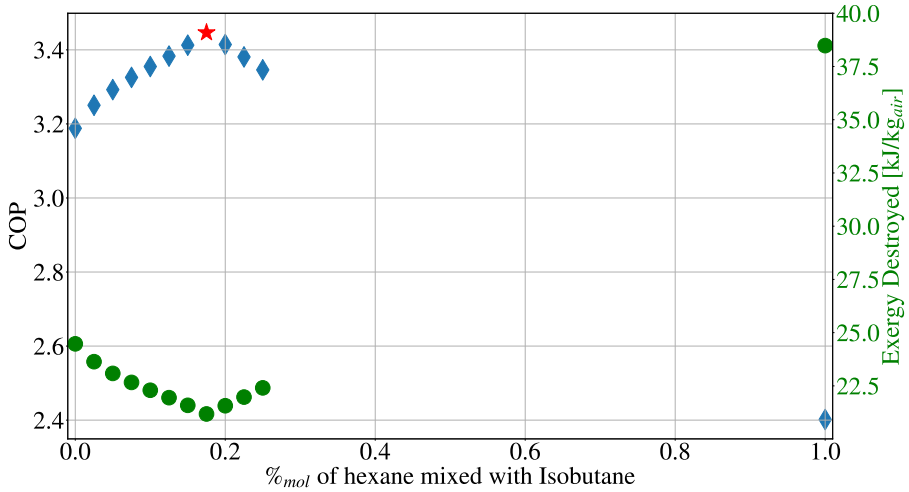

Figure 5.6: Comparison of COP (blue) and total destroyed exergy (green) of heat pump cycle using an Isobutane-Hexane mixture with highest COP marked with a red star

Figure 5.6 shows that not all mixture ratios were successfully calculated. Specifically, only 11 compositions were calculated and all those were in the range between 0 and 25$\%_{mol}$ Hexane. The sharp decrease in COP after the optimal mixture ratio of 17.5$\%_{mol}$ suggests that larger amounts of Hexane strongly negatively impact the cycle. Specifically, the deteriorating performance lies in an increase in compressor work demonstrated by the model's calculations of the PR for the optimal mixture (21.24) versus that of the last calculated refrigerant mixture, 25$\%_{mol}$ Hexane with a PR of 25.22 and the pure Hexane cycle's PR of 66.07. Also shown is the sum of exergy destroyed by each component of the calculated VCHP cycle as defined in section 3.1. The exergy destruction clearly mirrors the COP with a clear minimum reached at the optimal mixture with a value of 21.18 $\mathrm{kJ\,kg_{air}^{-1}}$. Given in Table 5.1 is the exergy destruction per component of the optimal mixture and the pure Isobutane cycle.

Table 5.1: Comparison of COP and exergy destruction (given in $\mathrm{kJ\,kg_{air}^{-1}}$) of optimal mixture cycle versus pure refrigerant cycle for heat pump integrated dryer

Refrigerant	COP	Ex$_d$ Condenser	Ex$_d$ Compressor	Ex$_d$ evaporator	Ex$_d$ Expansion valve	Total Ex$_d$
100 % Isobutane	3.19	3.95	9.47	6.67	4.38	24.47
82.5% Isobutane-Hexane	3.45	6.69	8.62	3.24	2.64	21.18

It is clear that the COP has increased, rising from 3.19 to 3.45 representing an 8.15% increase in performance. When comparing the exergy destruction the effect of glide matching in the evaporator is explicitly demonstrated as the exergy destroyed in this component has reduced from 6.67 to 3.24 $\mathrm{kJ\,kg_{air}^{-1}}$. In contrast, the exergy destroyed in the condenser has increased from 3.95 to 6.69 $\mathrm{kJ\,kg_{air}^{-1}}$,

indicating that the glide matching is worse than in the pure Isobutane cycle. A comparison between the two cycles in a T-s diagram is given in Figure 5.7 to investigate this.

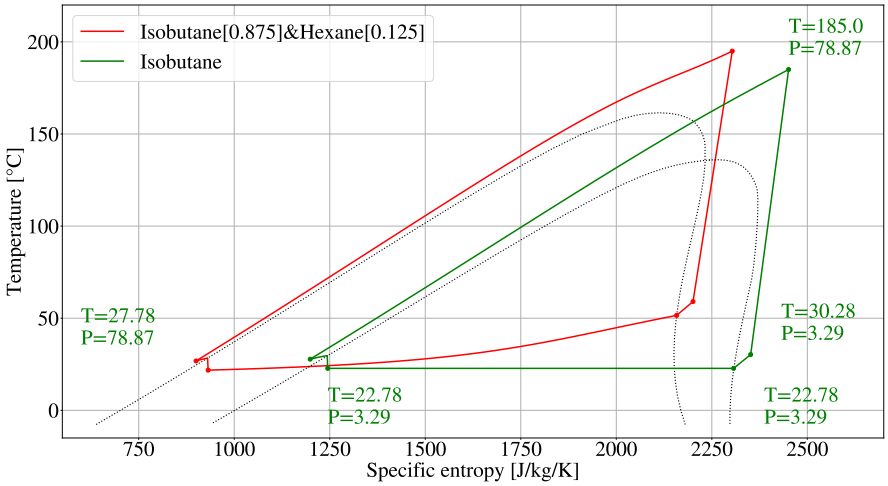

Figure 5.7: T-s diagram of optimal refrigerant mixture (red) and pure refrigerant (green) heat pump cycles

Figure 5.7 shows, in addition to the mixture cycle in red as in Figure 5.4, the pure Isobutane cycle given in green. The shape of the red and green supercritical isobars are not that notably different but the compressor outlet temperature of the mixture is equal to 194.97 °C in contrast to the 185.0 °C of the pure cycle. Both cycles are plotted within their respective two-phase regions and here the effect of glide-matching is clearly visible. The pure Isobutane enters and leaves the two-phase region at 22.78 °C, an isothermal phase change characteristic of pure refrigerants. The isothermal evaporation of pure Isobutane at 22.78 °C is in contrast to the temperature increase of the mixture experienced within the two-phase region from 21.82 to 51.55 °C. The effect of glide matching is most apparent when investigating the pure cycle T-Q diagram shown in Figure 5.8.

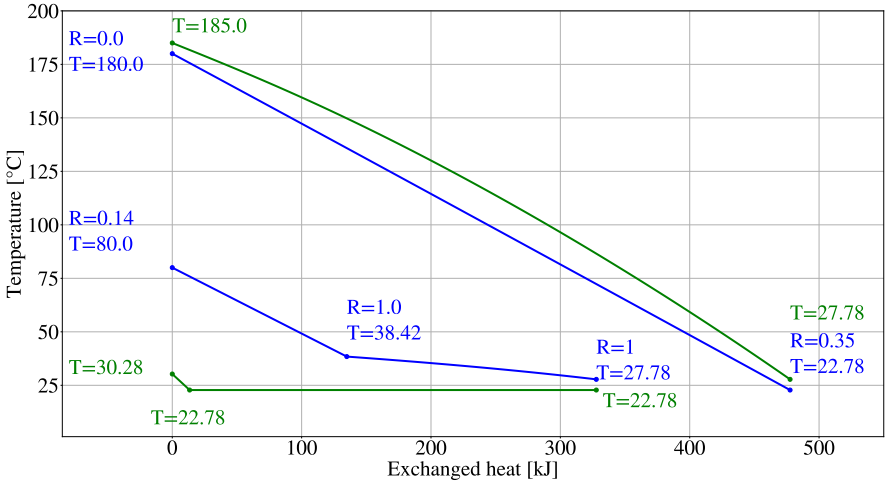

Figure 5.8: T-Q diagram of a pure Isobutane VCHP cycle showing the heat transfer within the evaporator and the condenser with refrigerant in green and (humid) air in blue

The unmatched glide within the pure Isobutane cycle's evaporator is clearly visible with the temperature difference becoming as large as 49.72 °C. In contrast to the evaporator, the pure Isobutane does maintain a smaller temperature difference than the mixture and is at exactly the design PPTD at both the in- and outlet, diverging during heat transfer to approximately 15 °C due to the pseudo-condensation

behaviour. The mixture's isobar travels closer to the saturated liquid boundary than the pure Isobutane cycle which causes the former's expansion valve to destroy less exergy as the isenthalpic expansion is nearly isentropic in the two-phase region.
Evaluating the cause for the increase in COP of the optimal mixture compared to the pure cycle is best done by its definition given in Eq. (3.1). The COP increases when $\dot{Q}_{out}$ is larger or $\dot{W}_c$ is smaller. Given that the heat output is the sum of the work done by the compressor and the heat input as stated in Eq. (4.1) the COP can also be written as

$$COP = \frac{\dot{W}_c + \dot{Q}_{in}}{\dot{W}_c} \tag{5.1}$$

and in this form it is evident that the COP increases when more heat is absorbed from the heat source for the same amount of compressor work. The heat absorbed in the pure and mixture cycles is given by the distance of the teal and red lines along the x-axis in Figures 5.8 and 5.5 respectively. The amount of heat the pure Isobutane absorbs in the evaporator is equal to 327.79 $\mathrm{kJ\,kg_r^{-1}}$. The mixture absorbs 388.09 $\mathrm{kJ\,kg_r^{-1}}$ in its evaporator meaning an 18.4% increase in absorbed heat from the humid air. Comparing the compressor work of both cycles, depicted in the TQ diagrams as the difference in distance along the x-axis of the red and green lines, values for $\dot{W}_c$ of 149.8 and 158.62 $\mathrm{kJ\,kg_r^{-1}}$ are found for the pure and mixture cycle respectively. An increase from 149.8 to 158.62 $\mathrm{kJ\,kg_r^{-1}}$ in the compressor equals an increase of 5.89%. For an increase in compressor work of 5.89%, 18.4% more heat was absorbed in the evaporator leading to an increase in COP of 8.15%. One cause for more heat being absorbed in the mixture cycle is that the pressure of the pure refrigerant evaporator had to be higher due to the PPTD placement at the inlet. If the pure Isobutane had been at the mixture evaporator pressure of 2.64 bar instead of its own 3.29 bar the amount of heat that was absorbed would have been 19.01 $\mathrm{kJ\,kg_r^{-1}}$ higher. Another reason for improved heat absorption is the significantly higher heat capacity of Hexane, equal to 143.26 $\mathrm{J\,mol^{-1}\,K^{-1}}$ at 300 $^\circ\,\mathrm{K}$, compared to that of Isobutane being 97.15 $\mathrm{J\,mol^{-1}\,K^{-1}}$.

Thus the mixture improves upon the pure refrigerant both by enabling lower operating pressures where more latent heat can be stored as well as by adding 12.5%$_{mol}$ of a compound with greater sensible heat storage. The maximum pressure of 56.03 bar is not an extreme when compared to the rest of the dataset presented in Figure 5.3 ranging from 48 and 100 bar.

5.1.2. Best performing cycle feasible with two-stage compression

The Isobutane-Hexane cycle requires a PR of 21.2 which, assuming a single-stage PR smaller than 4.6, requires a three-stage compressor. The use of a three-stage compression introduces more equipment with associated higher CapEx and more complex operation. Given the complexity and costs associated with three-stage compression cycles ,it is preferred to consider a cycle that is feasible with two-stage compression.

The cycle with the highest COP that can be expected to require only two compressor stages is the 87.5%$_{mol}$ Isobutane and Ethane mixture. The Isobutane-Ethane mixture has a PR of 16.5 and thus a single-stage PR of 4.062 if achieved using two compression stages. A single-stage PR of 4.062 is at the upper bound of a screw compressor's range for η_c equal to 70%. The Isobutane-Ethane mixture was calculated to have a COP of 3.38 and a P_{max} of 86 bar and the T-s and T-Q diagrams are given in Figures 5.9 and 5.10 respectively.

Shown in the T-s and T-Q diagram is that the glide matching of Isobutane when mixed with Ethane is convex which is in contrast with the concave glide matching achieved when mixed with Hexane. This does allow a small ΔT for significant parts of the humid air heat exchange but fails to achieve a saturated vapour temperature as high as the Hexane mixture, the latter curving around the dew point instead of plateauing beneath it. The worse glide matching of the Ethane-based mixture is also demonstrated by the exergy destruction of the cycle. The Exergy destruction per component of the Isobutane-Ethane cycle is given in Table 5.2 below.

Table 5.2: Comparison of COP and Ex$_d$ (Given in kJ per kg air) of pure Isobutane and a mixture with 12.5%$_{mol}$ Ethane

Refrigerant	COP	Ex$_d$ Condenser	Ex$_d$ Compressor	Ex$_d$ Evaporator	Ex$_d$ Expansion valve	Total Ex$_d$
100 % Isobutane	3.19	3.95	9.47	6.67	4.38	24.47
87.5% Isobutane-Ethane	3.38	4.11	8.97	4.14	4.78	21.99

The exergy destruction of the total cycle was improved from 24.47 to 21.99 meaning a 10.1% reduction, less than the 13.4% reduction achieved by the Hexane mixture. The largest reduction in destroyed exergy by the Ethane mixture was in the evaporator, showing that even imperfect glide matching still provides a major gain compared to pure refrigerants. In contrast to the Hexane mixture, the condenser's exergy destruction was barely increased and the dominant exergy destroyer of the Ethane mixture is the compressor, accounting for 40.8% of the destroyed exergy.

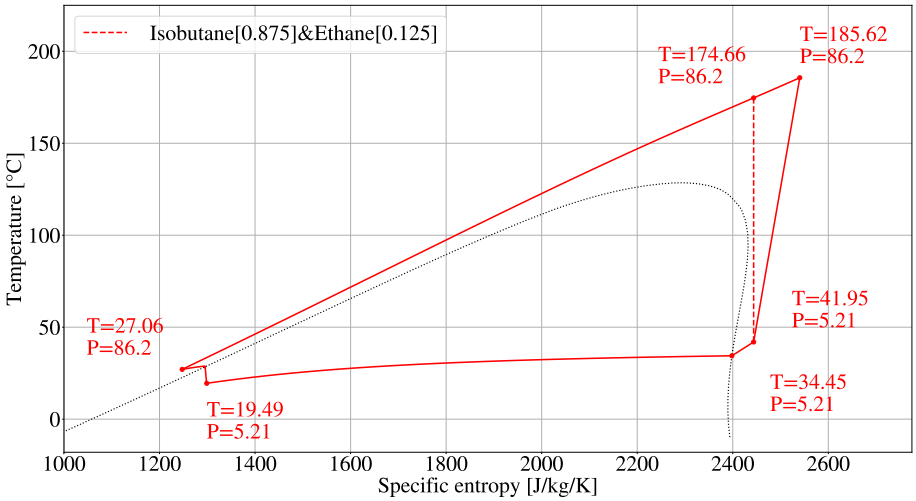

Figure 5.9: T-s diagram of highest COP cycle with two-stage compression for a dryer operating between 180 and 80 °C

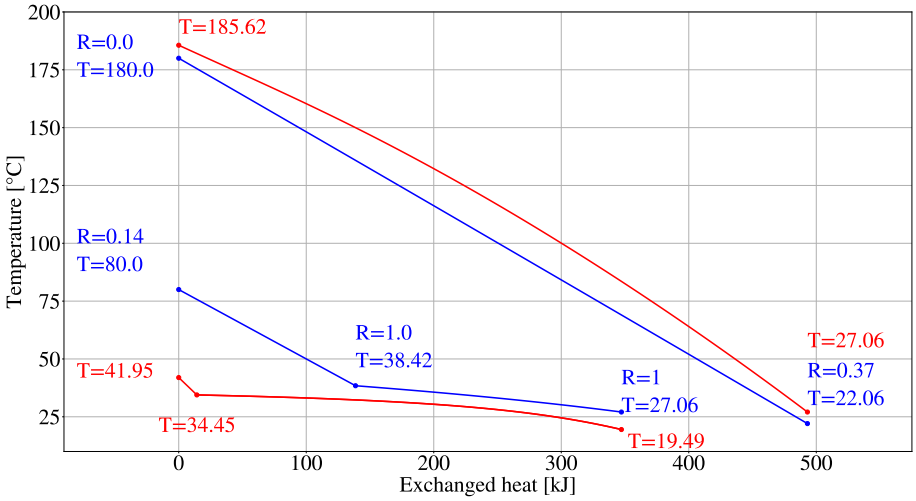

Figure 5.10: T-Q diagram of highest COP cycle with two-stage compression for a dryer operating between 180 and 80 °C with refrigerant marked in red and (Humid) air marked in blue

The larger exergy destruction of the Ethane mixture cycle's compressor is also visual in its T-s diagram in the form of the distance travelled along the x-axis during compression. Comparing Figure 5.9 to Figure 5.4, it is clear that the angle of the line between R2 and R3 is greater for the Ethane mixture. Given that the exergy destruction is directly coupled to entropy change following Eq. (3.2) this directly explains the dominant Ex_d contribution of the Ethane mixture cycle's compressor.

5.2. Effects of zeotropic mixture

51 refrigerant pairs were calculated to have the highest COP when a mixture was used. The isomers of Butane were dominantly present both in the number of successfully resolved pairs as well as in the twenty highest COPs. As stated in section 5.1, the fact that the Butane isomers both present great modelling success and performance makes these refrigerants worth studying in detail. Presented in Figure 5.11 and 5.12 are the COPs of every n-Butane and Isobutane based refrigerant pair respectively at their optimal composition.

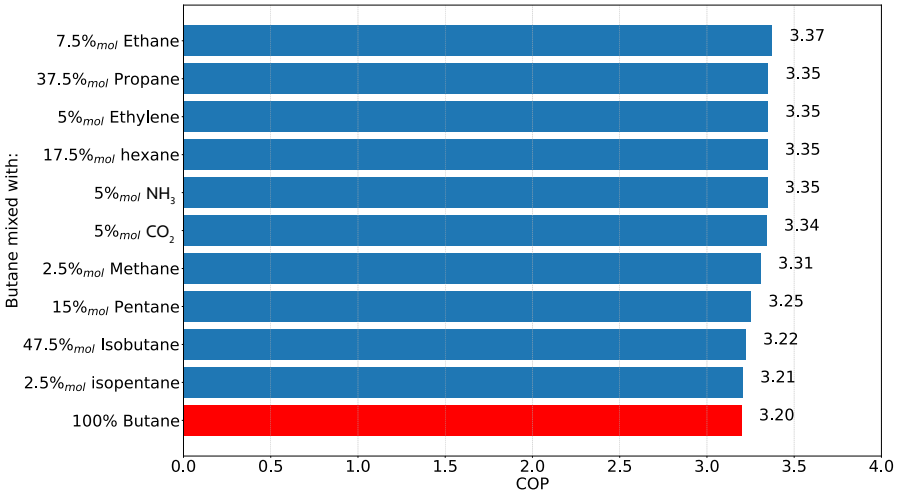

Figure 5.11: Comparison of the COP of n-Butane mixture VCHP cycles (blue) in reference to the pure Butane cycle (red)

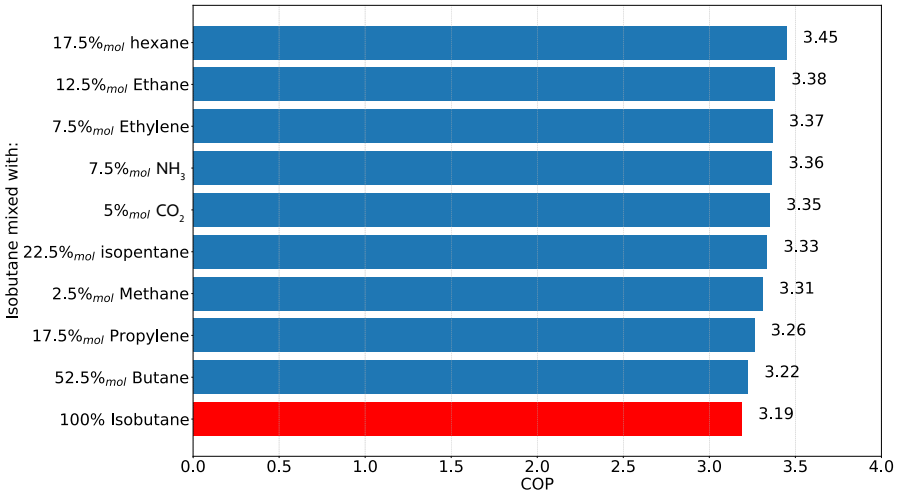

Figure 5.12: Comparison of the COP of Isobutane mixture VCHP cycles (blue) in reference to the pure Butane cycle (red)

N-Butane and Isobutane are very similar chemicals, being isomers of one another, and thus can be expected to perform similarly which, given their respective pure cycle COPs or 3.20 and 3.19, is also implied by the modelling results. However, once the two Butane isomers are mixed the behaviour does begin to vary. For example, when both isomers are proposed to be mixed with isopentane the model returns an optimal addition of 2.5 and 22.5 $\%_{mol}$ for n-Butane and Isobutane respectively with COPs of 3.21 and 3.33. The difference in results between the two compounds shows that in spite of their chemical similarity they can present different performance and mixture characteristics. To further demonstrate the difference in mixture behaviour not just at the optimal mixture composition Figure 5.13 is provided.

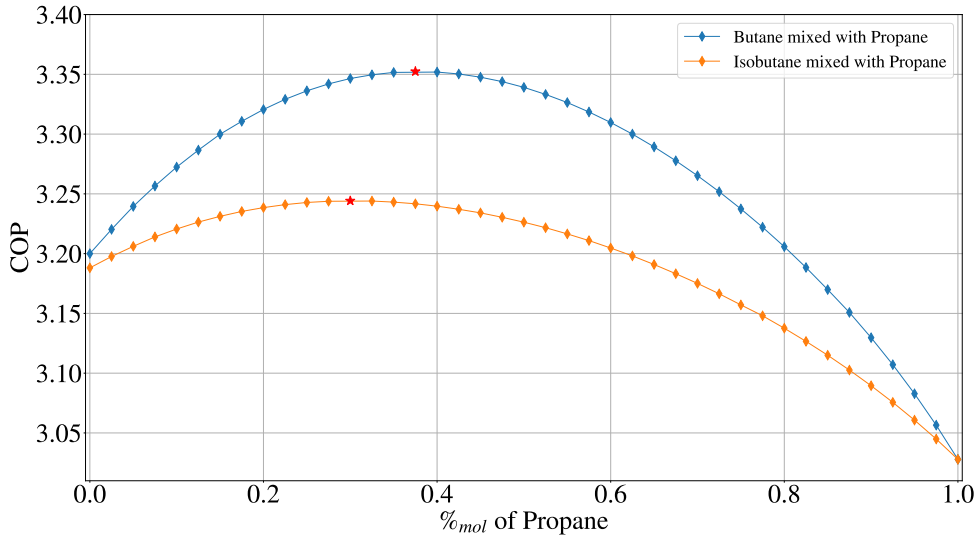

Figure 5.13: Coefficient of performance of Propane mixed with either n-Butane (orange) or Isobutane (blue) with their respective best-performing composition marked in red

Shown is the calculated COP in terms of mol percentage of Propane added to n-Butane, shown in blue, and Isobutane shown in orange with maximum cops highlighted. Clearly demonstrated in Figure 5.13 is that the response of n-Butane to an addition of Propane is very different. Both isomers have maxima that are in the region of 30 to 40$\%_{mol}$ Propane thus favouring a smaller amount of Propane. While both butanes have better performance when mixed the effect is far less pronounced for Isobutane. The maximum improvement in COP to Isobutane is 1.76% compared to 4.76% for Butane. This demonstrates that while two refrigerants can be chemically similar and have comparable pure cycle performances their behaviour within a mixture is not the same.

Evaluating probable causes for the difference in COP response reveals that while the isomers share a molecular weight and have comparable critical properties the boiling point at standard conditions is different being 272.66 and 261.4°K for n-Butane and Isobutane respectively [67, 68]. While the boiling points are not massively different from one another, the difference between boiling points of the two mixture constituents is the enabling property causing glide matching and thus is an important factor. Compared to the boiling point of Propane 231.185°K the difference with Butane is larger and thus the possible glide is larger [69]. The analysis of better performance with larger differences in boiling points holds for other examples as well. Hexane is the other compound in the best-performing Isobutane mixture and yielded the highest COP of all results and has a normal boiling point of 341.88°K [66]. As with Propane, the Butane isomer that has the largest difference in boiling point has the greatest performance enhancement, an 8.15% increase for Isobutane compared to only 4.69% for n-Butane. Thus the trend that the defining factor in mixture improvement potential is the difference in boiling points between the two mixture components.

While the improvement of COP as a consequence of zeotropic mixture use is widely encountered in the produced data, for example for the Propane mixtures shown in Figure 5.13, the opposite is also encountered. As discussed in Section 4.3, the compressor outlet temperature may require increasing beyond 185 $^{\circ}\mathrm{C}$ if either the pinch analysis of the condenser or the wet-compression avoidance in the compressor requires this. A pure refrigerant that did not violate pinch or perform wet compression may result in a mixture that does if it is blended with refrigerants that have an undesirable two-phase boundary or p_{max} isobar. The undesirable two-phase boundary can be encountered in refrigerants with a high critical temperature and when the dew line has a slop of $\mathrm{d}s/\mathrm{d}T$ as is the case for Hexane and the Pentane isomers. The two-phase boundary is the reason the Pentane-Isopentane mixture failed to resolve as was presented in Figure 5.2. The effect of an unfavourable isobar is demonstrated using Figure 5.14 where various refrigerants are mixed with NH_3, a refrigerant with an unfavourable trans-critical isobar.

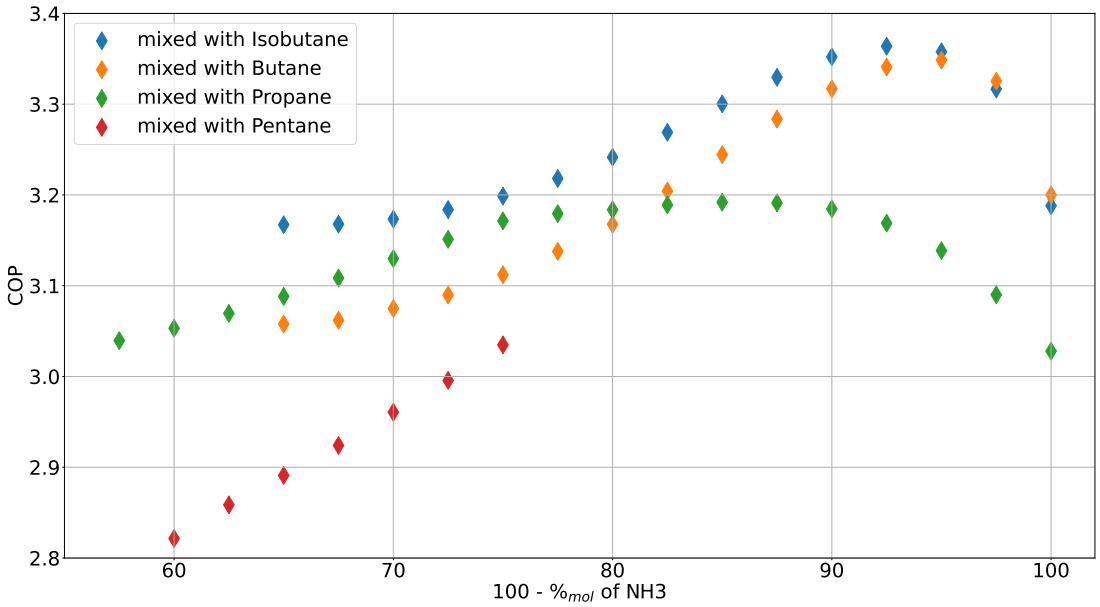

Figure 5.14: Selected coefficient of performance of Ammonia mixed with Isobutane (blue), Butane (orange), Propane (green) and Pentane (red) between 40 to 0 $\%_{mol}$ Ammonia

Shown in Figure 5.14 is the COP as a function of the fraction of several refrigerant mixtures that is not NH_3. The pure COPs, plotted on the right of the image, are all improved by small fractions of NH_3. As the fraction of NH_3 increases all four mixtures begin to experience sharp declines in COP. As a consequence of an increasing NH_3 fraction, the mixture's isobar increasingly takes on the shape of the Ammonia isobar. This isobar has an incredibly unfavourable pinch point which will be further discussed and shown in Section 6.1 but means that a pure NH_3 cycle requires a compressor outlet temperature of 311.97 $^{\circ}\mathrm{C}$ as to not violate the PPTD.

Upon the introduction of approximately 10$\%_{mol}$ NH_3 or more, the Ammonia mixtures start requiring higher outlet temperatures and consequently higher outlet pressures as well. For example, when examining the Isobutane-Ammonia data, the exit temperature of the compressor is 185 $^{\circ}\mathrm{C}$ for 0$\%_{mol}$ Ammonia and 196.63 $^{\circ}\mathrm{C}$ at 35$\%_{mol}$ Ammonia. This temperature makes for elevated pressures which in turn requires greater amounts of work from the compressor which reduces the COP. The same cause can be found when investigating the Butane, Pentane and Propane mixture cycles. While the steepest drop is caused in the pentane mixture, all mixtures have increasing compressor outlet temperatures and decreasing cycle COPs for past a certain critical fraction of Ammonia. The highest value for T_{R3} between the mixture cycles is 214.79 $^{\circ}\mathrm{C}$ for a 40$\%_{mol}$ Ammonia fraction with Pentane which is also the lowest COP at 2.82.

6

Simple cycle temperature sensitivity study

This chapter presents an investigation of the effect of the in- and outlet temperature of the drying section on the performance of the integrated VCHP cycle. It especially highlights whether the improvements of zeotropic mixtures are more or less pronounced in reference to the baseline results presented in Chapter 5. An additional inlet temperature of 50 $^{\circ}\mathrm{C}$ is considered and the outlet temperature is also calculated at 120 $^{\circ}\mathrm{C}$, representing a different segment of the drying industry. The additional in- and outlet temperatures modelled mean that in, addition to the case presented in Chapter 5, three additional dryer conditions are calculated and evaluated in reference to the original conditions. Operating conditions which produce cycles with non- or lightly flammable refrigerants are given specific attention.

6.1. Effect of reduced dryer outlet temperature

The outlet temperature of 80 $^{\circ}\mathrm{C}$ was selected as it was encountered both in the drying industry, as presented by Laurijssen (2013), and in the food industry, as reported by FrieslandCampina (2024) [23, 42]. Given the modeling of the dryer as adiabatic and isenthalpic and following the Mollier diagram shown in Figure 2.3, different temperatures along the isenthalp are possible and will lead to different humidities and thus different temperature glides. Different temperature glides might cause the effects of mixtures to become more or less pronounced or may cause different mixtures to present with the highest COP.

Reducing the dryer outlet temperature means a larger amount of the heat is now stored as latent heat. As was observed in Figure 4.5, a higher relative humidity means that the temperature difference between the T_{A3} and T_{dp} is smaller and the glide is flatter. The same 3198 refrigerant mixtures that were proposed in Chapter 5 were calculated for 50 $^{\circ}\mathrm{C}$. The modeling output remains consistent in successfully resolved pairs with 71 successful and 7 failed mixture pairs as was the case for the 80 $^{\circ}\mathrm{C}$ outlet temperature and is again sorted and presented in a Sankey diagram given in Figure 6.1 with the data available in Appendix B.2. The modelling stability was improved slightly, with an increase in successfully calculated cycles from 44.25% to 47.25% which equates to 1511 successfully calculations.

In comparison to the 80 $^{\circ}\mathrm{C}$ outlet, the same seven mixture pairs fail to resolve indicating that the condenser and not the evaporator condition is a determining factor in this. The mixtures that successfully improved COP are now even more dominated by the Butane isomers, now making up 21 of the 50 successful mixtures. Ammonia no longer presents in the category ”Pure refrigerant cycle has highest COP” and is now successfully presenting in pairs that improve the COP with two predominantly NH_3 mixtures now being calculated as optimal.

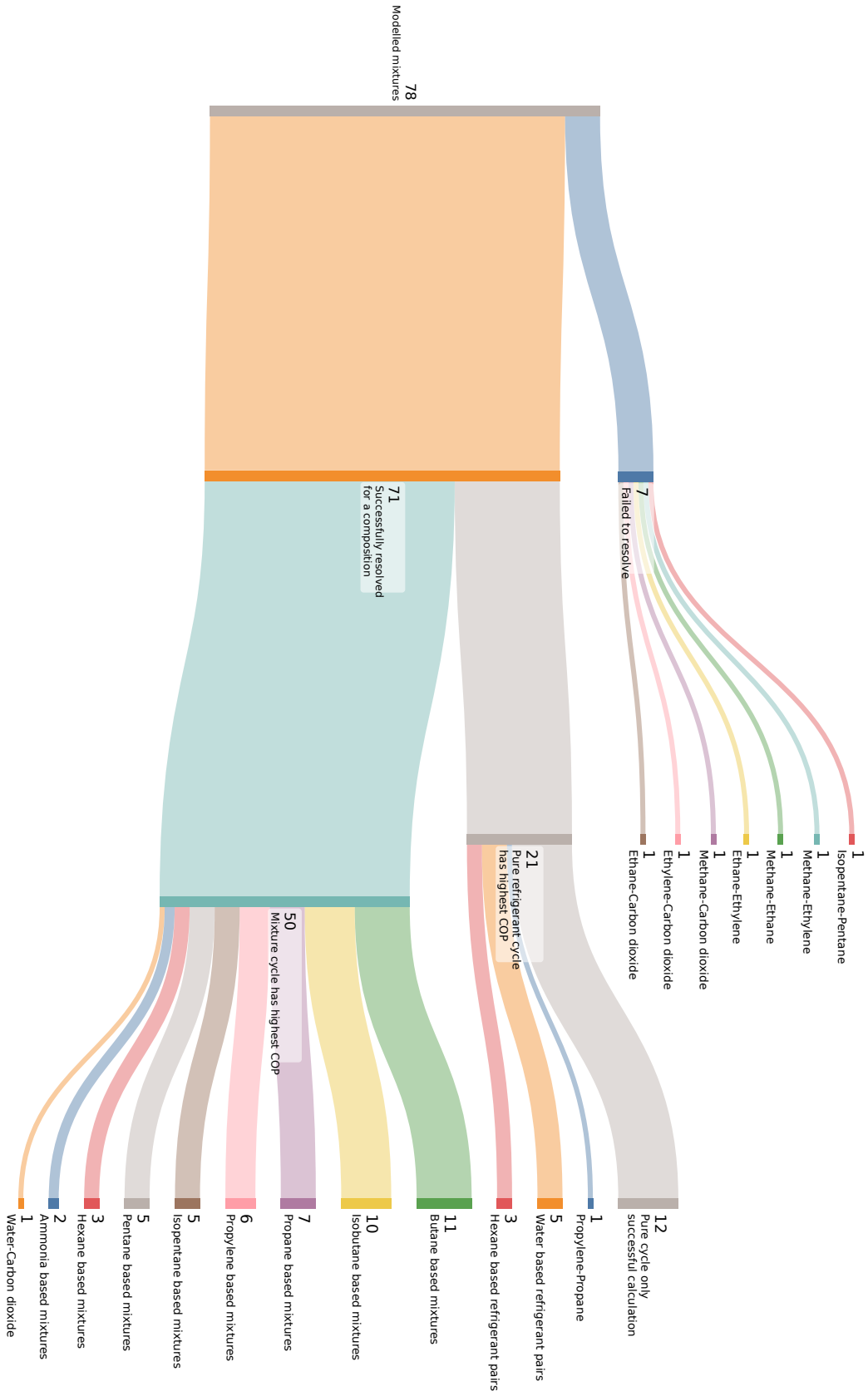

Figure 6.1: Sankey diagram classifying the modelling outputs in terms of successes and failures and further specifying primary compounds per category for reduced T_{A3}

The 20 mixtures with the highest COPs are given in Figure 6.2 with the cycle's PR and p_{max}.

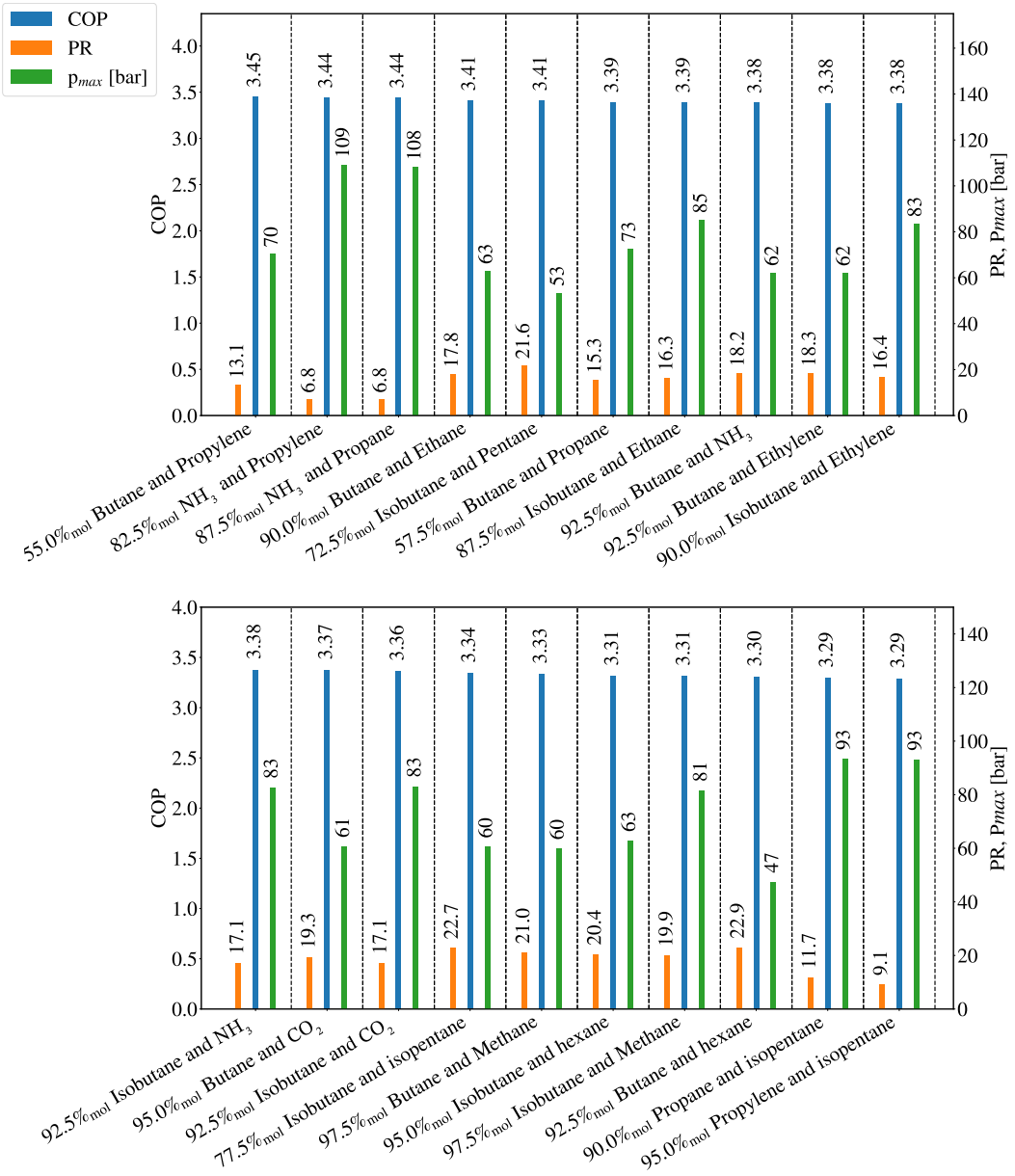

Figure 6.2: 20 mixtures with the highest calculated COP in a VCHP-integrated dryer operating between 180 and 50 °C with COP (blue), highest encountered pressure (green)and PR (orange) shown

Lowering the dryer's outlet temperature has not affected the highest achieved COP, although the mixture that achieved this COP has changed. Instead of 82.5% Isobutane-Hexane now the top performing mixture is 55% Butane-Propylene. It is also important that while Butane and Isobutane are still extremely dominantly present in the top 20, their presence has reduced to 16 out of 20 top mixtures with two predominantly Ammonia cycles now also present. The cycles generally present with comparable COPs and p_{max} to the 80 °C outlet but with notably reduced PR's, ranging from 6.8 to 22.9 compared to the original range of 11.3 to 26.1. This is also represented by the fact that the top 3 cycles are feasible with two-stage compression whereas three-stage compression was required for the 80 °C outlet. Given that Isobutane and Butane cycles were already explored in Chapter 5 and that Ammonia-based mixtures are interesting as Ammonia is classified as B2L meaning that while toxic, it has a low flammability index and thus provides an additional factor of interest. The Ammonia-Propane mixture has the highest fraction of Ammonia, its T-s diagram and T-Q diagram are given in Figures 6.3 and 6.4.

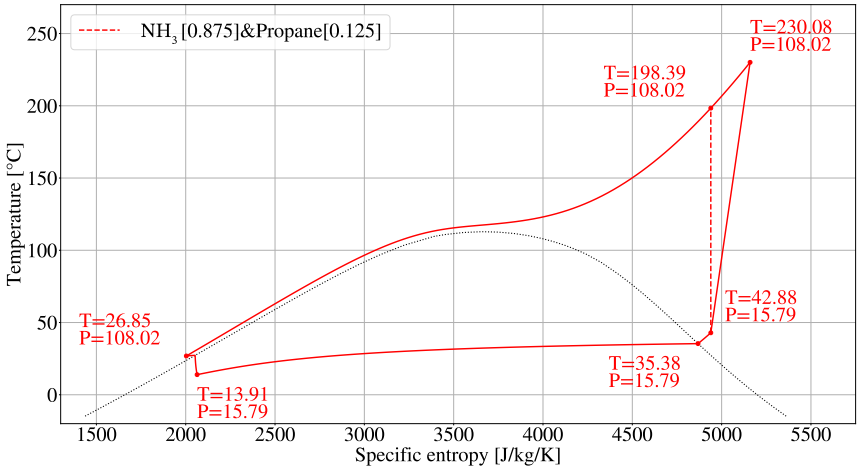

Figure 6.3: T-s diagram of Ammonia-based mixture optimised with an inlet of 180 °C and outlet of 50 °C

Shown in the T-s diagram given in Figure 6.3 is that the cycle is trans-critical, requiring a pressure of 108.02 bar in the condenser. The pressure level after the expansion valve is also elevated at 15.79 bar and thus while pressure levels are significantly elevated the PR is only 6.84. The COP of the mixture cycle is 3.44 compared to the pure NH_3 cycle COP of 3.09 representing an 11.33% increase, larger than the 8.15% increase for the top mixture with T_{A3} equal to 80°C. The compression line and the two-phase boundary move away from one another meaning that no risk of droplet formation will be present. Evaluating the temperatures it is immediately apparent that the temperature at the compressor outlet, T_{R3}, is far beyond the required PPTD. The T-Q diagram of the cycle, given in Figure 6.4, shows that this is due to the pinch point located before the start of pseudo-condensation around 400 $\frac{kJ}{kg_R}$ of exchanged heat.

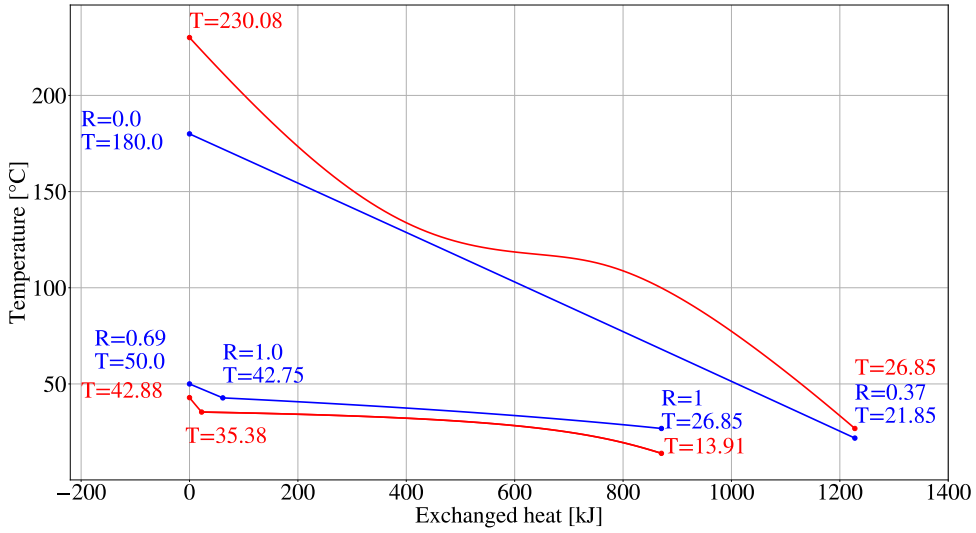

Figure 6.4: T-Q diagram of Ammonia-based mixture optimised with an inlet of 180 °C and outlet of 50 °C

As was also discussed in Section 5.2, the unfavourable trans-critical isobar of NH_3 affects the value of T_{R3} heavily. An unfortunate additional effect of the isobar shape is that the pinch point is now encountered within the HEX instead of at the in- or outlet. A pinch point within the HEX is the most undesired place as there is then no recourse but to heat through it and may mean greater PPTDs must be considered. An example of the effect an increased PPTD would have is available in appendix C and for the NH_3-Propane mixture the COP is reduced from 3.44 to 3.21 when the PPTD is doubled.

6.2. Effect of reduced inlet temperature

As presented in Chapter 2, the drying industry is heterogeneous in terms of process conditions both between and within industrial sectors. The highest feasible temperature required for drying was 180 $^{\circ}\mathrm{C}$ and was classified as being in the very high temperature drying regime.

It is valuable to investigate how well VCHPs integrate with lower temperature drying regimes to determine if zeotropic mixtures have added value across the entire drying industry. Specifically, it is interesting to determine if the performance improvement of zeotropic mixtures is more or less pronounced than for the very high temperature drying regime. The high temperature drying regime is one regime lower than the case presented in Chapter 5 and was defined as having a T_{db} between 100 and 150 $^{\circ}\mathrm{C}$. An intermediate temperature within this range of 120 $^{\circ}\mathrm{C}$ is selected, representative of air used in multi-cylinder drying and the high temperature drying of solid food products such as corn as described in sections 2.2.1 and 2.2.2 respectively.

Shown in Figure 6.5 is the sorted output of the model applied to the lower drying temperature, given in a Sankey diagram with the data available in Appendix B.3. Reducing the inlet temperature to 120 $^{\circ}\mathrm{C}$ Decreased the number of mixtures that did not resolve from 7 to 4 with Water, Isopentane and Pentane mixed with one another as well as Methane-Ethylene being the refrigerant pairs that failed to resolve. Compared to the higher inlet temperature, lower-order hydrocarbon mixtures now resolve much better and are found to be generally more suited to the lower temperature heat sinks. The failure to resolve the Pentane isomers is consistent between calculations and the addition of the water cycle is a consequence of the air-to-air HEX, with T_{A3} being lower than T_{A1} plus the PPTD making the component unfeasible. If the Air-to-air HEX is removed from the model the water cycle resolves successfully.

The successful resolution rate has increased only a little, from 1415 to 1424 for a success rate of 44.53%. The increases in resolved refrigerant pairs combined with the near-constant success rate implies that while more refrigerant pairs are possible, fewer combinations within a pair are feasible. The presence of the Butane isomers in the successful mixtures has reduced compared to the 180 $^{\circ}\mathrm{C}$ inlet condition and a more diverse result set has been produced.

The reduction in inlet temperature with a constant outlet temperature effectively means a larger amount of waste heat will be sensible and thus a steeper glide will be encountered in the evaporator. The much steeper glide encountered in these operating conditions means that a very different severity of glide matching is required. The different glide requirement is most clearly reflected in the mixtures that do not improve the COP. Compared to the 180 $^{\circ}\mathrm{C}$ inlet, all mixtures that do not improve the COP are now different, with the exception of Propylene-Propane. As was demonstrated in Section 5.2, a determining factor in glide matching is the difference in boiling points. For a lower inlet temperature, with a majority of heat in the evaporator available as sensible heat, A steep glide matching is needed thus requiring large differences in the boiling point of the mixture constituents. The mixtures that do not improve the COP are predominantly Ethane and CO_2 based, two refrigerants with very low boiling points, -89 and -78.46 $^{\circ}\mathrm{C}$ respectively. The refrigerant that Ethane and CO_2 do not improve when mixed with are either very close in boiling point, thus not providing the glide match needed by this drying condition, or the other constituent caused an elevated compressor outlet temperature as was also shown for select refrigerants in Section 5.2.

31 out of 51 successful mixtures were either mainly a Butane isomer or Propane and its alkene. These four most often encountered refrigerants posses boiling points at the mean of the 13 proposed refrigerants. The only refrigerant at the boiling point mean that isn't a common dominant constituents is NH_3, likely caused by its unfavourable trans-critical behaviour. The propensity for the model to return mixtures with a large amount of a refrigerant with a mean boiling point mixed with a small amount of a refrigerant with an extreme boiling point is a valuable insight into how glides can be constructed in zeotropic VCHP cycles.

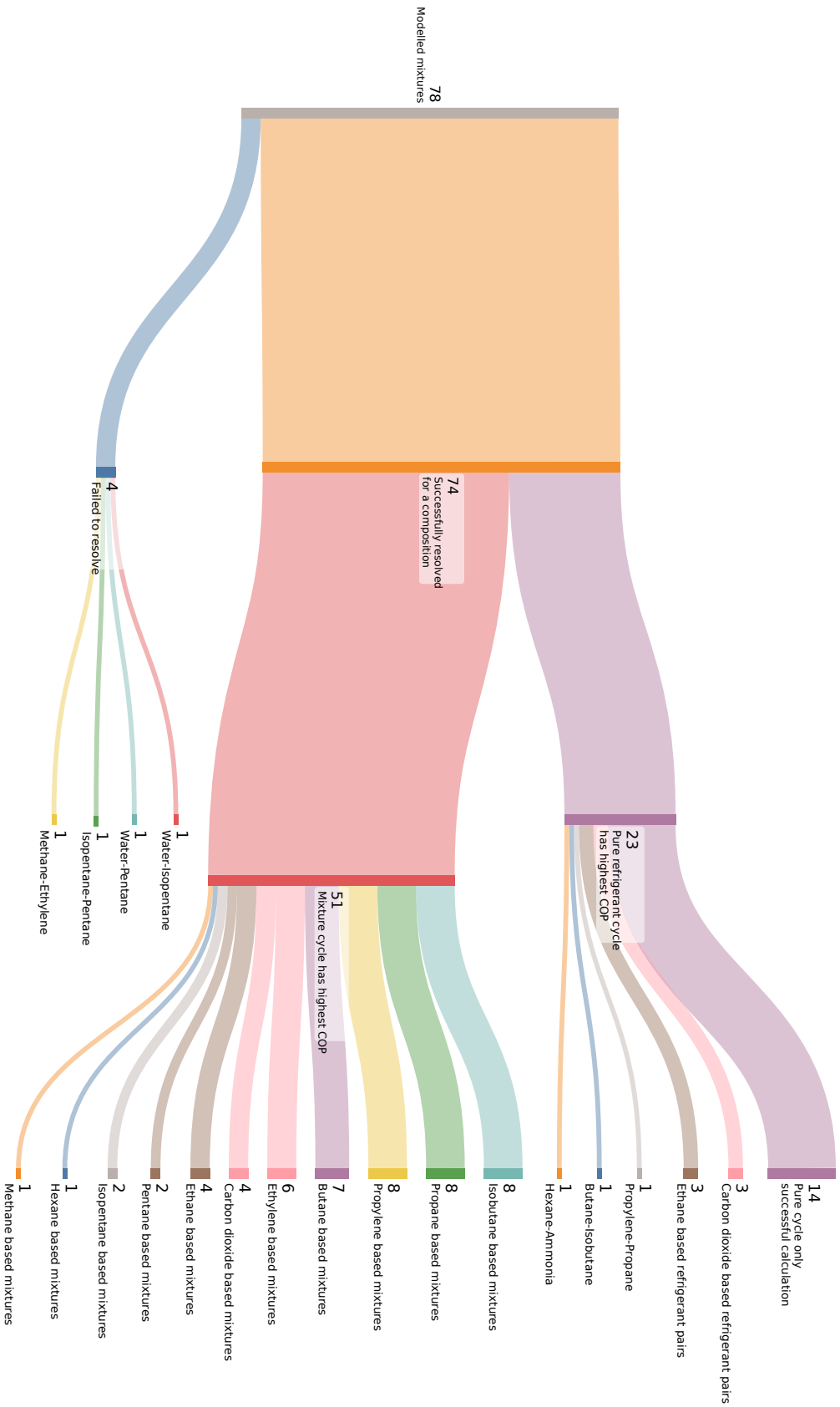

Figure 6.5: Sankey diagram classifying the modelling outputs in terms of successes and failures and further specifying primary compounds per category

Evaluating the 20 mixtures with the highest COP as given in Figure 6.6 shows that for this drying regime, the Butane isomers are no longer the dominantly present in the top performing mixtures.

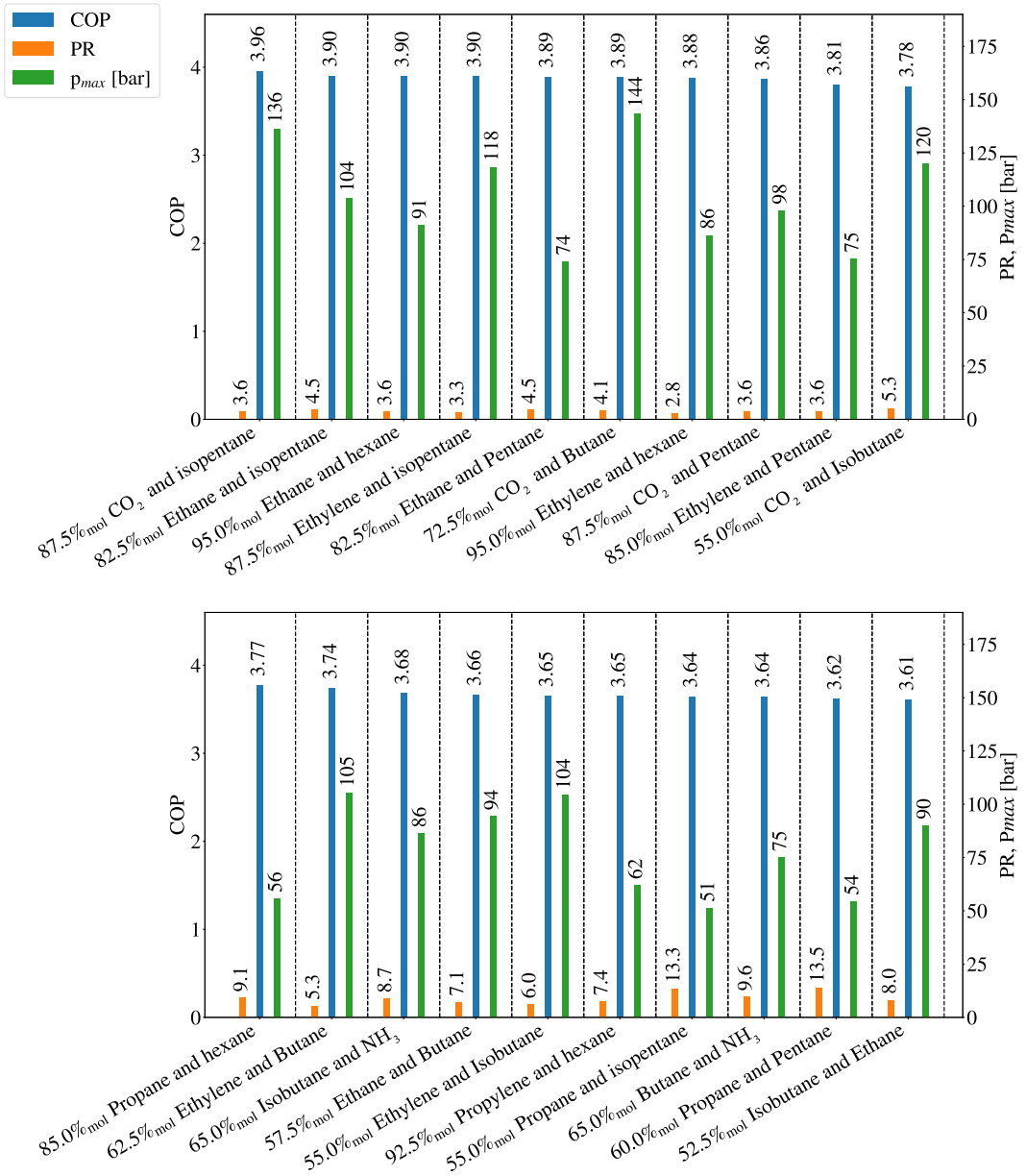

Figure 6.6: 20 refrigerant mixtures with the highest calculated COP for a dryer operating between 120 and 80 °C with COP, PR and p_{max} reported in blue, orange and green respectively

It is immediately striking that the calculated PRs now range between 2.5 and 13.5 which is a significant reduction compared to T_{R3} equal to 180 °C and is fully feasible with two-stage compression. Additionally, PRs below 4.0 can even be expected to be achieved by single compressor stages. As was the case for the 180 °C inlet, when PRs are lower the p_{max} is higher and indeed higher pressures are encountered in Figure 6.6, ranging from 144 to 51 bar.

The three most encountered mixture bases are CO_2, Ethane and Ethylene. Of the three base compounds CO_2 performs with the highest COP when mixed with 12.5%$_{mol}$ Isopentane yielding a COP of 3.96 with a PR of 3.6 and a p_{max} of 136 bar. CO_2 is a highly desirable mixture base as it is classified as A1 being a non-flammable and non-toxic compound. The top 20 results have COPs between 3.96 and 3.61, notably higher than the 180 °C results.

Given the advantageous refrigerant properties of CO_2, feasible single-stage compression and the highest calculated COP, the CO_2-Isopentane cycle is further explored using the T-s and T-Q diagrams given in Figures 6.7 and 6.8 respectively.

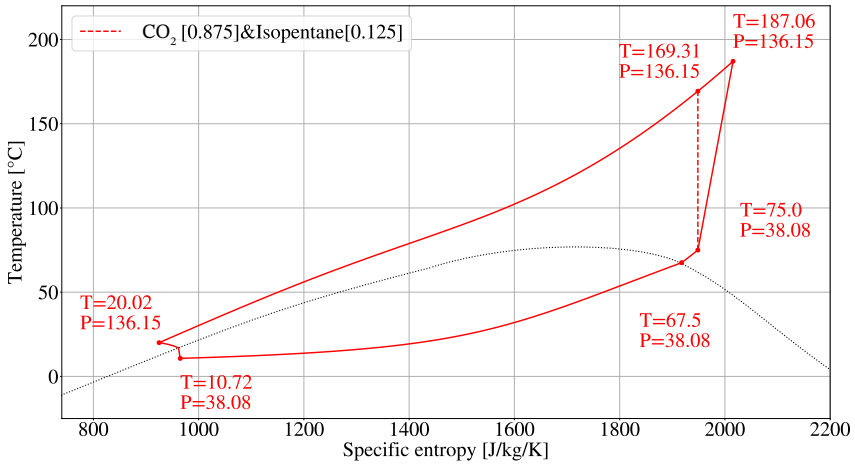

Figure 6.7: Temperature (T)-specific entropy(s) diagram depicting the best-performing cycle calculated for a dryer operating between 120 and 80 °C with refrigerant states marked and interconnected in solid red and isentropic compression shown using dashed red

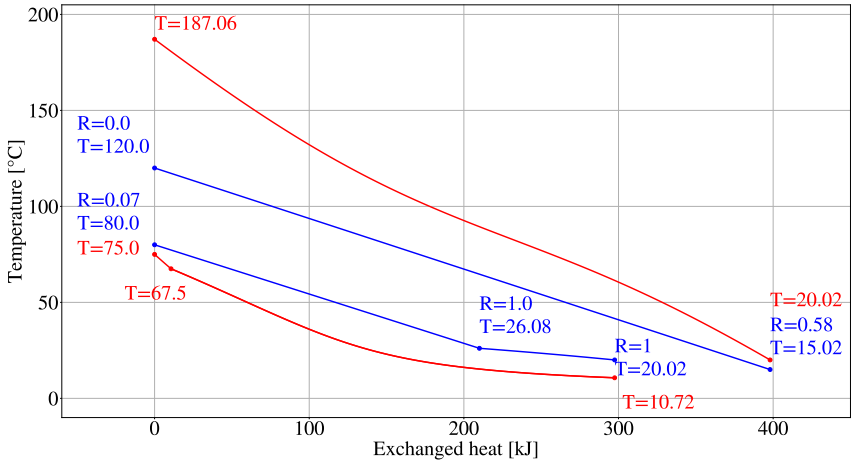

Figure 6.8: Temperature (T)-exchanged heat(Q) diagram depicting the best-performing cycle calculated for a dryer operating between 120 and 80 °C with refrigerant shown in red and (humid) air in blue

Visible in both the T-s and T-Q diagram is the severe glide matching performed by the mixture. The CO_2-Isopentane mixture enters the two-phase region at a temperature of 10.72 °C and exits at a temperature of 67.50 °C meaning a temperature increase of 56.78 °C during the evaporation which occurs at 38.08 bar. As expected, a steep glide is required to match that of the humid air dryer outlet, shown in Figure 6.8, exiting the dryer at the specified temperature of 80 °C with a φ of only 7%. Shown in Figure 6.8 is a temperature difference between T_{A3} and T_{dp}, the steep part of the glide, of 53.92 °C with sensible heat accounting for 70.60% of the 297.5 $\mathrm{kJ/kg_R}$ of exchanged heat.

Evaluating the temperatures in the condenser, the outlet temperature of the compressor is 187.06 °C, higher than what would be required by the minimum PPTD though not by much. The elevated value for T_{R3} is the consequence of the mixture's trans-critical isobar and specifically the fact that the heat capacity before pseudo-condensation is lower than after. The average heat capacity of the refrigerant mixture is 1.817$\mathrm{kJ/(kg_R\,K)}$ during the first 100 kJ of heat exchange, 2.538$\mathrm{kJ/(kg_R\,K)}$ during the second

100 kJ and 2.727$\mathrm{kJ}/(\mathrm{kg_R\ K})$ during the heat exchange beyond 200 kJ. Due to the lower heat capacity before pseudo-condensation, the temperature diverges in this region leading to the large compressor outlet temperature. The Pinch point in the condenser is encountered at the outlet where the refrigerant is exactly the PPTD above the incoming pre-heated ambient air at 15.02 $^\circ\mathrm{C}$.

The pinch point in the evaporator is located at the outlet and is thus the temperature of the superheated refrigerant T_{R2}. The heat capacity in the superheated region is significantly smaller as there is no longer any latent heat storage upon exiting the two-phase region. The lack of latent heat storage causes the glide in the initial 10.6 kJ of heat exchange to diverge from the humid air profile which carries through the entire heat exchange. The early divergence means that after the dew point, even though the glides are nearly perfectly parallel, the temperature difference remains 9.3 $^\circ\mathrm{C}$.

The optimal CO_2-Isopentane mixture was calculated to have a COP of 3.96. Comparing the COP of the optimal composition to the other calculated compositions can be done using Figure 6.9, giving the COP and exergy destroyed per kilogram of air.

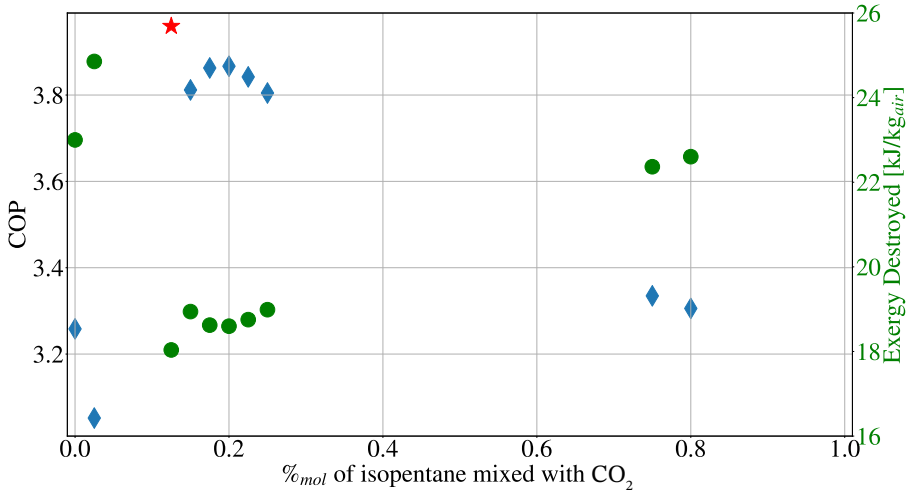

Figure 6.9: Calculated COP and Ex_d of VCHP cycles using CO_2-Isopentane integrated in a dryer operating between 120 and 80 $^\circ\mathrm{C}$

It is immediately apparent that the mixture presented with modelling instabilities at certain compositions, as only 10 out of 41 proposed compositions were calculated. The COP is not improved at all composition, compared to a pure CO_2 cycle with a COP of 3.26 an addition of only 2.5%$_{mol}$ Isopentane causes a drop in COP to a value of 3.05, a 6.44% decrease. As was observed for Ammonia mixtures presented in Figure 5.14, sudden drops in COP can be the result of increased compressor outlet temperatures as a consequence of wet compression avoidance or PPTD adherence. Investigating the value of T_{R3} for the pure both compositions reveals it has increased from 152.84 to 180.03 $^\circ\mathrm{C}$ upon the 2.5%$_{mol}$ Isopentane addition to the CO_2 cycle. It is important to note that while an increase in T_{R3} can cause a drop in COP it is not guaranteed as the optimal composition presents with the highest value for T_{R3} of all with 189.75 $^\circ\mathrm{C}$. The optimal cycle demonstrates that an elevated T_{R3}, while a possible cause, is only one factor affecting COP and it should not be extrapolated as an assured indicator of cycle performance. Furthermore, it is also important to compare the CO_2-Isopentane response to mixture fraction to that of more well-behaved examples like those given in Figure 5.13 for Propane mixed with Butane and Isobutane. It should be explicitly noted, as demonstrated by the CO_2-Isopentane mixture, that not every mixture presents as a gradual and consistent dome-shaped improvement towards an optimal COP at a given fraction. Figure 6.9 demonstrates the unpredictability and multi-variable dependence of a VCHP cycle's response to a mixture.

The COP of 3.96 for the optimal fraction is an improvement of 21.47% when compared to the pure CO_2 cycle with a COP of 3.26. An improvement of 21.47% on the pure cycle COP is far greater than the 8.15% increase calculated in Chapter 5 and the 11.33% increase calculated in Section 6.1, showing that indeed the COP improvement caused by zeotropic mixture use varies per drying regime.

6.3. Effect of reducing inlet and outlet temperature

As was done for the very high temperature drying regime, It is valuable to investigate whether a larger amount of heat available as latent heat affects the performance of the VCHP-integrated dryers as well as the relative improvement caused by zeotropic mixture introduction. To investigate how a larger latent heat fraction affects the VCHPs the drying condition with the reduced inlet of 120 $^{\circ}\mathrm{C}$ is combined with the reduced outlet of 50 $^{\circ}\mathrm{C}$. The same 3198 mixtures were calculated and resulted in the highest success rate thus far with 1668 successfully calculated cycles accounting for 52.16% of proposed mixtures. The sorted modelling output is given in Figure 6.11 with the data available in Appendix B.4.

The sorted modelling output shows that the number of failed mixture pairs has reduced to 1 with only Methane-Ethylene still failing to resolve at least once. It is no coincidence that Methane and Ethylene are the two refrigerants with the lowest boiling points of the thirteen considered refrigerants. Given the boiling points of the rejected mixture pair it follows that while these refrigerant can make good additions to other, higher boiling point having, refrigerants neither makes a good dominant constituent.

The number of refrigerant pairs wherefore a pure cycle is calculated to be the best is higher than for any other drying condition with 15 (subtracting highest by default results) pairs having the highest COP for a pure refrigerant. Hexane mixtures account for a third of refrigerant pairs that were calculated to be unimproved by zeotropic mixture introduction. Hexane-based mixtures with low boiling point partners like Propane, Ammonia, Methane etc. would be expected to perform well as Hexane has a high boiling point allowing for a large range of glide matching. However, low boiling point mixture partners are fully rejected by the model for Hexane due to its saturated vapour border as visible in the T-s diagram of Hexane's two-phase region given in Figure 6.10.

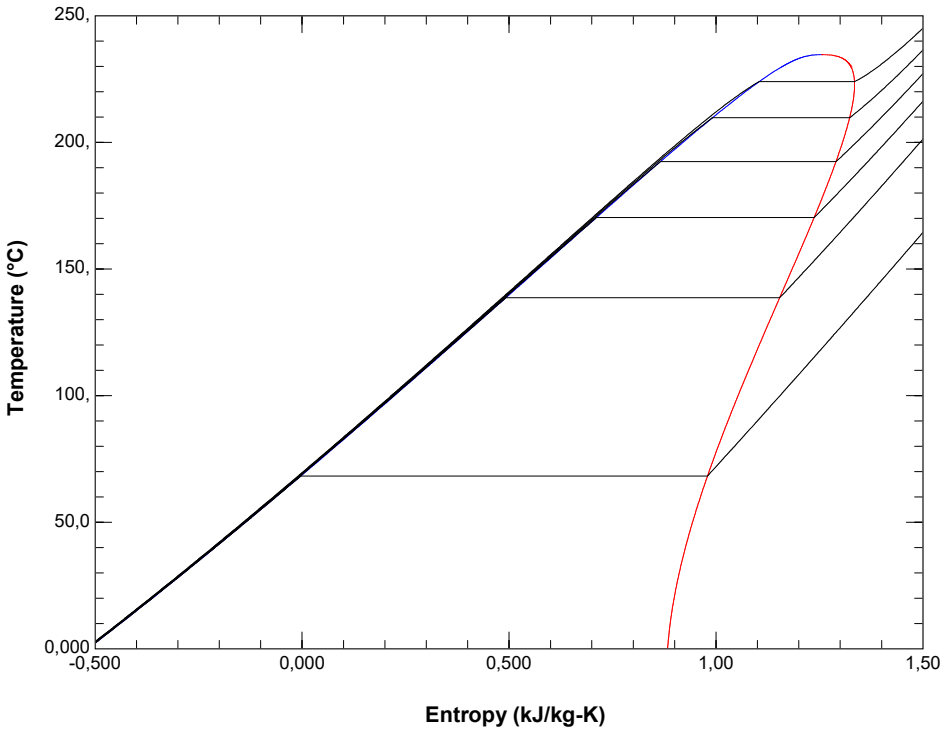

Figure 6.10: T-s diagram of pure Hexane's two-phase region with 6 isobars shown

Given in blue is the saturated liquid phase and in red the saturated vapour phase with 6 isobars plotted equidistantly between 1 and 26 bar. The red saturated vapour boundary clearly has a strong positive $\mathrm{d}s/\mathrm{d}T$ relation that, in order to ensure dry compression, must be avoided by increasing T_{R3}.

The other mixture constituent often encountered in the highest COP for pure cycle class is water. Water based cycles encounter a rarer issue namely that the superheated isobars for water have an extremely steep $\mathrm{d}s/\mathrm{d}T$ relation. The superheated water isobars are such that in practice it is common to inter-cool between compressor stages and as this was not an implemented feature of the python model the introduction of water into other refrigerants quickly has a negative impact on the COP.

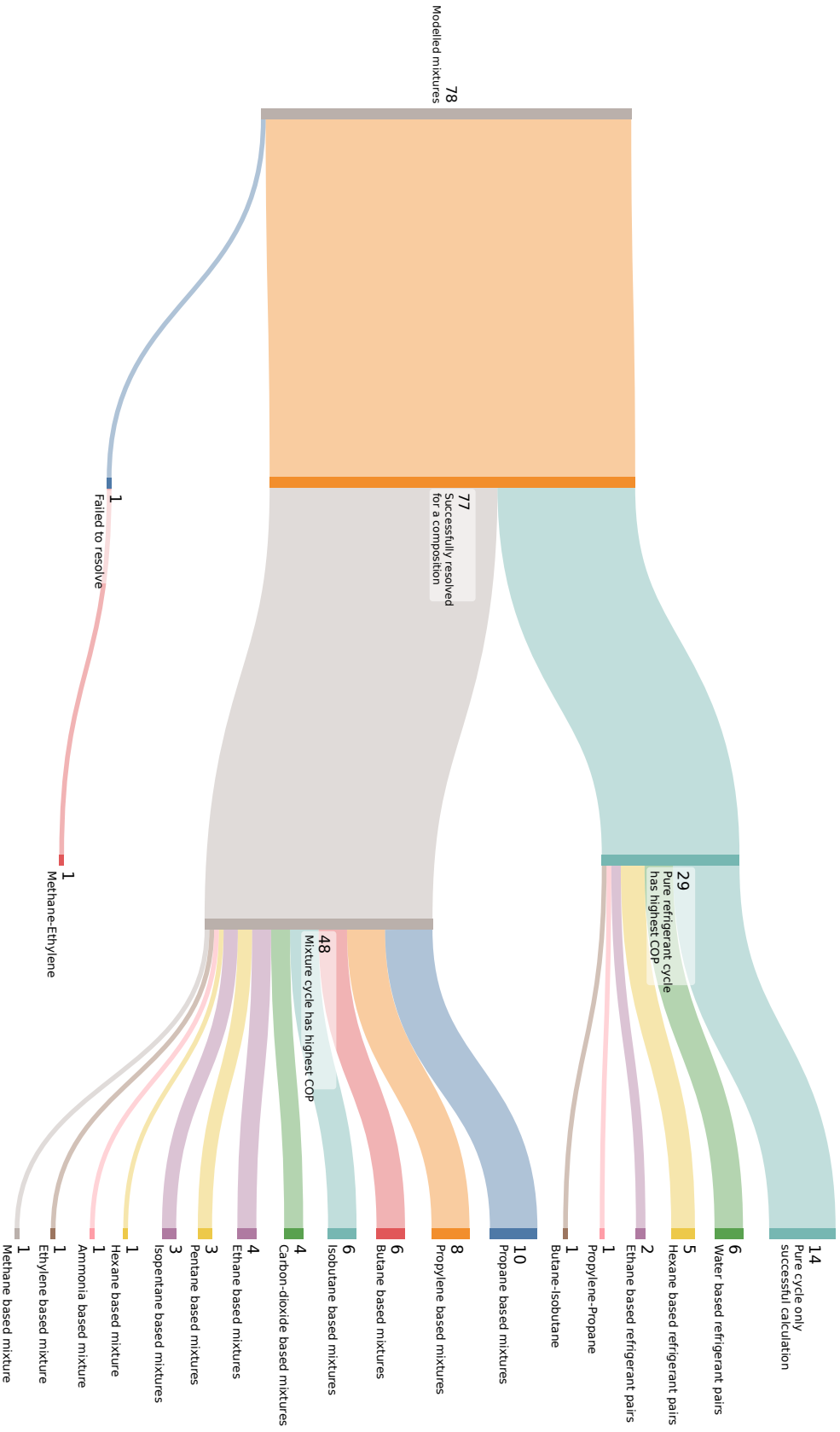

Figure 6.11: Sankey diagram classifying the modelling outputs in terms of successes and failures and further specifying primary compounds per category with reduced T_{A2} and T_{A3}

Only 48 mixture pairs were calculated to successfully improve the COP by introducing zeotropic mixtures, the smallest amount of successful improvements for the four investigated dryer operating conditions. Propane and Propylene together account for 37.5% of the successful mixtures and in contrast to previous results the number of Butane- and Isobutane-dominant mixtures is at the lowest value of all dryers. Investigating the 20 highest COPs reveals that, as was the case for the Butane isomers for T_{A2} equal to 180 °C and T_{A3} equal to 80 °C, refrigerants that are most often encountered also perform best. The 20 refrigerant mixtures with the highest COP are given in Figure 6.12 with their PR and p_{max}.

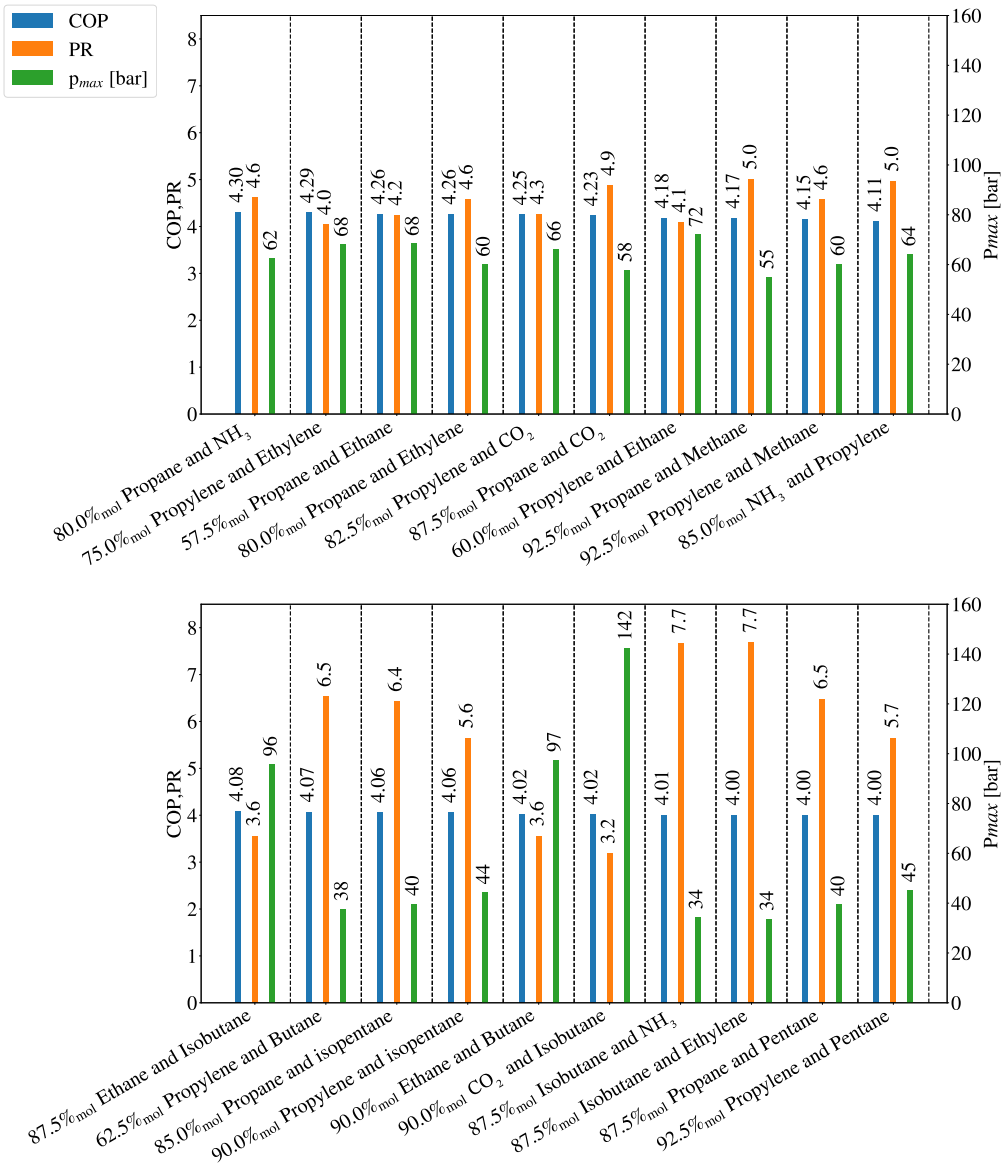

Figure 6.12: 20 mixtures with the highest calculated COP in a VCHP-integrated dryer operating between 120 and 50 °C with COP (blue), highest encountered pressure (green)and PR (orange) shown

Propane and Propylene dominate the top 20 with 14 of these mixtures being dominantly one of these refrigerant. PRs range between 3.2 and 7.7 meaning all are possible with two-stage compression and some with a single stage. The values for p_{max} range between 34 and 142 and again the PRs and p_{max} values are inversly correlated with the highest pressures at the lowest PRs. The COPs range between 4.30 and 4.00 presenting the highest values thus far.

The top performing mixture is an 80$\%_{mol}$ Propane-Ammonia mixture with a COP of 4.3, a PR of 4.61 and a top pressure of 62.5 bar of which the TS and TQ diagrams are shown in Figures 6.13 and 6.14 respectively.

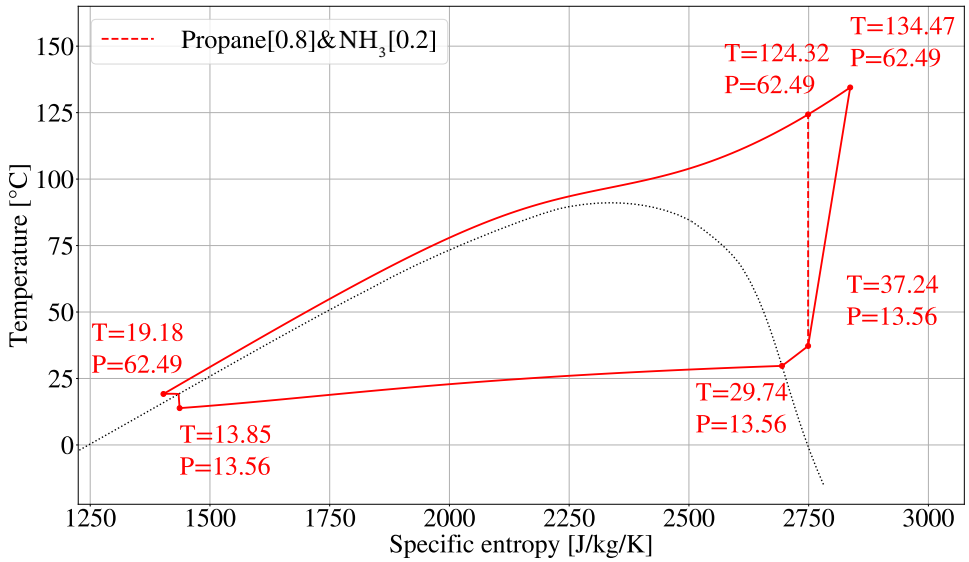

Figure 6.13: Temperature (T) specific entropy (s) diagram showing the VCHP cycle using an 80$\%_{mol}$ Propane - Ammonia refrigerant mixture

Shown in Figure 6.13 is the optimal cycle for T_{A2} equal to 120 °C and T_{A3} equal to 50 °C accomplished by an 80$\%_{mol}$ Propane-Ammonia mixture. Once more the highest COP is achieved by a trans-critical cycle, a consistent result for all drying conditions. The crossing of the widom line and the associated pseudo-condensation is observable in the flattening of the isobar around the critical point with the 20 $\%_{mol}$ NH_3 introducing some of its undesired non-linearity.

Clearly visible within the two-phase region is that the isobar for 13.56 bar is not isothermal, given the temperature increaes of the refrigerant within the two-phase region from 13.85 to 29.74 °C. The temperature at the exhaust of the compressor is higher than the minimum amount required which would be 125 °C, given the distance of the compression line to the two-phase boundary this is a consequence of the PPTD set for the condenser and not a wet compression risk. The adherence to the PPTD is more clearly visible when investigating the TQ plot of the HEXs given in Figure 6.14.

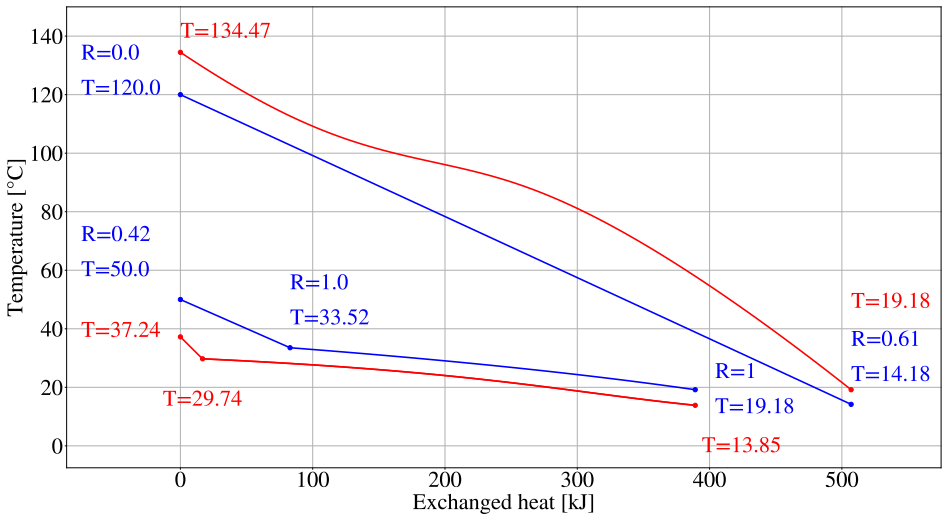

Figure 6.14: Temperature (T) exchanged heat (Q) diagram showing the 80$\%_{mol}$ Propane - Ammonia refrigerant cycle's condenser and evaporator with (humid) air given in blue and the refrigerant mixture in red

The T-Q plot given in Figure 6.14 shows the heat exchanged in the condenser (R3 to R4) and the evaporator (R5 to R2) in red. The air is preheated from ambient conditions such that T_{A1*} is 14.18 °C which is thus the inlet temperature for the VCHP cycle. The top blue line shows the pre-heated air reaching the targeted dryer inlet of 120 °C. The top red line is the "condensing" refrigerant which starts the heating at exactly the PPTD higher than the air such that T_{R5} is 19.18 °C. The maximum temperature T_{R3} is greater than what is required by the PPTD indicating a PPTD constraint encountered by the model. In addition to the pinch point at the evaporator outlet the refrigerant encounters a second point where the ΔT with the air grows small. The second constraining point in the condenser is encountered at approximately 100 kJ exchanged and has a ΔT of approximately 10 °C. The required value for T_{R3} to maintain a PPTD of 5.0 °C was calculated to be 134.47 °C.

Evaluating the evaporator, the design value of T_{A3} = 50 °C is found with φ_{A3} equal to 0.42, a result of the isenthalpic dryer assumption. The T_{dp} is calculated to be 33.52 °C where-after the slope of the humid air significantly flattens indicating the condensation of the evaporated water. The wet air exits the evaporator at 19.18 °C which is the heat source for the air pre-heater (not shown). The refrigerant's temperature at the expansion valve outlet, T_{R5}, is calculated to be 13.85 °C. T_{R5} is lower than the PPTD, required by the slight curve upwards that the refrigerant shows between T_{R5} and T_{R1} with the closest distance between the two streams around 200 kJ of heat exchanged. The degree of superheat is set to be 7.5 and as a direct consequence, T_{R2} is found to be equal to 37.24 °C.

The PR of 4.61 is slightly higher than the optimal values presented for screw compressors in section 3.4 but is still feasible with η_c between 65% and 70%. the top-performing refrigerant mixture uses 20$\%_{mol}$ Ammonia which is classified as B2L being mildly flammable and toxic. As discussed in 4.6, the flammability and toxicity of constituents can be suppressed by the use of mixtures. As the work by Fernandez et al. (2022) required at least 60 $\%_{mol}$ of non-flammable (A1) refrigerant be added to a highly flammable (A3) refrigerant to bring it down to "marginally flammable" (A2L) classification it is not expected that a 20$\%_{mol}$ addition of a "marginally flammable" type refrigerant to an A3 refrigerant will bring the mixture's rating down to A2L. Nevertheless, while the presence of the Ammonia cannot be expected to lead to a different classification, it will suppress flame propagation speed, the defining difference between A2 and A2L classification and a desired property. In the same sense, the toxicity of the mixture will be significantly lower (though not zero) than a pure Ammonia cycle would be.

The COP change as a function of mixture fraction is given in Figure 6.15.

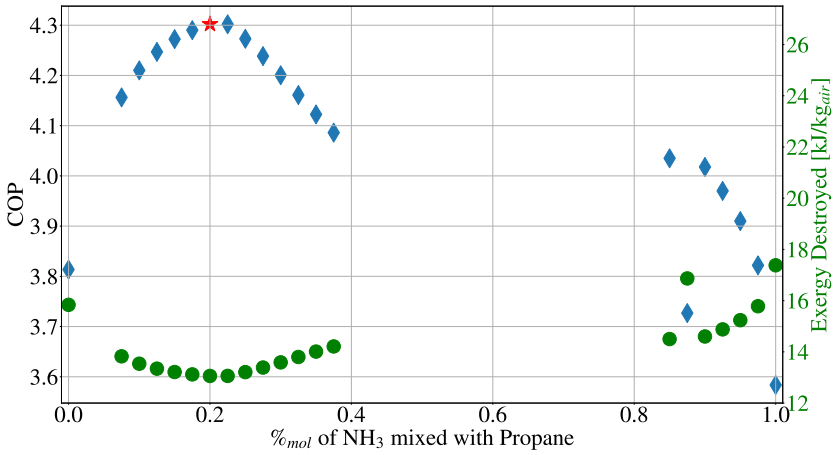

Figure 6.15: COP (blue) and exergy destruction (green) as a function of mixture fraction for the top performing refrigerant pair

Visible is the COP, given in blue, as a function of the mol fraction of NH_3 and the exergy destruction in green in $\mathrm{kJ\,kg_{air}^{-1}}$ with the maximum COP marked in red. The model failed to resolve around the 50% ratio but clearly demonstrates again the coupling of exergy destruction minimisation with COP optimisation and gives a clear maximum COP at 20$\%_{mol}$ NH_3. Also shown in figure 6.15 are two distinct declines in COP, first after the optimum is reached but the second as the fraction of NH_3 approaches 100%, a consequence of its trans-critical isobar shape. In comparison to the pure propane COP, the addition of 20$\%_{mol}$ NH_3 caused a COP increase of 12.81%.

If the selection is restricted to only consider mixtures that can be expected to have an A2L classification the first high COP cycle that meets this criteria is the 90%$_{mol}$ CO_2-Isobutane cycle, entry 16 in Figure 6.12. As was the case for Section 6.2, the use of a CO_2 comes with the benefits of having a predominantly A1 (non-flammable, non-toxic) refrigerant mixture with low GWP and no ODP. Given the benefits of CO_2, the cycle may be preferred in spite of its lower COP. The T-s and T-Q diagrams of the CO_2 mixture cycle are given in Figures 6.16 and 6.17 respectively.

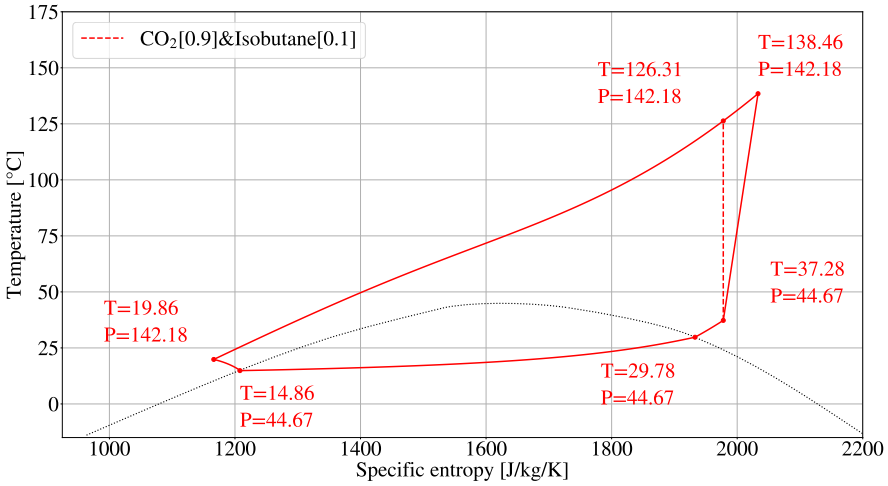

Figure 6.16: Temperature (T) specific entropy (s) diagram showing the VCHP cycle using a 90%$_{mol}$ CO_2-Isobutane refrigerant mixture

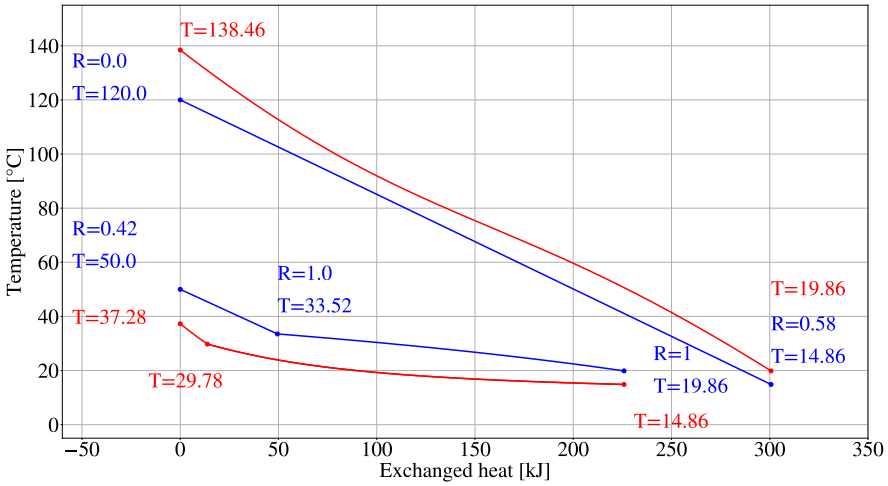

Figure 6.17: Temperature (T) exchanged heat (Q) diagram showing the 80%$_{mol}$ Propane - Ammonia refrigerant cycle's condenser (blue and purple) and evaporator (red and teal)

This marginally flammable, non-toxic alternative to the cycle shown in Figure 6.13 has a COP of 4.02, a PR of 3.2 and a p_{max} of 142 bar. The COP, while lower than the optimal, is competitive with values presented in Section 6.2 for the same drying regime and has feasible single stage compression. One downside inherent to CO_2 VCHPs is that the pressure is high and thus will affect the piping sizing if this cycle was to be constructed. The pinch in the evaporator is encountered at the refrigerant inlet and diverges to a ΔT of approximately 15.0 $^{\circ}\mathrm{C}$. The glide matching in the condenser was relatively successful thanks to the CO_2 trans-critical isobar shape with a divergence around 75 kJ of exchanged heat caused by the Isobutane leading to a maximum for ΔT of 18.45 $^{\circ}\mathrm{C}$ at the condenser inlet.

7

Novel cycle modelling

As was presented in section 4.5, a novel cycle is proposed to decouple glide matching in the evaporator and the condenser. The decoupling is accomplished using a flash tank to separate the saturated liquid and vapour from one another which, by nature of zeotropic mixture use, will have different compositions. This chapter presents a proof of concept for this cycle using an isopentane-Propylene mixture integrated into a dryer with the same inlet temperature as presented in Chapter 5 being 180 $^{\circ}\mathrm{C}$. An outlet temperature of 60 $^{\circ}\mathrm{C}$ is selected as the results of Chapter 6 showed that at this dryer inlet performance does not vary for outlet temperatures between 80 and 50 $^{\circ}\mathrm{C}$. The novel cycle was not calculated and optimised on a large scale as described in section 4.3 and instead was defined through user input. Given the reliance on user input the chapter opens with a discussion on the design procedure before presenting the result of the cycle and evaluating its performance.

7.1. Design procedure

Given the design of the novel cycle, in contrast to the basic cycle, was not automated this procedure must be performed manually. The feasibility conditions placed upon the basic cycle, adhered to by the model, are also placed on the novel cycle being the adherence of a PPTD of 5.0 $^{\circ}\mathrm{C}$ in both the evaporator and condenser as well as an avoidance of wet compression. The design of a cycle requires a mass and energy balance between the refrigerant and the air in both HEXs as well as between the inlets and outlets of the flash tank.

The very first step in the proof of concept cycle design is a selection of the mixture pair to be used. The 78 refrigerant pairs specified in 4.6 were divided into fractions with steps of 20%$_{mol}$ and the resulting 468 mixtures were each plotted in T-s diagrams. The two-phase regions of each mixture were plotted with several isobars such that of each mixture it could be evaluated if the mixture presented with profiles like those schematically given of the perfect novel cycle presented in section 4.5 and Figure 4.6. The mixtures that present with desirable isobars must also be evaluated if the required mixture composition is feasible in the evaporator. The evaporator is part of the bottom loop and thus will have the composition of the saturated liquid in the flask tank. The saturated liquid phase will favour the higher boiling point of the two mixture constituents and thus mixtures that require the low boiling point refrigerant to be dominantly present in the evaporator must be rejected. To give an example: Isopentane-Ammonia has, when the latter is 80%$_{mol}$ of the mixture, a very suitable glide in the two-phase region for interaction with humid air. In spite of the suitable glide the mixture is unfeasible for the novel cycle as Ammonia will never be more present than Isopentane in the liquid phase given the former has a boiling point of -33.33 $^{\circ}\mathrm{C}$ compared to the latter's of 27.83 $^{\circ}\mathrm{C}$.

Upon selecting a compound with an appropriate two-phase composition and an approximately linear trans-critical isobar the conditions in the flask tank must be specified. As the pressure of the flash tank is also that of the evaporator it affects the glide matching in this component directly. The shape of the isobar is generally defined by the composition but the temperatures between which the glide presents is directly defined by the pressure.

The equilibrium temperature is defined by the mass and energy balance of the HEXs and the flash tank which are given in as

$$\begin{aligned} \dot{m}_{air}(h_{A2} - h_{A1}) &= \dot{m}_{sat\_vap}(h_{V2} - h_{V3}) \\ \dot{m}_{air}(h_{A3} - h_{A4}) &= \dot{m}_{sat\_liq}(h_{L2} - h_{L1}) \\ (\dot{m}_{sat\_vap} + \dot{m}_{sat\_liq})c_{p,Fl}T_{Fl} &= \dot{m}_{sat\_vap}h_{V1} + \dot{m}_{sat\_liq}h_{L1} = \dot{m}_{sat\_vap}h_{V4} + \dot{m}_{sat\_liq}h_{L2} \end{aligned} \tag{7.1}$$

where $h_{i,n}$ is the specific enthalpy given for loop i given at thermodynamic state n, $\dot{m}_i$ is the massflow of a given loop, T_{fl} is the equilibrium temperature within the flash tank and $c_{p,i}$ is the heat capacity here defined for the equilibrium composition in the flash tank denoted by Fl.

The system of equations given in Eq. 7.1 is done using the following two definitions. First is the vapour quality given as

$$x = \frac{m_{sat\_vap}}{m_t} \tag{7.2}$$

which describes the fraction of the total mass (m_t) that is in the saturated vapour state (m_{sat_vap}). Second is the mass ratio given as

$$r_{mass} = \frac{m_{air}}{m_{sat\_liq}} \tag{7.3}$$

Which defines the mass of air that is heated (m_{air}) in relation to the mass of liquid refrigerant (m_{sat_liq}). Eq 7.2 and 7.3 are substituted into the system of equations given in Eq. (7.1) which yields

$$r_{mass} = \frac{x}{1-x}\frac{h_{V2} - h_{V3}}{h_{A2} - h_{A1}} = \frac{h_{L2} - h_{L1}}{h_{A3} - h_{A4}} \tag{7.4}$$

$$c_{p,Fl}T_{Fl} = xh_{V1} + (1-x)h_{L1} = xh_{V4} + (1-x)h_{L2} \rightarrow \frac{x}{1-x}(h_{V1} - h_{V4}) = h_{L2} - h_{L1} \tag{7.5}$$

relating the various enthalpies encountered at thermodynamic states within to the system to one another using only the vapour quality and mass ratio. The expressions given in Eq. (7.4) and 7.5 can be combined given their shared quality factor which yields

$$\frac{h_{L2} - h_{L1}}{h_{V1} - h_{V4}}\frac{h_{V2} - h_{V3}}{h_{L2} - h_{L1}} = \frac{h_{A2} - h_{A1}}{h_{A3} - h_{A4}} \xrightarrow{h_{V3}=h_{V4}} \frac{h_{V2} - h_{V3}}{h_{V1} - h_{V3}} = \frac{h_{A2} - h_{A1}}{h_{A3} - h_{A4}} \tag{7.6}$$

$$\frac{q_{out,v\_ref}}{q_{out,v\_ref} - w_c} = \frac{q_{in,air}}{q_{out,air}} \tag{7.7}$$

Which demonstrates that in addition to a direct coupling of $\dot{Q}$, as was given in Eq. (7.1), the specific heat and work of the refrigerant and the air are also coupled. The temperature defines the amount and composition of the saturated vapour state which, following Eq. (4.4), defines the amount of heat rejected by determining m_{sat_vap} which also fixes m_{sat_liq} through the mass balance as given in Eq. (4.5). The composition of m_{total} and the ratio between mass of refrigerant and mass of air, r_{mass}, can be set to match the total exchanged heat in the evaporator to the dry air and in the condenser to the humid air. The interconnection of the mass- and heatflows mean that while several user defined values are present they all affect one another and so they cannot be freely selected.

7.2. Proof of concept result

The modelling of a cycle using the state definitions presented in Table 4.4 were used to calculate a demonstration using a mixture of Isopentane-Propylene. The cycle has several degrees of freedom that were user-defined that are given in Table 7.1.

Table 7.1: Overview of user inputs used to design the novel cycle proof of concept

Design parameter	Symbol	Value
molar fraction isopentane	x	0.68
Flash tank temperature	T_{Fl}	20.38 °C
Flash tank pressure	p_{Fl}	1.415 bar
Air to refrigerant ratio	r_{mass}	3.655
Drying outlet temperature	T_{A3}	60 °C

By defining the molar fraction of isopentane the amount of propylene is also determined as it is a two-compound mixture. The flash tank temperature, molar fraction and mass ratio are three variables that influence the mass and energy balance and as such can be user defined but this must be done in proportion to one another. The resulting cycle is shown in a T-s diagram in Figure 7.1 and a T-Q diagram in Figure 7.2.

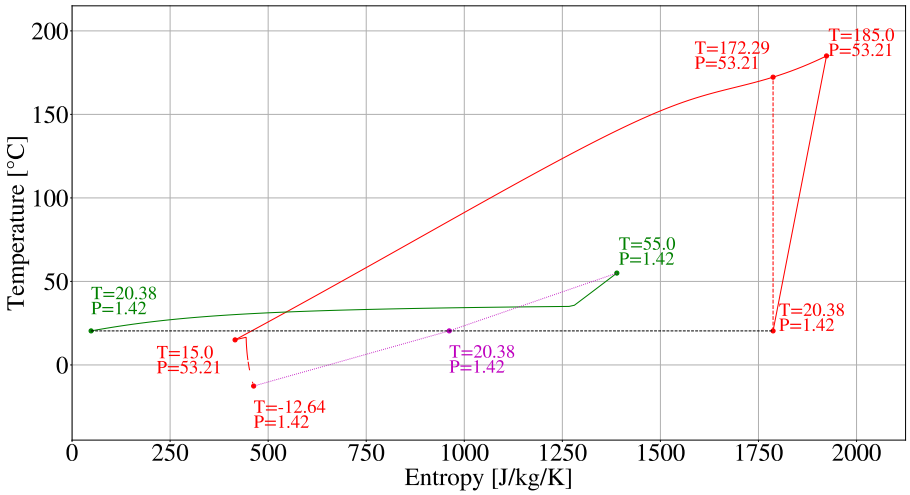

Figure 7.1: T-s diagram of proof of concept novel heat pump cycle using a flash tank (purple) to create a saturated vapour evaporation loop (green) and a saturated vapour condensation loop (red)

Visible in the T-s diagram is the successful calculation of the novel cycle concept heating air from 10 to 180 °C such that there is no air-to-air pre-heater in this cycle. The cycle's has a composition of 51%$_{mol}$ Isopentane-Propylene in the condenser and a 91%$_{mol}$ isopentane concentration in the evaporator. The COP of the cycle is calculated to be 2.81 with a PR of 37.6. The pressure ratio requires a three-stage compressor with a single-stage PR of 3.35. The quality in the flash tank is 0.57 and so slightly more mass flows in the top loop than the bottom. The mass of air is defined to be 3.655 $\mathrm{kg\,kg_{sat\_liq}^{-1}}$.

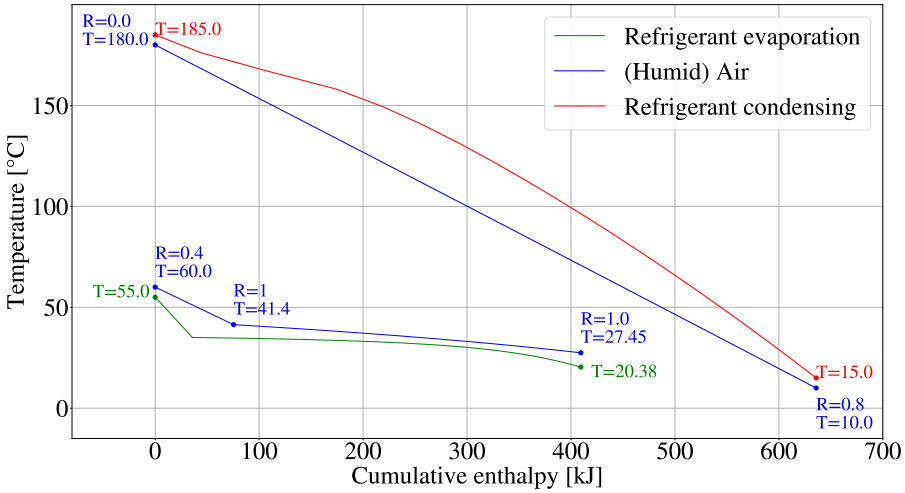

Figure 7.2: T-Q diagram of proof of concept novel heat pump cycle exchanging heat with (humid) air shown in blue with the evaporating refrigerant given in green and the condensing refrigerant in red

The T-Q diagram given in Figure 7.2 shows the glide matching of this cycle. The outlet temperature of 60 $^{\circ}\mathrm{C}$ is an intermediate value between the two conditions studied in Chapter 6 and has a relative humidity of 0.4 which means about 80% of $\dot{Q}_{in}$ is available below T_{dp}. The glide matching performed in the evaporator is very effective with the temperature difference at the refrigerant inlet being 7.07 $^{\circ}\mathrm{C}$, narrowing to the PPTD during evaporator with a temporary divergence due to a mild mismatch between the placement of T_{dp} and the saturated vapour state. The exergy destroyed by the novel cycle per component is given in Table 7.2.

Table 7.2: determination of exergy destroyed, given in $\mathrm{kJ\,kg_{air}^{-1}}$ per component of the proof of concept novel cycle

COP	Ex_d flash tank	Ex_d Condenser	Ex_d Compressor	Ex_d Evaporator	Ex_d Expansion valve	Total Ex_d
2.81	9.54	7.07	11.67	1.56	4.06	33.9

The glide matching in the evaporator was indeed successful as the exergy destroyed in the evaporator of this cycle per mass of air is lower than any other cycle with a value of 1.56 $\mathrm{kJ\,kg_{air}^{-1}}$ compared to 3.24 and 4.14 for the optimal three- and two-stage compression cycle presented in Chapter 5. Unfortunately the cycle does destroy a significant amount of exergy in the compressor and the glide matching in the condenser was also sub-optimal with both values being higher than the optimal standard VCHP mixture cycles. Additionally, the novel cycle destroys exergy during mixing as well and this component accounts for 28.1% of exergy destroyed. The novel cycle does also perform the heating segment that the basic cycle performs using the air-to-air HEX of which the Ex_d was not included in analysis but this does not compensate for the 60% larger exergy destruction. While the novel concept enabled a more bespoke glide matching in the evaporator, the total cycle was evidently not optimised. The COP of 2.81 is also 18.55% lower than the optimal COP of 3.45. Given the COP can be written as

$$COP = \frac{\dot{Q}_{out}}{\dot{W}_{in}} = \frac{\dot{Q}_{in} + \dot{W}_{in}}{\dot{W}_{in}} = \frac{\dot{m}_{sat\_liq} * q_{in} + \dot{m}_{sat\_vap} * w_{in}}{\dot{m}_{sat\_vap} * w_{in}} \tag{7.8}$$

It becomes clear that a higher vapour quality negatively affects the COP as the COP goes towards 1 as m_{vap} goes to m_{tot}. This also makes intuitive sense as more gas is compressed and circulated that does not absorb any heat. An optimised novel cycle would have a larger amount of mass flowing into the evaporator such that a lot of refrigerant is absorbing heat and only a little is rejecting. One additional advantage this cycle does posses is that no single component besides the flash tank needs to be sized for the total refrigerant mass. The evaporator only needs to accommodate the liquid refrigerant, the compressor and condenser the compressed vapour fraction. The mass split means that individual components can, for the refrigerant, be smaller than for a classic VCHP.

8

Conclusions & Recommendations

In this chapter, the key conclusions drawn from the study will be presented, followed by the recommendations for future research on the subject. The 13 natural refrigerants water, ammonia, (iso)butane, (iso)pentane, methane, ethane, propane, CO_2, propylene, ethylene and hexane were combined into 78 binary pairs. Each binary pair was divided into 41 possible compositions for a total of 3198 possible refrigerant mixtures. These refrigerant mixtures were modelled within a VCHP cycle operating between the inlet and outlet of a dryer. Two temperatures for the inlet as well as for the outlet were calculated for a total of 4 dryer operating conditions and as such 12792 possible VCHP dryers were calculated and optimised.

8.1. Conclusion

For each drying condition the 20 mixtures with the highest COP were explored and per dryer a preferred cycle was selected based on COP, estimated compressor stages as well as flammability and toxicity. The selected cycle for every dryer, the used mixture and the cycle's COP and PR are summarized in table 8.1 below.

Table 8.1: Overview of best performing mixtures for each studied drying condition

	Dryer outlet temperature					
	80 $^\circ$C			50 $^\circ$C		
Dryer inlet temperature	Mixture	COP	PR	Mixture	COP	PR
180 $^\circ$C	87.5$\%_{mol}$ Isobutane-Ethane	3.38	16.53	87.5$\%_{mol}$ NH_3-Propane	3.44	6.84
120 $^\circ$C	87.5$\%_{mol}$ CO_2-Isopentane	3.96	3.58	90$\%_{mol}$ CO_2-Isobutane	4.02	3.18

The highest COP for an inlet temperature of 180°C was calculated to be 3.45 for both outlet temperatures. Both optimal mixtures for 180°C were predominately isomers of butane and the investigation of the top 20 mixtures revealed these were the main component of the majority of top performing cycles. Both T_{A2} = 180 $^\circ$C cycles with a COP of 3.45 were rejected, for the T_{A3} = 80 $^\circ$C condition this was due to a requirement of three compressor stages and for T_{A3} = 50 $^\circ$C it was because cycles were available with comparable performance but a lower expected flammability rating. The outlet temperature of 50°C differentiates itself from the higher outlet temperature by enabling less flammable refrigerants. Additionally, the lower outlet temperature dryer has a lower PR, that being 6.84 compared to 16.53 for the high temperature outlet. PRs deemed likely to be achievable using less compressor stages were given preference due to CapEx and operational complexity concerns introduced by having multiple compressor that are interconnected.

For an inlet temperature of 120°C CO_2 based refrigerant mixtures presented themselves with high COPs and low PRs with the additional benefit of an A1 rating using the ASHRAE-34 classification and low GWP and ODP. For the higher outlet temperature the highest COP of 3.96 was achieved by an 87.5%$_{mol}$ CO_2-Isopentane mixture. In addition to a high COP the cycle also has a low PR of 3.58 which could be performed using only a single compression stage. For the low outlet temperature the highest COP of 4.3 was rejected as it was achieved by a mostly Propane mixture. Instead the choice was made

to explore the top COP A2L mixture which was achieved by a 90%$_{mol}$ CO_2-Isobutane mixture. While the COP is 6.51% lower than the top cycle's the large presence of CO_2 was deemed preferable and with a PR of 3.18 single stage compression is also possible for this cycle. As discussed in Section 4.6, work by Fernandez et al. (2022) demonstrated that a mixture comprised of a highly flammable (A3) and a non-flammable (A1) mixture can have a rating of lightly flammable (A2L) provided the A1 refrigerant is the dominant compound. The possibility of an A2L classification is an advantage of the CO_2-mixture cycles that was given strong emphasis as it makes safety concerns smaller when the proposed cycle is brought into practice. One downside of using mostly CO_2 mixtures is that values for p_{max} are typically large and as such the sizing of piping will require thicker walls to safely handle the stresses imposed.

It was demonstrated in a broad sense that zeotropic refrigerant mixtures improve the COP of VCHP-integrated dryers for at least 51 refrigerant pairs for a dryer operating between 180 and 80 $^{\circ}\mathrm{C}$ with the number reducing for other conditions with a minimum of 48 refrigerant pairs for dryer operation between 120 and 50 $^{\circ}\mathrm{C}$. Mixtures that failed to resolve or failed to improve upon the pure cycle COP were repeatedly discussed. Some refrigerants struggled to adhere to the PPTD and dry compression requirements leading to highly elevated compressor outlet temperatures. Specifically Hexane was found to have an inconvenient saturated vapour line. Ammonia was repeatedly observed to have an undesirable trans-critical isobar shape with significant changes to its heat capacity during condensation. Water cycles were often rejected by the model or failed to resolve and this was attributed to the compression definition as water VCHPs often have intercooling between compression stages to avoid extremely elevated compressor outlet temperatures.

The dominant constituent of many refrigerant mixtures was repeatedly found to be one around the median boiling point value. It was observed that the most used refrigerant shifted between the Butane isomers, the two refrigerants with a boiling point directly above the median, and Propane and Propylene, the two refrigerants directly below the median depending on drying conditions. The shifting between above and below median boiling point refrigerants indicates a relation between the drying temperature and the most stable dominant refrigerant constituent. It was valuable to observe that for all drying cases the dominant constituent is a near-median refrigerant and this insight can be used for theorising future cycles.

The highest COP was achieved by a Butane mixture but when compared to the pure cycle COP the COP of Butane can be improved by mixing it with 8 other refrigerants as shown in figure 5.6. Another commonly found mixture compound was Isobutane which also showed that a pure Isobutane COP can be improved through mixing it with 8 different refrigerants. While Isobutane and Butane are both encountered often in well performing mixtures and the fact that one is the isomer of the other they are not interchangeable. As shown by comparing both refrigerants when mixed with Propane, the behavior both in COP values as well as the relation of COP to mixture ratio was different. This shows that even comparable refrigerants warrant inclusion in analysis as both the mixing behavior as well as the performance in a heat pump cycle can be different.

A recurring result across all drying conditions and their top COP cycles was that these cycles operated trans-critically. As shown in the schematic TS-diagram given in figure 4.5 the isobar of the refrigerant mixture in the super-critical region closely matched the temperature glide of dry air. This presents an addition to the discussion on how VCHP cycles can glide match that was presented in chapter 3. Zeotropic mixtures and trans-critical cycles are commonly presented as two different methods to achieve glide matching. It was consistently demonstrated, across all drying conditions, that the top performing cycles were both zeotropic and trans-critical. The choice between trans-critical and zeotropic mixture VCHPs is a false dichotomy as it is clearly demonstrated that the best performance is achieved by trans-critical zeotropic mixture cycles, a combination of both methods.

The main research question of the present work was: *"How can future-proof binary zeotropic refrigerant mixtures be used to increase the performance of heat pumps applied to the waste heat recovery of industrial drying processes."*

It was clearly demonstrated that future-proof binary zeotropic mixtures increase the performance of VCHP-integrated dryers across all relevant temperature ranges, by as much as 21.47%. The greatest performance increase is found when zeotropic refrigerant mixtures are used together with trans-critical operation. The performance increase does vary across drying conditions as does the best performing refrigerant mixture. Zeotropic mixtures can also be used to conceptualise new cycles that were not possible for pure refrigerants as was demonstrated using the novel cycle. Zeotropic mixtures improve the COP of VCHP-dryers and should be utilised for non-isothermal processes like drying.

8.2. Recommendations

One aspect in which the present work can be improved is by introducing an accounting of the pressure drops within the VCHP cycle. As Bell et al. (2021) discussed based on the work of Mclinden et al. (2017), pressure drop models are required to make truly fair comparisons between refrigerants. As was done in the work by Mclinden et al. (2017), the current model can serve as an identifier of high potential cycles which are then provided into a second, more realistic model that also accounts for pressure drops. The developed model for large scale analysis of optimal VCHP integrated dryers can also be applied to a larger set of refrigerants and a higher resolution temperature sensitivity study can be performed. Such a wide-scale deployment of the model will realistically require use of a high performance computing cluster such as DelftBlue.

Given that water cycles are of specific interest to industry due to its availability and safety, the used python model is recommended to be modified such that intercooling can be modelled. It would be valuable to investigate water-based refrigerant mixtures specifically, modelling just water paired with each other refrigerant and optimising the cycle and the compression stage. A water-based refrigerant mixture cycle optimisation would be a valuable addition to the present work.

Instead of producing a large scale dataset using large amounts of computing power, it is more effective to use the developed model applied to dryers currently in operation. Ideally, accurate data of the dryer in- and outlet conditions is supplied to the model, an optimised mixture is calculated by the model and that VCHP cycle is then physically constructed and tested. Specific points of attention are the behaviour of refrigerant mixtures in the supercritical region, with fractionation concerns being most pressing, and heat transfer profile investigation to validate and improve assumptions made about the PPTD, especially when trans-critical mixtures are to be used. Alternatively, or, preferably in parallel, molecular simulations can be performed investigating the behaviour of refrigerant mixtures as well. If simulations are performed it is once again recommended to focus attention on predicting super-critical behaviour as a merger of trans-critical cycles with zeotropic refrigerant cycles has been consistently shown to result in the highest COPs across all drying regimes and latent to sensible heat storage ratios.

Two additional areas of study would be a techno-economic study of select high-performance cycles from the results. At several point within the present work reference is made to CapEx considerations. For example CapEx factors into the pressure levels through pipe sizing, PRs and associated compressor stages in amount of required equipment as well as PPTD optimisation. A PPTD optimisation also leads to the second area of study as it is recommended to perform a dimensioning of the HEXs both in the VCHP cycles as well as the air-to-air HEX. Given the interaction with air, it is not expected that the heat transfer coefficient of the refrigerant will be a limitation. Nevertheless, trans-critical refrigerants can have unexpectedly low heat transfer coefficients and including mixtures with different boiling points into this warrants a proper study.

The novel cycle proposed demonstrated that the consideration of the potential of zeotropic refrigerant mixtures can go beyond their introduction into a standard heat pump cycle. The novel cycle proposed in the present work allowed for different glide matching in the evaporator and condenser. The optimisation of the novel cycle did prove more complex than the standard heat pump and the proof of concept cycle presented with lower COPs than the optimised standard cycles. One identified reason for this is the COPs dependence on the quality in the flash tank with higher COPs achieved when a larger amount of the refrigerant mixture stays liquid and absorbs heat. A model that optimises the novel cycle, as was done in the present work for the basic cycle, would be a valuable addition to this rapport. Additionally, the novel cycle should be constructed for the purposes of testing and be investiagted as to identify the steady-state as well as the dynamic operation behaviour.

References

[1] Hamed Abedini, Elias Vieren, Toon Demeester, Wim Beyne, Steven Lecompte, Sylvain Quoilin, and Alessia Arteconi. “A comprehensive analysis of binary mixtures as working fluid in high temperature heat pumps”. en. In: *Energy Conversion and Management* 277 (Feb. 2023), p. 116652. ISSN: 01968904. DOI: 10.1016/j.enconman.2022.116652. URL: https://linkinghub.elsevier.com/retrieve/pii/S0196890422014303 (visited on 03/20/2024).

[2] *ANSI/ASHRAE standard 34-2019 designation and Safety Classification of Refrigerants*. 2019.

[3] Gholamreza Bamorovat Abadi and Kyung Chun Kim. “Investigation of organic Rankine cycles with zeotropic mixtures as a working fluid: Advantages and issues”. en. In: *Renewable and Sustainable Energy Reviews* 73 (June 2017), pp. 1000–1013. ISSN: 13640321. DOI: 10.1016/j.rser.2017.02.020. URL: https://linkinghub.elsevier.com/retrieve/pii/S1364032117302253 (visited on 03/20/2024).

[4] Ian H. Bell, Piotr A. Domanski, Mark O. McLinden, and Gregory T. Linteris. “The hunt for nonflammable refrigerant blends to replace R-134a”. en. In: *International Journal of Refrigeration* 104 (Aug. 2019), pp. 484–495. ISSN: 01407007. DOI: 10.1016/j.ijrefrig.2019.05.035. URL: https://linkinghub.elsevier.com/retrieve/pii/S0140700719302361 (visited on 03/22/2024).

[5] Ian H. Bell, Jorrit Wronski, Sylvain Quoilin, and Vincent Lemort. “Pure and Pseudo-pure Fluid Thermophysical Property Evaluation and the Open-Source Thermophysical Property Library CoolProp”. In: *Industrial & Engineering Chemistry Research* 53.6 (2014), pp. 2498–2508. DOI: 10.1021/ie4033999. eprint: http://pubs.acs.org/doi/pdf/10.1021/ie4033999. URL: http://pubs.acs.org/doi/abs/10.1021/ie4033999.

[6] Giuseppe Bianchi, Gregoris Panayiotou, Lazaros Aresti, Soteris A. Kalogirou, Georgios A. Florides, Kostantinos Tsamos, Savvas A. Tassou, and Paul Christodoulides. “Estimating the waste heat recovery in the European Union Industry”. In: *Energy, ecology and environment (Online)* 4.5 (Sept. 2019), pp. 211–221. DOI: 10.1007/s40974-019-00132-7. URL: https://doi.org/10.1007/s40974-019-00132-7.

[7] R. de Boer. *Strengthening Industrial Heat Pump Innovation - Decarbonizing Industrial Hea*. Tech. rep. TNO, 2020.

[8] Marina Brancaccio. “Modelling of Non-Equilibrium Wet Compression in Compression-Resorption Heat Pumps”. MA thesis.

[9] Richard P. Brent. *Algorithms for minimization without derivatives*. Courier Corporation, June 2013.

[10] S Buysse. “The dryer section of a paper machine”. English. MA thesis. Delft: TU Delft, Sept. 2021. URL: http://resolver.tudelft.nl/uuid:2f064fad-d4e0-44bf-a81f-28ba25fe4678.

[11] *Check humidity in Amsterdam by month | Accurate Insights*. URL: https://weather-and-climate.com/average-monthly-Humidity-perc,Amsterdam,Netherlands.

[12] K.J. Chua, S.K. Chou, and W.M. Yang. “Advances in heat pump systems: A review”. en. In: *Applied Energy* 87.12 (Dec. 2010), pp. 3611–3624. ISSN: 03062619. DOI: 10.1016/j.apenergy.2010.06.014. URL: https://linkinghub.elsevier.com/retrieve/pii/S030626191000228X (visited on 03/13/2024).

[13] “COP28 Agreement”. In: The United Nations Climate Change Conference. Dec. 2023.

[14] Alexandre C. Dimian, Costin S. Bildea, and Anton A. Kiss. “Pinch Point Analysis”. In: *Computer Aided Chemical Engineering*. Vol. 35. Elsevier, 2014, pp. 525–564. ISBN: 978-0-444-62700-1. DOI: 10.1016/B978-0-444-62700-1.00013-9. URL: https://linkinghub.elsevier.com/retrieve/pii/B9780444627001000139 (visited on 08/27/2024).

[15] Piotr A Domanski and Mark O McLinden. “A simplified cycle simulation model for the performance rating of refrigerants and refrigerant mixtures”. In: *International Journal of Refrigeration* 15.2 (Jan. 1992), pp. 81–88. DOI: 10.1016/0140-7007(92)90031-o. URL: https://doi.org/10.1016/0140-7007(92)90031-o.

[16] *Drogen in de papier en karton industrie*. 2014. URL: https://nwgd.nl/kennisbank/drogen-in-de-papier-en-karton-industrie/.

[17] *Drying in the chemical industry*. Oct. 8, 2020. URL: https://nwgd.nl/kennisbank/drying-in-the-chemical-industry/ (visited on 04/07/2024).

[18] Editor Engineeringtoolbox. *Moist Air - The Mollier Diagram*. Oct. 23, 2023. URL: https://www.engineeringtoolbox.com/psychrometric-chart-mollier-d_27.html.

[19] Stefan Elbel and Pega Hrnjak. “Experimental validation of a prototype ejector designed to reduce throttling losses encountered in transcritical R744 system operation”. In: *International Journal of Refrigeration* 31.3 (May 1, 2008), pp. 411–422. DOI: 10.1016/j.ijrefrig.2007.07.013. URL: https://doi.org/10.1016/j.ijrefrig.2007.07.013.

[20] Adrián Fernández-Moreno, Adrián Mota-Babiloni, Pau Giménez-Prades, and Joaquín Navarro-Esbrí. “Optimal refrigerant mixture in single-stage high-temperature heat pumps based on a multiparameter evaluation”. en. In: *Sustainable Energy Technologies and Assessments* 52 (Aug. 2022), p. 101989. ISSN: 22131388. DOI: 10.1016/j.seta.2022.101989. URL: https://linkinghub.elsevier.com/retrieve/pii/S2213138822000418 (visited on 03/20/2024).

[21] *Final energy consumption in industry - detailed statistics*. Aug. 23, 2023. URL: https://ec.europa.eu/eurostat/statistics-explained/index.php?title=Final_energy_consumption_in_industry_-_detailed_statistics#Energy_products_used_in_the_industry_sector (visited on 04/07/2024).

[22] George E. Forsythe, Michael A. Malcolm, and Cleve B. Moler. *Computer methods for mathematical computations*. Jan. 1977. URL: https://ci.nii.ac.jp/ncid/BA01265412.

[23] FrieslandCampina. *Harnessing the heat: FrieslandCampina Ingredients and Atlas Copco team up to develop energy-saving heat recovery system concept*. Feb. 6, 2024. URL: https://www.frieslandcampinaingredients.com/insight/harnessing-the-heat-frieslandcampina-ingredients-and-atlas-copco-team-up-to-develop-energy-saving-heat-recovery-system-concept/.

[24] P. Ganesan and Trygve M. Eikevik. “New zeotropic CO2-based refrigerant mixtures for cascade high-temperature heat pump to reach heat sink temperature up to 180 °C”. en. In: *Energy Conversion and Management: X* 20 (Oct. 2023), p. 100407. ISSN: 25901745. DOI: 10.1016/j.ecmx.2023.100407. URL: https://linkinghub.elsevier.com/retrieve/pii/S2590174523000636 (visited on 02/21/2024).

[25] Ajit Ghosh. *Fundamentals of Paper Drying – Theory and Application from Industrial Perspective*. Sept. 2011. DOI: 10.5772/21594. URL: https://doi.org/10.5772/21594.

[26] Walter Grassi. *Heat pumps*. Jan. 1, 2018. DOI: 10.1007/978-3-319-62199-9. URL: https://doi.org/10.1007/978-3-319-62199-9.

[27] *Heat up Carbon down*. URL: https://www.man-es.com/process-industry/campaigns/heat-up-carbon-down.

[28] Sebastian Herrmann, Hans-Joachim Kretzschmar, and Donald P. Gatley. “Thermodynamic Properties of Real Moist Air, Dry Air, Steam, Water, and Ice (RP-1485)”. en. In: *HVAC&R Research* 15.5 (Sept. 2009), pp. 961–986. ISSN: 1078-9669, 1938-5587. DOI: 10.1080/10789669.2009.10390874. URL: https://www.tandfonline.com/doi/full/10.1080/10789669.2009.10390874 (visited on 03/26/2024).

[29] K. Hooman. *lecture notes on Heat exchangers: Introduction*. 2023.

[30] Marcia Huber, Allan Harvey, Eric Lemmon, Gary Hardin, Ian Bell, and Mark McLinden. *NIST Reference Fluid Thermodynamic and Transport Properties Database (REFPROP) Version 10 - SRD 23*. 2018. DOI: 10.18434/T4/1502528. URL: https://www.nist.gov/srd/refprop (visited on 03/28/2024).

[31] IEA. *World Energy Outlook 2023*. Tech. rep. IEA, 2023. URL: https://www.iea.org/reports/world-energy-outlook-2023.

[32] Blechschmidt J. *Taschenbuch der Papiertechnik*. Tech. rep. Carl Hanser Verlag GmbH Co KG, 2013.

[33] Mateo Jesper, Florian Schlosser, Felix Pag, Timothy Gordon Walmsley, Bastian Schmitt, and Klaus Vajen. "Large-scale heat pumps: Uptake and performance modelling of market-available devices". In: *Renewable & Sustainable Energy Reviews* 137 (Mar. 1, 2021), p. 110646. DOI: 10.1016/j.rser.2020.110646. URL: https://doi.org/10.1016/j.rser.2020.110646.

[34] Jiatong Jiang, Bin Hu, R.Z. Wang, Na Deng, Feng Cao, and Chi-Chuan Wang. "A review and perspective on industry high-temperature heat pumps". en. In: *Renewable and Sustainable Energy Reviews* 161 (June 2022), p. 112106. ISSN: 13640321. DOI: 10.1016/j.rser.2022.112106. URL: https://linkinghub.elsevier.com/retrieve/pii/S1364032122000351 (visited on 03/20/2024).

[35] H.P. Karbstein. *Projektkurzbericht 2018 - Kombination konventioneller Trocknungsverfahren zur Erhöhung der Energieeffizienz und zur Verbesserung der Qualität von getrocknetem Obst und Gemüse*. Tech. rep. FEI, 2018. URL: https://www.fei-bonn.de/gefoerderte-projekte/projektdatenbank/aif-18250-n.projekt.

[36] Ian Kemp. "Reducing dryer energy use by process integration and pinch analysis". In: *Drying technology* 23.9-11 (Sept. 1, 2005), pp. 2089–2104. DOI: 10.1080/07373930500210572. URL: https://doi.org/10.1080/07373930500210572.

[37] Anton Alexandru Kiss and Carlos Alberto Infante Ferreira. *Heat pumps in th chemical process industry*. eng. Boca Raton London New York: CRC Press, Taylor & Francis Group, 2017. ISBN: 978-1-4987-1895-0.

[38] T. Kudra. "Energy Performance of Convective Dryers". en. In: *Drying Technology* 30.11-12 (Sept. 2012), pp. 1190–1198. ISSN: 0737-3937, 1532-2300. DOI: 10.1080/07373937.2012.690803. URL: http://www.tandfonline.com/doi/abs/10.1080/07373937.2012.690803 (visited on 02/02/2024).

[39] Tadeusz Kudra. "Energy aspects in drying". In: *Drying technology* 22.5 (Dec. 31, 2004), pp. 917–932. DOI: 10.1081/drt-120038572. URL: https://doi.org/10.1081/drt-120038572.

[40] O Kunz and Wolfgang Wagner. "The GERG-2008 Wide-Range Equation of State for Natural Gases and Other Mixtures: An expansion of GERG-2004". In: *Journal of chemical and engineering data* 57.11 (Oct. 31, 2012), pp. 3032–3091. DOI: 10.1021/je300655b. URL: https://doi.org/10.1021/je300655b.

[41] H.J. Laue. *Application of Industrial Heat Pumps, Annex 35*. Tech. rep. International Energy Agency (IEA), 2014.

[42] Jobien Laurijssen. "Energy use in the paper industry". en. PhD thesis. 2013.

[43] Jobien Laurijssen, Frans J. De Gram, Ernst Worrell, and Andre Faaij. "Optimizing the energy efficiency of conventional multi-cylinder dryers in the paper industry". en. In: *Energy* 35.9 (Sept. 2010), pp. 3738–3750. ISSN: 03605442. DOI: 10.1016/j.energy.2010.05.023. URL: https://linkinghub.elsevier.com/retrieve/pii/S0360544210002938 (visited on 01/29/2024).

[44] S. Lecompte, B. Ameel, D. Ziviani, M. Van Den Broek, and M. De Paepe. "Exergy analysis of zeotropic mixtures as working fluids in Organic Rankine Cycles". en. In: *Energy Conversion and Management* 85 (Sept. 2014), pp. 727–739. ISSN: 01968904. DOI: 10.1016/j.enconman.2014.02.028. URL: https://linkinghub.elsevier.com/retrieve/pii/S0196890414001472 (visited on 03/20/2024).

[45] Da Qing Li and Eckhard A. Groll. "Transcritical CO2 refrigeration cycle with ejector-expansion device". In: *International Journal of Refrigeration* 28.5 (Aug. 1, 2005), pp. 766–773. DOI: 10.1016/j.ijrefrig.2004.10.008. URL: https://doi.org/10.1016/j.ijrefrig.2004.10.008.

[46] Ting Liang, Andrea Vecchi, Kai Knobloch, Adriano Sciacovelli, Kurt Engelbrecht, Yongliang Li, and Yulong Ding. “Key components for Carnot Battery: Technology review, technical barriers and selection criteria”. en. In: *Renewable and Sustainable Energy Reviews* 163 (July 2022), p. 112478. ISSN: 13640321. DOI: 10.1016/j.rser.2022.112478. URL: https://linkinghub.elsevier.com/retrieve/pii/S1364032122003823 (visited on 03/13/2024).

[47] Aldé B. T. Loemba, Baraka Kichonge, and Thomas Kivevele. “Comprehensive assessment of heat pump dryers for drying agricultural products”. en. In: *Energy Science & Engineering* 11.8 (Aug. 2023), pp. 2985–3014. ISSN: 2050-0505, 2050-0505. DOI: 10.1002/ese3.1326. URL: https://onlinelibrary.wiley.com/doi/10.1002/ese3.1326 (visited on 01/29/2024).

[48] Gustav Lorentzen. “Revival of carbon dioxide as a refrigerant”. In: *International Journal of Refrigeration* 17.5 (Jan. 1, 1994), pp. 292–301. DOI: 10.1016/0140-7007(94)90059-0. URL: https://doi.org/10.1016/0140-7007(94)90059-0.

[49] Gustav Lorentzen. *Trans-critical vapour compression cycle device*. 1990.

[50] Andrew Marina, S. Spoelstra, H.A. Zondag, and A.K. Wemmers. “An estimation of the European industrial heat pump market potential”. In: *Renewable & Sustainable Energy Reviews* 139 (Apr. 1, 2021), p. 110545. DOI: 10.1016/j.rser.2020.110545. URL: https://doi.org/10.1016/j.rser.2020.110545.

[51] Mark O. McLinden, J. Steven Brown, Riccardo Brignoli, Andrei F. Kazakov, and Piotr A. Domanski. “Limited options for low-global-warming-potential refrigerants”. In: *Nature Communications* 8.1 (Feb. 17, 2017). DOI: 10.1038/ncomms14476. URL: https://doi.org/10.1038/ncomms14476.

[52] Mohsen Mehdizadeh-Fard, Fathollah Pourfayaz, and Akbar Maleki. “Exergy analysis of multiple heat exchanger networks: An approach based on the irreversibility distribution ratio”. In: *Energy Reports* 7 (Nov. 1, 2021), pp. 174–193. DOI: 10.1016/j.egyr.2020.11.166. URL: https://doi.org/10.1016/j.egyr.2020.11.166.

[53] Dariusz Mikielewicz and Jan Wajs. “Performance of the very high-temperature heat pump with low GWP working fluids”. en. In: *Energy* 182 (Sept. 2019), pp. 460–470. ISSN: 03605442. DOI: 10.1016/j.energy.2019.05.203. URL: https://linkinghub.elsevier.com/retrieve/pii/S0360544219310916 (visited on 03/13/2024).

[54] Anthony F. Mills and Carlos F.M. Coimbra. *Basic heat and mass transfer*. Jan. 2015. ISBN: 978-0-9963053-0-3.

[55] Michael J. Moran, Howard N. Shapiro, Daisie D. Boettner, and Margaret B. Bailey. *Moran’s Principles of Engineering Thermodynamics*. June 29, 2018.

[56] Arun S. Mujumdar. *Handbook of industrial drying*. eng. third edition. Boca Raton (Fla.): CRC/Taylor & Francis, 2007. ISBN: 978-1-57444-668-5.

[57] Lisa Neumaier, Dennis Roskosch, Johannes Schilling, Gernot Bauer, Joachim Gross, and André Bardow. “Refrigerant Selection for Heat Pumps: The Compressor Makes the Difference”. en. In: *Energy Technology* 11.4 (Apr. 2023), p. 2201403. ISSN: 2194-4288, 2194-4296. DOI: 10.1002/ente.202201403. URL: https://onlinelibrary.wiley.com/doi/10.1002/ente.202201403 (visited on 03/13/2024).

[58] *NFPA 704: Standard system for the identification of the hazards of materials for emergency response*. 2022. URL: https://www.nfpa.org/codes-and-standards/nfpa-704-standard-development/704.

[59] Wilson R. Nyemba, Simon Chinguwa, Batsirayi L. Marango, and Charles Mbohwa. “Evaluation and feasibility assessment of the sustainability of refrigeration systems devoid of harmful refrigerants for storage of vaccines”. In: *Procedia Manufacturing* 35 (Jan. 1, 2019), pp. 291–297. DOI: 10.1016/j.promfg.2019.05.042. URL: https://doi.org/10.1016/j.promfg.2019.05.042.

[60] *Registry of restriction intentions until outcome - ECHA*. URL: https://echa.europa.eu/registry-of-restriction-intentions/-/dislist/details/0b0236e18663449b.

[61] D. Sánchez, R. Larrondo, F. Vidan-Falomir, and R. Cabello. “Experimental evaluation of the CO2-based mixtures CO2/R32, CO2/R1234yf and CO2/R1270 in a transcritical refrigerating plant considering the effect of the internal heat exchanger (IHX)”. en. In: *Applied Thermal Engineering* 236 (Jan. 2024), p. 121473. ISSN: 13594311. DOI: 10.1016/j.applthermaleng.2023.121473. URL: https://linkinghub.elsevier.com/retrieve/pii/S1359431123015028 (visited on 03/13/2024).

[62] Sigurd Sannan, Michael Bantle, Michael Lauermann, and Veronika Wilk. “DryFiciency: Waste Heat Recovery in Industrial Drying Processes”. en. In: ().

[63] Elisabeth Schröder, Klaus Neumaier, Fabian Nagel, and Christian Vetter. “Study on heat transfer in heat exchangers for a new supercritical organic rankine Cycle”. In: *Heat Transfer Engineering* 35.18 (Apr. 29, 2014), pp. 1505–1519. DOI: 10.1080/01457632.2014.897558. URL: https://doi.org/10.1080/01457632.2014.897558.

[64] “The Kigali amendment to the Montreal protocol”. In: 2016.

[65] *VDI Heat Atlas*. Jan. 1, 2010. DOI: 10.1007/978-3-540-77877-6. URL: https://doi.org/10.1007/978-3-540-77877-6.

[66] V. Vesovic. *HEXANE*. Aug. 2008. DOI: 10.1615/atoz.h.hexane. URL: https://doi.org/10.1615/atoz.h.hexane.

[67] V. Vesovic. *ISO-BUTANE*. Aug. 2008. DOI: 10.1615/atoz.i.iso-butane. URL: https://doi.org/10.1615/atoz.i.iso-butane.

[68] V. Vesovic. *N-BUTANE*. Aug. 2008. DOI: 10.1615/atoz.b.n-butane. URL: https://doi.org/10.1615/atoz.b.n-butane.

[69] V. Vesovic. *PROPANE*. June 2011. DOI: 10.1615/atoz.p.propane. URL: https://doi.org/10.1615/atoz.p.propane.

[70] Elias Vieren, Toon Demeester, Wim Beyne, Alessia Arteconi, Michel De Paepe, and Steven Lecompte. “The thermodynamic potential of high-temperature transcritical heat pump cycles for industrial processes with large temperature glides”. en. In: *Applied Thermal Engineering* 234 (Nov. 2023), p. 121197. ISSN: 13594311. DOI: 10.1016/j.applthermaleng.2023.121197. URL: https://linkinghub.elsevier.com/retrieve/pii/S1359431123012267 (visited on 02/02/2024).

[71] Gardis J.E. Von Gersdorff, Michael Bantle, Oliver Hensel, and Barbara Sturm. “Drying and Chilling/Freezing of Perishable Foods in the Organic Sector”. en. In: *Sustainable Food Systems from Agriculture to Industry*. Elsevier, 2018, pp. 245–273. ISBN: 978-0-12-811935-8. DOI: 10.1016/B978-0-12-811935-8.00007-X. URL: https://linkinghub.elsevier.com/retrieve/pii/B978012811935800007X (visited on 02/02/2024).

[72] Chang Xu, Hua Yang, Xiaohui Yu, Hongting Ma, Mo Chen, and Mingchang Yang. “Performance analysis for binary mixtures based on R245fa using in high temperature heat pumps”. en. In: *Energy Conversion and Management: X* 12 (Dec. 2021), p. 100123. ISSN: 25901745. DOI: 10.1016/j.ecmx.2021.100123. URL: https://linkinghub.elsevier.com/retrieve/pii/S2590174521000489 (visited on 03/20/2024).

[73] Weicong Xu, Ruikai Zhao, Shuai Deng, Li Zhao, and Samuel S. Mao. “Is zeotropic working fluid a promising option for organic Rankine cycle: A quantitative evaluation based on literature data”. en. In: *Renewable and Sustainable Energy Reviews* 148 (Sept. 2021), p. 111267. ISSN: 13640321. DOI: 10.1016/j.rser.2021.111267. URL: https://linkinghub.elsevier.com/retrieve/pii/S1364032121005542 (visited on 03/20/2024).

[74] Dazhang Yang, Yang Li, Jing Xie, and Jinfeng Wang. “Research and application progress of transcritical CO2 refrigeration cycle system: a review”. In: □*The* □*international journal of low carbon technologies* 17 (Dec. 8, 2021), pp. 245–256. DOI: 10.1093/ijlct/ctab086. URL: https://doi.org/10.1093/ijlct/ctab086.

[75] Michele Zehnder. “Efficient air-water heat pumps for high temperature lift residential heating, including oil migration aspects”. In: (Jan. 2004). DOI: 10.5075/epfl-thesis-2998.

[76] An Zhao, Rene Pecnik, and Jurriaan W.R. Peeters. “Thermodynamic analysis and heat exchanger calculations of transcritical high-temperature heat pumps”. en. In: *Energy Conversion and Management* 303 (Mar. 2024), p. 118172. ISSN: 01968904. DOI: 10.1016/j.enconman.2024.118172. URL: https://linkinghub.elsevier.com/retrieve/pii/S0196890424001134 (visited on 03/11/2024).

[77] Benjamin Zühlsdorf. *High-Temperature Heat Pumps, Annex 58*. Tech. rep. IEA, 2023.

[78] Benjamin Zühlsdorf, Jonas Kjær Jensen, Stefano Cignitti, Claus Madsen, and Brian Elmegaard. “Analysis of temperature glide matching of heat pumps with zeotropic working fluid mixtures for different temperature glides”. en. In: *Energy* 153 (June 2018), pp. 650–660. ISSN: 03605442. DOI: 10.1016/j.energy.2018.04.048. URL: https://linkinghub.elsevier.com/retrieve/pii/S0360544218306522 (visited on 03/11/2024).

A

Excerpts from python model

Listing A.1: Python code implementation of air and refrigerant state calculation

```
def calc_init_states(self,fluid,T_pinch,T_airout,T_airin,R_airin,etac,T_wetout,R_wetout):
        #Define air boundary conditions
        self.airdry1 = states.ThermoStateHumid("TR", T_airin+kelvin, R_airin)
        self.airdry1_init = self.airdry1
        H_init = self.airdry1.H
        S_init = self.airdry1.S
        self.airdry2 = states.ThermoStateHumid("TW", T_airout+kelvin, self.airdry1.W)
        self.airwet1 = states.ThermoStateHumid("TH", T_wetout + kelvin, self.airdry2.H)
        self.airwet2 = states.ThermoStateHumid("TR", self.airwet1.Tdp, 1.0)
        #Define known refrigerant states
        self.ts1    = states.ThermoState("TQ", self.airwet2.T - T_pinch, 1.0, fluid)
        self.ts2    = states.ThermoState("TP", self.airwet1.T-T_pinch, self.ts1.P, fluid)

        #Determine the isobar wherefore ts3is.S = ts2.S, T_max = airdry2.T+ PPTD and etac =
            set value
        def objective(p):
            ts3is_H = PropsSI("H", "S", self.ts2.S, "P", p, self.fluid)
            ts3_H = PropsSI("H", "T", self.airdry2.T + T_pinch, "P", p, self.fluid)
            etac_calc = (ts3is_H - self.ts2.H) / (ts3_H - self.ts2.H)
            return abs(etac_calc - self.etac)

        p_max = PropsSI('P',"T",self.airdry2.T + T_pinch,"S",self.ts2.S,self.fluid)
        bounds = (self.ts2.P,p_max)
        res = minimize_scalar(objective,bounds = bounds, method = 'bounded', options = {'
            maxiter': max_iter,'xatol':error, "disp": 1})
        p_chosen = res.x

        #calculate other refrigerant state
        self.ts3is = states.ThermoState("PS", p_chosen, self.ts2.S, self.fluid)
        self.ts3 = states.ThermoState("TP", self.airdry2.T + T_pinch, p_chosen, self.fluid)
        self.r_mass = (self.ts3.H - PropsSI("H","T",self.airdry1.T + T_pinch,"P",self.ts3.P,
            fluid))/(self.airdry2.H-self.airdry1.H)
        self.ts4    = states.ThermoState("PH",self.ts3.P, self.ts3.H - ((self.airdry2.H -
            self.airdry1.H)*self.r_mass),fluid)
        self.ts5    = states.ThermoState("PH", self.ts1.P, self.ts4.H, fluid)
        #calculate wet air outlet
        self.airwet3 = states.ThermoStateHumid("HR", self.airwet1.H-(self.ts2.H-self.ts5.H)/
            self.r_mass, 1)
```

Listing A.2: Python code implementation of PPTD and wet compression check

```
dT_min_wet = 0
       for i in range(int(discretization/5)):
           dH_check = np.linspace(0, self.ts3.H - self.ts4.H,  discretization, endpoint=True
               )
           dH_check_evap = np.linspace(0, self.ts2.H - self.ts5.H,  discretization, endpoint
               =True)
           dT_min = None
           dT_min_evap = None

           #Identify pinch point in condenser
           for i, dH in enumerate(dH_check):
             T_refrigerant = CP.PropsSI("T", "H", self.ts3.H - dH, "P", self.ts3.P, fluid)
             T_air = CP.HAPropsSI("T", "H", self.airdry2.H - (dH/self.r_mass), "P", self.
                 airdry2.P, "W", self.airdry1.W)
             dT = T_refrigerant - T_air

             if dT_min == None:
                 dT_min = dT

             elif dT < dT_min:
                 dT_min = dT

           #Identify pinch in evaporator
           for x, dH in enumerate(dH_check_evap):
               T_refrigerant = CP.PropsSI("T", "H", self.ts2.H - dH, "P", self.ts1.P, fluid)
               if (self.airwet1.H - dH/self.r_mass) > self.airwet2.H:
                   T_air = CP.HAPropsSI("T", "H", self.airwet1.H - (dH/self.r_mass), "P",
                       self.airwet1.P, "W", self.airwet1.W)
               else:
                   T_air = CP.HAPropsSI("T","H",self.airwet1.H - (dH/self.r_mass),"P",self.
                       airwet1.P,"R",1.0)
               dT =  T_air - T_refrigerant

               if dT_min_evap == None:
                   dT_min_evap = dT

               elif dT < dT_min_evap:
                 dT_min_evap = dT

           dS_check = np.linspace(0,self.ts3.S - self.ts2.S, discretization, endpoint = True
               )

           for x, dS in enumerate(dS_check):
               a = (self.ts3.T-self.ts2.T)/(self.ts3.S-self.ts2.S)
               T = a*dS + self.ts2.T
               Q = PropsSI("Q","T",T,"S",self.ts2.S + dS,fluid)
               #print(f"Quality is {round(Q,2)}")
               try:
                   T_sat = PropsSI("T","Q",1,"S",self.ts2.S + dS,fluid)
                   print(f"Succesfully␣resolved␣the␣saturated␣vapour,␣T_sat␣is␣{T_sat}␣
                       degrees␣Kelvin")
               except ValueError:
                   pass
               if 0 <= Q <= 1.0:
                   dT_min_wet += 1
                   continue
```

Listing A.3: Python code implementation of mixturesweep.py as presented in modelling hierarchy

```
class Mixturesweep:
def __init__(self, compound1, compound2, N_step, T_pinch, T_airout, T_airin, R_airin,
    etac, T_wetin, R_wetin, plot = False):
    self.mixtures = np.array([f"REFPROP::␣{compound1}[{round(f,␣4)}]&{compound2}[{round(1
        ␣-␣f,␣4)}]" for f in np.linspace(0, 1, N_step)], dtype=str)
    self.heatpumps = np.empty(len(self.mixtures), dtype=object)  # Empty array for
        Heatpump objects
    self.failures = 0
    self.optimal_cop = None
    self.optimal_mixture = None
    SweepCOP = []
    SweepMix = []
    SweepExd = []
    SweepExdcon = []
    SweepExdcom = []
    SweepExdeva = []
    SweepExdthr = []
    SweepTmax = []
    SweepPR  = []
    for i, mixture in enumerate(self.mixtures):
        try:
            self.heatpumps[i] = Simplified.Heatpump(mixture, T_pinch, T_airout, T_airin,
                R_airin, etac, T_wetin)
            SweepCOP.append(round(self.heatpumps[i].COP,4))
            SweepMix.append(self.mixtures[i])
            SweepExd.append(round(self.heatpumps[i].Exergy_destruction/1000,4))
            SweepExdcon.append(round(self.heatpumps[i].Exd_condenser/1000,4))
            SweepExdcom.append(round(self.heatpumps[i].Exd_compressor/1000,4))
            SweepExdeva.append(round(self.heatpumps[i].Exd_evaporator/1000,4))
            SweepExdthr.append(round(self.heatpumps[i].Exd_throttle/1000,4))
            SweepTmax.append(self.heatpumps[i].ts3.T)
            SweepPR.append(self.heatpumps[i].PR)

            if self.optimal_cop is None or self.heatpumps[i].calc_COP() > self.
                optimal_cop:
                try:
                    self.optimal_cop = self.heatpumps[i].calc_COP()
                    self.optimal_mixture = self.heatpumps[i].fluid
                    self.optimal_PR = self.heatpumps[i].PR
                    self.optimal_Phigh = self.heatpumps[i].ts3.P
                    self.optimal_Plow = self.heatpumps[i].ts1.P
                    self.airpreheat = self.heatpumps[i].airdry1.T
                    self.Tsat = self.heatpumps[i].ts1.T
                    self.Tmax = self.heatpumps[i].ts3.T
                except ValueError:
                    continue

        except ValueError:
            self.failures += 1
            continue

    df = pd.DataFrame({
        'Mixture': SweepMix,
        'COP': SweepCOP,
        'Exergy␣Destroyed': SweepExd,
        'Exd␣Condenser': SweepExdcon,
        'Exd␣in␣Compressor': SweepExdcom,
        'Exd␣in␣evaporator': SweepExdeva,
        'Exd␣in␣throttle': SweepExdthr,
        'Maxmimum␣temperature': SweepTmax,
        'Pressure␣Ratio': SweepPR

    })

    df.to_excel(f'sweepdata_{compound1}_and_{compound2}_{date.today()}.xlsx',index=False)
    print(f"␣N_failures␣for␣{compound1}␣and␣{compound2}:␣{self.failures}/{N_step}␣({np.
        round(100*(N_step␣-␣self.failures)/N_step,2)}%␣succesrate)")


```

```
compounds = ["CO2", "Pentane", "Butane", "Propane", "Isobutane", "isopentane", "hexane","
    Ethane","Methane", "Ethylene", "Propylene","water","NH3"]

mixture_divisions = 41
pptd = 5
hotair_t = 180  # deg C
inputair_t = 10  # deg C
inputair_r = 0.8  # (-) relative humidity
etac = 0.7
waste_humid_air_t = 80

solutions = []
for compound1, compound2 in combinations(compounds, 2):
  solution = Mixturesweep(compound1, compound2, N_step=mixture_divisions, T_pinch=pptd,
                          T_airout=hotair_t, T_airin=inputair_t, R_airin=inputair_r, etac=
                              etac,
                          T_wetin=waste_humid_air_t)
  solutions.append(solution)
```

B

Complete model outputs for integrated dryer performance simulation

Mixture	COP	PR	P_high [bar]	P_low [bar]	Air_Preheat [Kelvin]	T_max [degC]	Successes
REFPROP:: Isobutane[0.825]&hexane[0.175]	3.45	21.24	56.03	2.64	294.97	194.97	12
REFPROP:: Pentane[0.3]&Isobutane[0.7]	3.40	22.57	54.26	2.40	295.13	187.42	12
REFPROP:: Isobutane[0.875]&Ethane[0.125]	3.38	16.53	86.20	5.21	295.21	185.62	39
REFPROP:: Butane[0.925]&Ethane[0.075]	3.37	19.58	64.59	3.30	295.23	187.67	40
REFPROP:: Butane[0.6]&Propylene[0.4]	3.37	15.21	75.90	4.99	295.25	191.11	41
REFPROP:: Isobutane[0.925]&Ethylene[0.075]	3.37	17.55	82.94	4.73	295.26	185.39	34
REFPROP:: Isobutane[0.925]&NH3[0.075]	3.36	17.31	83.95	4.85	295.27	185.71	19
REFPROP:: Propane[0.775]&isopentane[0.225]	3.36	13.27	88.69	6.68	295.27	193.83	25
REFPROP:: Butane[0.625]&Propane[0.375]	3.35	16.77	74.58	4.45	295.31	188.18	41
REFPROP:: Butane[0.95]&Ethylene[0.05]	3.35	20.28	63.34	3.12	295.32	187.53	36
REFPROP:: CO2[0.05]&Isobutane[0.95]	3.35	18.46	82.38	4.46	295.32	185.34	38
REFPROP:: Butane[0.825]&hexane[0.175]	3.35	26.12	48.02	1.84	295.32	195.82	9
REFPROP:: Butane[0.95]&NH3[0.05]	3.35	20.41	63.98	3.14	295.33	188.04	19
REFPROP:: CO2[0.05]&Butane[0.95]	3.34	20.23	63.76	3.15	295.34	187.78	36
REFPROP:: Pentane[0.175]&Propane[0.825]	3.34	12.87	91.91	7.14	295.37	197.64	26
REFPROP:: Isobutane[0.775]&isopentane[0.225]	3.33	22.98	61.27	2.67	295.38	185.63	10
REFPROP:: Butane[0.975]&Methane[0.025]	3.31	21.88	62.40	2.85	295.47	187.37	32
REFPROP:: Isobutane[0.975]&Methane[0.025]	3.31	19.99	81.77	4.09	295.47	185.14	30
REFPROP:: isopentane[0.15]&Propylene[0.85]	3.27	11.31	100.35	8.87	295.62	203.57	27
REFPROP:: Isobutane[0.825]&Propylene[0.175]	3.26	18.72	83.54	4.46	295.66	185.40	41
REFPROP:: Pentane[0.15]&Butane[0.85]	3.25	26.28	52.33	1.99	295.68	187.84	4
REFPROP:: Propane[0.3]&Isobutane[0.7]	3.24	18.14	86.76	4.78	295.72	185.39	41
REFPROP:: Pentane[0.125]&Propylene[0.875]	3.24	11.27	104.13	9.24	295.74	208.45	27
REFPROP:: Butane[0.525]&Isobutane[0.475]	3.22	23.97	65.50	2.73	295.80	185.46	41
REFPROP:: Butane[0.975]&isopentane[0.025]	3.21	25.95	57.79	2.23	295.86	186.46	2
REFPROP:: Butane[1.0]&water[0.0]	3.20	25.85	58.59	2.27	295.89	186.34	2
REFPROP:: Propane[0.925]&hexane[0.075]	3.20	13.07	106.79	8.17	295.90	209.74	18
REFPROP:: Propane[0.85]&NH3[0.15]	3.19	9.66	144.35	14.94	295.92	188.54	23
REFPROP:: Isobutane[1.0]&water[0.0]	3.19	24.01	78.87	3.29	295.94	185.00	2
REFPROP:: CO2[0.1]&Propane[0.9]	3.17	10.25	139.15	13.57	296.02	187.53	24
REFPROP:: CO2[0.125]&Propylene[0.875]	3.16	8.43	142.33	16.88	296.06	191.65	36
REFPROP:: Propane[0.875]&Ethylene[0.125]	3.15	10.24	138.80	13.55	296.07	186.87	32
REFPROP:: Methane[0.05]&Propylene[0.95]	3.14	9.05	134.10	14.82	296.11	190.22	22
REFPROP:: Propane[0.95]&Methane[0.05]	3.14	10.99	136.00	12.38	296.14	186.57	20
REFPROP:: Ethylene[0.15]&Propylene[0.85]	3.13	8.53	142.17	16.66	296.15	190.25	31
REFPROP:: Propylene[0.85]&NH3[0.15]	3.09	9.27	134.96	14.55	296.31	192.40	33
REFPROP:: Propane[0.8]&Ethane[0.2]	3.09	10.49	143.66	13.69	296.32	186.62	38
REFPROP:: Ethane[0.15]&Propylene[0.85]	3.07	9.35	137.99	14.77	296.39	189.23	39
REFPROP:: isopentane[0.75]&NH3[0.25]	3.06	29.05	56.80	1.96	296.47	197.05	5
REFPROP:: hexane[0.025]&Propylene[0.975]	3.04	11.01	118.15	10.73	296.51	209.40	17
REFPROP:: Pentane[0.75]&NH3[0.25]	3.03	34.46	48.60	1.41	296.55	200.73	9
REFPROP:: Propane[0.0]&Propylene[1.0]	3.03	10.88	120.73	11.09	296.56	189.22	41
REFPROP:: Propylene[1.0]&water[0.0]	3.03	10.88	120.73	11.09	296.56	189.22	2
REFPROP:: Propane[1.0]&water[0.0]	3.03	13.45	123.05	9.15	296.58	185.90	2
REFPROP:: isopentane[0.75]&Ethylene[0.25]	3.01	28.92	57.00	1.97	296.64	195.08	26
REFPROP:: CO2[0.225]&isopentane[0.775]	2.98	30.23	57.37	1.90	296.80	195.53	10
REFPROP:: Pentane[0.75]&Ethylene[0.25]	2.95	33.64	50.35	1.50	296.90	198.15	24
REFPROP:: isopentane[0.7]&Ethane[0.3]	2.94	27.68	61.14	2.21	296.97	195.10	27
REFPROP:: hexane[0.0]&NH3[1.0]	2.91	11.61	112.60	9.70	297.09	311.97	5
REFPROP:: water[0.0]&NH3[1.0]	2.91	11.61	112.60	9.70	297.09	311.97	3
REFPROP:: CO2[0.0]&NH3[1.0]	2.91	11.61	112.60	9.70	297.09	311.97	1
REFPROP:: Ethane[0.0]&NH3[1.0]	2.91	11.61	112.60	9.70	297.09	311.97	1
REFPROP:: Ethylene[0.0]&NH3[1.0]	2.91	11.61	112.60	9.70	297.09	311.97	1
REFPROP:: Methane[0.0]&NH3[1.0]	2.91	11.61	112.60	9.70	297.09	311.97	1
REFPROP:: Pentane[0.675]&Ethane[0.325]	2.89	31.02	54.95	1.77	297.16	199.53	25
REFPROP:: CO2[0.25]&Pentane[0.75]	2.88	35.00	52.96	1.51	297.23	200.14	25
REFPROP:: Pentane[0.8]&Methane[0.2]	2.84	37.05	50.06	1.35	297.39	197.02	29
REFPROP:: isopentane[0.7]&Methane[0.3]	2.64	28.68	62.34	2.17	298.32	197.64	23
REFPROP:: CO2[0.05]&water[0.95]	2.64	60.54	2.98	0.05	298.34	720.66	13
REFPROP:: CO2[0.95]&hexane[0.05]	2.63	6.30	167.59	26.59	298.37	261.56	22
REFPROP:: hexane[0.575]&Ethane[0.425]	2.59	53.89	40.06	0.74	298.57	204.64	22
REFPROP:: hexane[0.625]&Ethylene[0.375]	2.59	58.38	37.63	0.64	298.59	203.67	25
REFPROP:: Ethylene[0.0]&water[1.0]	2.55	82.61	2.72	0.03	298.79	790.10	16
REFPROP:: Ethane[0.0]&water[1.0]	2.55	82.61	2.72	0.03	298.79	790.10	12
REFPROP:: Methane[0.0]&water[1.0]	2.55	82.61	2.72	0.03	298.79	790.10	7
REFPROP:: hexane[0.0]&water[1.0]	2.55	82.61	2.72	0.03	298.79	790.10	2
REFPROP:: isopentane[0.0]&water[1.0]	2.55	82.61	2.72	0.03	298.79	790.10	1
REFPROP:: Pentane[0.0]&water[1.0]	2.55	82.61	2.72	0.03	298.79	790.10	1
REFPROP:: hexane[1.0]&Methane[0.0]	2.40	66.07	14.16	0.21	299.56	185.00	13
REFPROP:: isopentane[0.0]&hexane[1.0]	2.40	66.07	14.16	0.21	299.56	185.00	1
REFPROP:: Pentane[0.0]&hexane[1.0]	2.40	66.07	14.16	0.21	299.56	185.00	1

Figure B.1: All model outputs for a VCHP integrated dryer heating dry air from 10 to 180 °C using the humid air exiting the dryer at 80 °C with results having the pure refrigerant COP as highest marked red

Mixture	COP	PR	P_high [bar]	P_low [bar]	Air_Preheat [Kelvin]	T_max [degC]	Succeses
REFPROP:: Butane[0.55]&Propylene[0.45]	3.45	13.08	70.26	5.37	294.96	185.00	41
REFPROP:: Propylene[0.175]&NH3[0.825]	3.44	6.80	109.15	16.06	294.99	226.49	35
REFPROP:: Propane[0.125]&NH3[0.875]	3.44	6.84	108.02	15.79	295.00	230.08	20
REFPROP:: Butane[0.9]&Ethane[0.1]	3.41	17.76	62.89	3.54	295.10	185.00	40
REFPROP:: Pentane[0.275]&Isobutane[0.725]	3.41	21.58	53.26	2.47	295.10	185.02	12
REFPROP:: Butane[0.575]&Propane[0.425]	3.39	15.25	72.54	4.76	295.17	185.00	41
REFPROP:: Isobutane[0.875]&Ethane[0.125]	3.39	16.31	85.03	5.21	295.17	185.00	40
REFPROP:: Butane[0.925]&NH3[0.075]	3.38	18.21	62.10	3.41	295.20	185.00	17
REFPROP:: Butane[0.925]&Ethylene[0.075]	3.38	18.27	62.02	3.39	295.22	185.00	37
REFPROP:: Isobutane[0.9]&Ethylene[0.1]	3.38	16.43	83.33	5.07	295.23	185.00	38
REFPROP:: Isobutane[0.925]&NH3[0.075]	3.38	17.05	82.65	4.85	295.23	185.00	19
REFPROP:: CO2[0.05]&Butane[0.95]	3.37	19.27	60.64	3.15	295.24	185.02	36
REFPROP:: CO2[0.075]&Isobutane[0.925]	3.36	17.11	83.08	4.86	295.28	185.00	38
REFPROP:: Isobutane[0.775]&isopentane[0.225]	3.34	22.69	60.46	2.66	295.35	185.00	10
REFPROP:: Butane[0.975]&Methane[0.025]	3.33	21.01	59.84	2.85	295.39	185.06	32
REFPROP:: Isobutane[0.95]&hexane[0.05]	3.31	20.44	62.80	3.07	295.46	185.00	13
REFPROP:: Isobutane[0.975]&Methane[0.025]	3.31	19.93	81.49	4.09	295.46	185.00	34
REFPROP:: Butane[0.925]&hexane[0.075]	3.30	22.95	47.48	2.07	295.49	185.02	11
REFPROP:: Propane[0.9]&isopentane[0.1]	3.29	11.69	93.37	7.99	295.54	185.00	26
REFPROP:: isopentane[0.05]&Propylene[0.95]	3.29	9.14	93.09	10.18	295.56	185.09	27
REFPROP:: CO2[0.15]&Propylene[0.85]	3.28	7.41	131.56	17.76	295.57	185.00	37
REFPROP:: Pentane[0.15]&Butane[0.85]	3.27	25.14	49.95	1.99	295.61	185.07	7
REFPROP:: Pentane[0.05]&Propylene[0.95]	3.27	9.11	88.16	9.68	295.61	185.41	28
REFPROP:: Isobutane[0.775]&Propylene[0.225]	3.27	17.68	83.73	4.74	295.63	185.00	41
REFPROP:: Pentane[0.075]&Propane[0.925]	3.27	11.48	92.02	8.02	295.64	185.00	27
REFPROP:: Propane[0.325]&Isobutane[0.675]	3.25	17.66	86.72	4.91	295.69	185.00	41
REFPROP:: Butane[0.9]&isopentane[0.1]	3.24	25.52	53.78	2.11	295.73	185.06	5
REFPROP:: Methane[0.05]&Propylene[0.95]	3.23	8.38	123.59	14.76	295.75	185.00	27
REFPROP:: Ethylene[0.175]&Propylene[0.825]	3.23	7.67	134.34	17.51	295.76	185.00	38
REFPROP:: Butane[0.575]&Isobutane[0.425]	3.23	23.84	63.91	2.68	295.78	185.00	41
REFPROP:: CO2[0.1]&Propane[0.9]	3.22	9.81	132.94	13.55	295.82	185.00	23
REFPROP:: Butane[1.0]&water[0.0]	3.21	25.26	57.18	2.26	295.85	185.00	2
REFPROP:: Propane[0.85]&Ethylene[0.15]	3.19	9.55	136.75	14.33	295.91	185.00	33
REFPROP:: Isobutane[1.0]&water[0.0]	3.19	24.01	78.87	3.29	295.94	185.00	2
REFPROP:: Pentane[0.775]&NH3[0.225]	3.18	27.98	37.35	1.34	295.96	185.08	14
REFPROP:: Propane[0.975]&hexane[0.025]	3.18	11.27	91.22	8.09	295.97	185.00	22
REFPROP:: Propane[0.95]&Methane[0.05]	3.17	10.68	132.01	12.36	296.02	185.00	25
REFPROP:: Ethane[0.15]&Propylene[0.85]	3.14	8.79	128.99	14.67	296.11	185.00	38
REFPROP:: Propane[0.775]&Ethane[0.225]	3.12	9.96	142.06	14.26	296.20	185.00	37
REFPROP:: isopentane[0.75]&NH3[0.25]	3.11	24.79	46.36	1.87	296.23	185.00	4
REFPROP:: Propane[0.0]&Propylene[1.0]	3.09	10.25	112.97	11.03	296.32	185.00	41
REFPROP:: hexane[0.0]&Propylene[1.0]	3.09	10.25	112.97	11.03	296.32	185.00	18
REFPROP:: Propylene[1.0]&water[0.0]	3.09	10.25	112.97	11.03	296.32	185.00	5
REFPROP:: hexane[0.0]&NH3[1.0]	3.09	9.88	93.65	9.48	296.34	288.90	7
REFPROP:: water[0.0]&NH3[1.0]	3.09	9.88	93.65	9.48	296.34	288.90	2
REFPROP:: CO2[0.0]&NH3[1.0]	3.09	9.88	93.65	9.48	296.34	288.90	1
REFPROP:: Ethane[0.0]&NH3[1.0]	3.09	9.88	93.65	9.48	296.34	288.90	1
REFPROP:: Ethylene[0.0]&NH3[1.0]	3.09	9.88	93.65	9.48	296.34	288.90	1
REFPROP:: Methane[0.0]&NH3[1.0]	3.09	9.88	93.65	9.48	296.34	288.90	1
REFPROP:: Pentane[0.775]&Ethylene[0.225]	3.06	28.72	39.70	1.38	296.44	185.00	30
REFPROP:: isopentane[0.75]&Ethylene[0.25]	3.05	25.40	47.79	1.88	296.48	185.00	29
REFPROP:: Propane[1.0]&water[0.0]	3.04	13.24	120.94	9.13	296.52	185.00	9
REFPROP:: CO2[0.225]&isopentane[0.775]	3.03	25.99	47.60	1.83	296.56	185.00	10
REFPROP:: Pentane[0.725]&Ethane[0.275]	3.00	28.19	41.59	1.48	296.71	185.00	26
REFPROP:: isopentane[0.725]&Ethane[0.275]	2.99	25.77	50.23	1.95	296.76	185.00	26
REFPROP:: CO2[0.25]&Pentane[0.75]	2.95	28.77	41.19	1.43	296.92	185.80	28
REFPROP:: Pentane[0.8]&Methane[0.2]	2.92	30.11	40.39	1.34	297.03	185.18	30
REFPROP:: isopentane[0.725]&Methane[0.275]	2.72	25.59	49.32	1.93	297.92	185.13	27
REFPROP:: hexane[0.65]&Ethylene[0.35]	2.67	49.18	25.76	0.52	298.18	185.16	25
REFPROP:: CO2[0.05]&water[0.95]	2.64	60.19	2.97	0.05	298.32	719.30	15
REFPROP:: hexane[0.6]&Ethane[0.4]	2.63	47.70	27.02	0.57	298.36	185.57	25
REFPROP:: CO2[0.375]&hexane[0.625]	2.60	46.19	25.11	0.54	298.52	185.91	25
REFPROP:: Ethane[0.0]&water[1.0]	2.56	81.05	2.66	0.03	298.72	785.32	16
REFPROP:: Ethylene[0.0]&water[1.0]	2.56	81.05	2.66	0.03	298.72	785.32	16
REFPROP:: Methane[0.0]&water[1.0]	2.56	81.05	2.66	0.03	298.72	785.32	8
REFPROP:: hexane[0.0]&water[1.0]	2.56	81.05	2.66	0.03	298.72	785.32	2
REFPROP:: isopentane[0.0]&water[1.0]	2.56	81.05	2.66	0.03	298.72	785.32	1
REFPROP:: Pentane[0.0]&water[1.0]	2.56	81.05	2.66	0.03	298.72	785.32	1
REFPROP:: hexane[1.0]&Methane[0.0]	2.40	66.07	14.16	0.21	299.56	185.00	24
REFPROP:: isopentane[0.0]&hexane[1.0]	2.40	66.07	14.16	0.21	299.56	185.00	1
REFPROP:: Pentane[0.0]&hexane[1.0]	2.40	66.07	14.16	0.21	299.56	185.00	1

Figure B.2: All model outputs for a VCHP integrated dryer heating dry air from 10 to 180 °C using the humid air exiting the dryer at 50 °C with results having the pure refrigerant COP as highest marked red

Mixture	COP	PR	P_high [bar]	P_low [bar]	Air_Preheat [Kelvin]	Successes	T_max [Kelvin]
REFPROP:: CO2[0.875]&isopentane[0.125]	3.96	3.58	136.15	38.08	288.17	10	460.21
REFPROP:: isopentane[0.175]&Ethane[0.825]	3.90	4.50	103.88	23.06	288.31	27	448.57
REFPROP:: hexane[0.05]&Ethane[0.95]	3.90	3.63	91.14	25.14	288.33	23	441.21
REFPROP:: isopentane[0.125]&Ethylene[0.875]	3.90	3.35	118.19	35.29	288.33	26	442.43
REFPROP:: Pentane[0.175]&Ethane[0.825]	3.89	4.52	74.12	16.41	288.34	27	445.66
REFPROP:: CO2[0.725]&Butane[0.275]	3.89	4.05	143.58	35.42	288.36	36	458.94
REFPROP:: hexane[0.05]&Ethylene[0.95]	3.88	2.80	86.36	30.88	288.37	24	433.38
REFPROP:: CO2[0.875]&Pentane[0.125]	3.86	3.62	97.99	27.07	288.42	28	460.98
REFPROP:: Pentane[0.15]&Ethylene[0.85]	3.81	3.60	75.34	20.95	288.57	28	442.76
REFPROP:: CO2[0.55]&Isobutane[0.45]	3.78	5.33	119.93	22.48	288.63	40	455.73
REFPROP:: Propane[0.85]&hexane[0.15]	3.77	9.09	55.74	6.13	288.66	21	460.44
REFPROP:: Butane[0.375]&Ethylene[0.625]	3.74	5.30	105.24	19.86	288.75	34	455.39
REFPROP:: Isobutane[0.65]&NH3[0.35]	3.68	8.66	86.22	9.95	288.92	18	452.72
REFPROP:: Butane[0.425]&Ethane[0.575]	3.66	7.13	94.32	13.23	288.97	41	455.10
REFPROP:: Isobutane[0.45]&Ethylene[0.55]	3.65	5.98	104.19	17.41	289.00	34	449.70
REFPROP:: hexane[0.075]&Propylene[0.925]	3.65	7.43	61.96	8.34	289.02	12	462.23
REFPROP:: Propane[0.55]&isopentane[0.45]	3.64	13.30	51.30	3.86	289.02	27	449.97
REFPROP:: Butane[0.65]&NH3[0.35]	3.64	9.56	75.06	7.86	289.02	16	459.61
REFPROP:: Pentane[0.4]&Propane[0.6]	3.62	13.53	54.40	4.02	289.10	26	458.78
REFPROP:: Isobutane[0.525]&Ethane[0.475]	3.61	8.04	90.09	11.21	289.12	41	447.16
REFPROP:: Isobutane[0.725]&hexane[0.275]	3.58	20.47	40.36	1.97	289.20	13	458.06
REFPROP:: Pentane[0.325]&Propylene[0.675]	3.57	11.88	61.38	5.16	289.23	26	467.44
REFPROP:: isopentane[0.375]&Propylene[0.625]	3.56	12.44	59.14	4.75	289.26	27	460.43
REFPROP:: Propane[0.575]&Ethane[0.425]	3.53	6.35	106.85	16.82	289.36	38	433.30
REFPROP:: Propane[0.825]&NH3[0.175]	3.51	7.57	101.49	13.40	289.43	20	441.15
REFPROP:: Propane[0.8]&Ethylene[0.2]	3.51	7.23	98.19	13.58	289.43	32	437.87
REFPROP:: Propane[0.95]&Methane[0.05]	3.49	8.25	85.44	10.36	289.47	17	434.82
REFPROP:: CO2[0.125]&Propane[0.875]	3.49	7.81	96.01	12.30	289.47	24	439.23
REFPROP:: Isobutane[0.975]&Methane[0.025]	3.48	14.90	50.53	3.39	289.50	26	434.19
REFPROP:: Pentane[0.525]&NH3[0.475]	3.47	12.58	45.58	3.62	289.52	12	468.59
REFPROP:: Ethane[0.475]&Propylene[0.525]	3.46	5.69	114.64	20.17	289.56	39	432.25
REFPROP:: Butane[0.575]&Propylene[0.425]	3.45	13.29	58.79	4.43	289.59	38	448.52
REFPROP:: Butane[0.55]&Propane[0.45]	3.45	13.76	58.08	4.22	289.59	39	444.61
REFPROP:: Ethylene[0.3]&Propylene[0.7]	3.45	5.98	115.32	19.27	289.59	34	441.98
REFPROP:: isopentane[0.675]&NH3[0.325]	3.45	15.79	45.50	2.88	289.60	6	455.36
REFPROP:: Pentane[0.35]&Isobutane[0.65]	3.45	20.62	39.58	1.92	289.60	13	444.15
REFPROP:: Isobutane[0.875]&Propylene[0.125]	3.43	14.90	52.34	3.51	289.65	30	435.01
REFPROP:: Propane[0.425]&Isobutane[0.575]	3.43	13.02	60.18	4.62	289.67	40	437.01
REFPROP:: Isobutane[0.7]&isopentane[0.3]	3.42	19.61	40.88	2.08	289.68	11	439.10
REFPROP:: CO2[0.175]&Propylene[0.825]	3.42	6.78	109.61	16.16	289.69	37	446.59
REFPROP:: Methane[0.05]&Propylene[0.95]	3.40	7.57	94.72	12.52	289.76	18	442.68
REFPROP:: Butane[0.0]&Isobutane[1.0]	3.36	17.24	47.15	2.73	289.89	37	432.35
REFPROP:: Isobutane[1.0]&water[0.0]	3.36	17.24	47.15	2.73	289.89	1	432.35
REFPROP:: Butane[0.975]&Methane[0.025]	3.35	19.25	45.29	2.35	289.92	31	441.23
REFPROP:: Butane[0.825]&hexane[0.175]	3.33	25.57	39.54	1.55	289.96	9	456.93
REFPROP:: Propane[1.0]&Propylene[0.0]	3.33	10.00	76.88	7.69	289.99	41	433.29
REFPROP:: Propane[1.0]&water[0.0]	3.33	10.00	76.88	7.69	289.99	1	433.29
REFPROP:: Propylene[0.875]&NH3[0.125]	3.32	8.01	96.22	12.02	289.99	28	445.06
REFPROP:: Pentane[0.25]&Butane[0.75]	3.29	24.71	37.49	1.52	290.10	9	444.16
REFPROP:: Butane[0.8]&isopentane[0.2]	3.28	23.90	39.08	1.64	290.15	7	441.30
REFPROP:: Propylene[1.0]&water[0.0]	3.26	8.98	84.53	9.42	290.19	1	440.70
REFPROP:: CO2[1.0]&hexane[0.0]	3.26	3.99	220.14	55.18	290.21	23	425.99
REFPROP:: CO2[1.0]&Ethane[0.0]	3.26	3.99	220.14	55.18	290.21	12	425.99
REFPROP:: CO2[1.0]&Ethylene[0.0]	3.26	3.99	220.14	55.18	290.21	6	425.99
REFPROP:: CO2[1.0]&Methane[0.0]	3.26	3.99	220.14	55.18	290.21	2	425.99
REFPROP:: CO2[1.0]&NH3[0.0]	3.26	3.99	220.14	55.18	290.21	2	425.99
REFPROP:: CO2[1.0]&water[0.0]	3.26	3.99	220.14	55.18	290.21	2	425.99
REFPROP:: Butane[1.0]&water[0.0]	3.24	22.59	42.71	1.89	290.27	1	440.19
REFPROP:: hexane[0.0]&NH3[1.0]	3.23	9.15	71.53	7.81	290.29	5	543.08
REFPROP:: Ethane[0.0]&NH3[1.0]	3.23	9.15	71.53	7.81	290.29	2	543.08
REFPROP:: Ethylene[0.0]&NH3[1.0]	3.23	9.15	71.53	7.81	290.29	1	543.08
REFPROP:: Methane[0.0]&NH3[1.0]	3.23	9.15	71.53	7.81	290.29	1	543.08
REFPROP:: water[0.0]&NH3[1.0]	3.23	9.15	71.53	7.81	290.29	1	543.08
REFPROP:: Pentane[0.825]&Methane[0.175]	3.08	28.24	33.97	1.20	290.82	30	449.47
REFPROP:: Ethane[1.0]&water[0.0]	3.02	4.74	174.49	36.82	291.03	12	411.45
REFPROP:: Ethane[1.0]&Ethylene[0.0]	3.02	4.74	174.49	36.82	291.03	10	411.45
REFPROP:: Ethane[1.0]&Methane[0.0]	3.02	4.74	174.49	36.82	291.03	3	411.45
REFPROP:: isopentane[0.725]&Methane[0.275]	3.02	18.24	40.94	2.24	291.05	25	447.17
REFPROP:: hexane[0.6]&Methane[0.4]	2.58	32.82	30.11	0.92	292.76	18	465.34
REFPROP:: hexane[1.0]&water[0.0]	2.52	65.39	10.51	0.16	293.03	1	440.93
REFPROP:: isopentane[0.0]&hexane[1.0]	2.52	65.39	10.51	0.16	293.03	1	440.93
REFPROP:: Pentane[0.0]&hexane[1.0]	2.52	65.39	10.51	0.16	293.03	1	440.93
REFPROP:: Ethylene[0.6]&water[0.4]	2.29	17.04	6.55	0.38	294.13	15	629.42
REFPROP:: Methane[0.85]&water[0.15]	1.99	5.30	8.69	1.64	295.78	6	541.25

Figure B.3: All model outputs for a VCHP integrated dryer heating dry air from 10 to 120 °C using the humid air exiting the dryer at 80 °C with results having the pure refrigerant COP as highest marked red

Mixture	COP	PR	P_high [bar]	P_low [bar]	Air_Preheat [Kelvin]	T_max [Kelvin]	Successes
REFPROP:: Propane[0.8]&NH3[0.2]	4.30	4.61	62.49	13.56	287.33	407.62	21
REFPROP:: Ethylene[0.25]&Propylene[0.75]	4.29	4.04	67.99	16.84	287.35	407.94	32
REFPROP:: Propane[0.575]&Ethane[0.425]	4.26	4.24	68.29	16.11	287.42	404.03	39
REFPROP:: Propane[0.8]&Ethylene[0.2]	4.26	4.58	59.96	13.10	287.43	405.55	34
REFPROP:: CO2[0.175]&Propylene[0.825]	4.25	4.26	66.17	15.52	287.46	410.06	37
REFPROP:: CO2[0.125]&Propane[0.875]	4.23	4.87	57.75	11.85	287.51	406.12	23
REFPROP:: Ethane[0.4]&Propylene[0.6]	4.18	4.09	71.92	17.58	287.62	404.91	38
REFPROP:: Propane[0.925]&Methane[0.075]	4.17	5.01	54.94	10.97	287.63	404.68	25
REFPROP:: Methane[0.075]&Propylene[0.925]	4.15	4.57	60.25	13.19	287.69	408.54	26
REFPROP:: Propylene[0.15]&NH3[0.85]	4.11	4.96	64.13	12.92	287.79	460.26	20
REFPROP:: Isobutane[0.125]&Ethane[0.875]	4.08	3.56	95.69	26.89	287.85	405.63	37
REFPROP:: Butane[0.375]&Propylene[0.625]	4.07	6.53	37.60	5.76	287.88	412.97	39
REFPROP:: Propane[0.85]&isopentane[0.15]	4.06	6.43	39.72	6.18	287.92	412.87	31
REFPROP:: isopentane[0.1]&Propylene[0.9]	4.06	5.65	44.34	7.85	287.92	419.36	32
REFPROP:: Butane[0.1]&Ethane[0.9]	4.02	3.56	97.45	27.41	288.00	408.15	41
REFPROP:: CO2[0.9]&Isobutane[0.1]	4.02	3.18	142.18	44.67	288.01	411.61	39
REFPROP:: Isobutane[0.875]&NH3[0.125]	4.01	7.67	34.28	4.47	288.05	405.96	21
REFPROP:: Isobutane[0.875]&Ethylene[0.125]	4.00	7.69	33.66	4.38	288.06	405.21	38
REFPROP:: Pentane[0.125]&Propane[0.875]	4.00	6.48	39.61	6.11	288.06	415.61	33
REFPROP:: Pentane[0.075]&Propylene[0.925]	4.00	5.65	45.23	8.00	288.06	421.17	33
REFPROP:: CO2[0.925]&Butane[0.075]	4.00	3.15	145.46	46.21	288.06	411.97	40
REFPROP:: Butane[0.45]&Propane[0.55]	3.99	7.48	34.53	4.61	288.09	408.68	38
REFPROP:: CO2[0.975]&Pentane[0.025]	3.96	3.10	151.86	48.93	288.15	416.93	33
REFPROP:: CO2[0.975]&isopentane[0.025]	3.93	3.15	155.05	49.16	288.24	414.05	29
REFPROP:: Pentane[0.4]&Isobutane[0.6]	3.93	11.11	19.20	1.73	288.24	404.65	23
REFPROP:: Isobutane[0.9]&hexane[0.1]	3.91	9.76	22.84	2.34	288.29	409.33	21
REFPROP:: Isobutane[0.95]&Methane[0.05]	3.90	8.60	31.74	3.69	288.31	403.87	34
REFPROP:: Isobutane[0.125]&Propylene[0.875]	3.90	6.02	47.12	7.82	288.33	409.94	27
REFPROP:: Butane[0.9]&NH3[0.1]	3.89	9.18	26.93	2.93	288.34	407.46	17
REFPROP:: Propane[0.6]&Isobutane[0.4]	3.88	7.40	39.07	5.28	288.37	405.33	35
REFPROP:: Propane[0.975]&hexane[0.025]	3.87	6.37	45.52	7.14	288.40	416.14	28
REFPROP:: Butane[0.85]&hexane[0.15]	3.87	11.53	16.98	1.47	288.40	409.64	19
REFPROP:: Butane[0.9]&Ethylene[0.1]	3.87	9.21	26.90	2.92	288.41	406.92	38
REFPROP:: Pentane[0.025]&Ethane[0.975]	3.85	3.44	111.57	32.48	288.45	405.87	35
REFPROP:: hexane[0.0]&Propylene[1.0]	3.84	5.72	51.49	9.00	288.49	406.32	23
REFPROP:: Propylene[1.0]&water[0.0]	3.84	5.72	51.49	9.00	288.49	406.32	10
REFPROP:: Propane[0.0]&Propylene[1.0]	3.84	5.72	51.49	9.00	288.49	406.32	7
REFPROP:: Isobutane[0.55]&isopentane[0.45]	3.84	11.86	20.31	1.71	288.49	402.83	21
REFPROP:: Propane[1.0]&water[0.0]	3.81	6.48	47.93	7.40	288.55	402.86	6
REFPROP:: Butane[0.95]&Methane[0.05]	3.78	10.21	26.05	2.55	288.63	406.05	36
REFPROP:: isopentane[0.025]&Ethane[0.975]	3.77	3.52	115.05	32.69	288.67	400.49	33
REFPROP:: isopentane[0.85]&NH3[0.15]	3.76	13.15	16.23	1.23	288.70	404.31	14
REFPROP:: Pentane[0.875]&NH3[0.125]	3.75	15.61	12.96	0.83	288.73	405.18	16
REFPROP:: Pentane[0.45]&Butane[0.55]	3.74	13.99	16.53	1.18	288.75	404.06	21
REFPROP:: CO2[1.0]&hexane[0.0]	3.70	3.34	177.31	53.13	288.87	407.14	32
REFPROP:: CO2[1.0]&water[0.0]	3.70	3.34	177.31	53.13	288.87	407.14	8
REFPROP:: CO2[1.0]&Ethane[0.0]	3.70	3.34	177.31	53.13	288.87	407.14	5
REFPROP:: CO2[1.0]&NH3[0.0]	3.70	3.34	177.31	53.13	288.87	407.14	2
REFPROP:: CO2[1.0]&Ethylene[0.0]	3.70	3.34	177.31	53.13	288.87	407.14	1
REFPROP:: CO2[1.0]&Methane[0.0]	3.70	3.34	177.31	53.13	288.87	407.14	1
REFPROP:: isopentane[0.825]&Ethylene[0.175]	3.67	12.89	16.86	1.31	288.94	404.77	33
REFPROP:: Butane[0.575]&isopentane[0.425]	3.66	14.31	18.73	1.31	288.98	402.93	18
REFPROP:: Butane[0.0]&Isobutane[1.0]	3.66	10.98	29.21	2.66	288.99	402.00	41
REFPROP:: Isobutane[1.0]&water[0.0]	3.66	10.98	29.21	2.66	288.99	402.00	2
REFPROP:: Pentane[0.85]&Ethylene[0.15]	3.65	14.90	13.82	0.93	289.00	406.04	33
REFPROP:: water[0.0]&NH3[1.0]	3.58	7.20	54.30	7.54	289.20	510.60	24
REFPROP:: hexane[0.0]&NH3[1.0]	3.58	7.20	54.30	7.54	289.20	510.60	19
REFPROP:: Ethane[0.0]&NH3[1.0]	3.58	7.20	54.30	7.54	289.20	510.60	2
REFPROP:: Ethylene[0.0]&NH3[1.0]	3.58	7.20	54.30	7.54	289.20	510.60	1
REFPROP:: Methane[0.0]&NH3[1.0]	3.58	7.20	54.30	7.54	289.20	510.60	1
REFPROP:: Butane[1.0]&water[0.0]	3.57	13.11	23.96	1.83	289.25	404.26	6
REFPROP:: Pentane[0.875]&Methane[0.125]	3.53	15.44	13.53	0.88	289.35	405.66	35
REFPROP:: hexane[0.0]&Ethane[1.0]	3.38	3.94	140.99	35.79	289.81	398.28	30
REFPROP:: Ethane[1.0]&water[0.0]	3.38	3.94	140.99	35.79	289.81	398.28	11
REFPROP:: Ethane[1.0]&Ethylene[0.0]	3.38	3.94	140.99	35.79	289.81	398.28	4
REFPROP:: Ethane[1.0]&Methane[0.0]	3.38	3.94	140.99	35.79	289.81	398.28	2
REFPROP:: isopentane[0.8]&Methane[0.2]	3.33	12.90	17.47	1.35	289.98	404.99	31
REFPROP:: Pentane[1.0]&hexane[0.0]	3.32	20.81	10.41	0.50	289.99	400.07	2
REFPROP:: Pentane[1.0]&isopentane[0.0]	3.32	20.81	10.41	0.50	289.99	400.07	2
REFPROP:: Pentane[1.0]&water[0.0]	3.32	20.81	10.41	0.50	289.99	400.07	1
REFPROP:: isopentane[1.0]&hexane[0.0]	3.29	17.45	11.95	0.68	290.12	398.15	2
REFPROP:: isopentane[1.0]&water[0.0]	3.29	17.45	11.95	0.68	290.12	398.15	1
REFPROP:: hexane[0.75]&Ethylene[0.25]	3.26	22.05	7.40	0.34	290.20	407.42	30
REFPROP:: hexane[1.0]&Methane[0.0]	3.17	31.26	4.48	0.14	290.51	398.15	22
REFPROP:: hexane[1.0]&water[0.0]	3.17	31.26	4.48	0.14	290.51	398.15	1
REFPROP:: Ethylene[0.575]&water[0.425]	2.44	14.83	1.66	0.11	293.43	586.59	15
REFPROP:: Methane[0.825]&water[0.175]	1.78	7.80	2.49	0.32	297.11	550.96	7

Figure B.4: All model outputs for a VCHP integrated dryer heating dry air from 10 to 120 °C using the humid air exiting the dryer at 50 °C with results having the pure refrigerant COP as highest marked red

C

Cycle demonstrating the effect of a larger minimum pinch point temperature difference

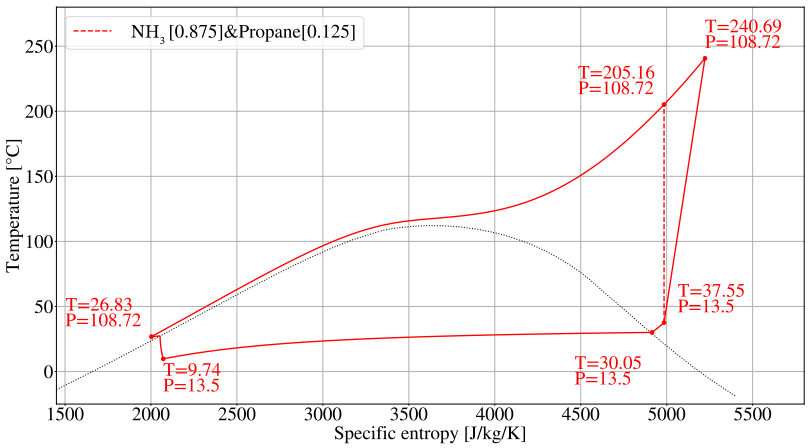

Figure C.1: T-s diagram of the Ammonia mixture cycle for T_{A2} = 180 °C and T_{A3} = 50 °C with PPTD = 10 °C

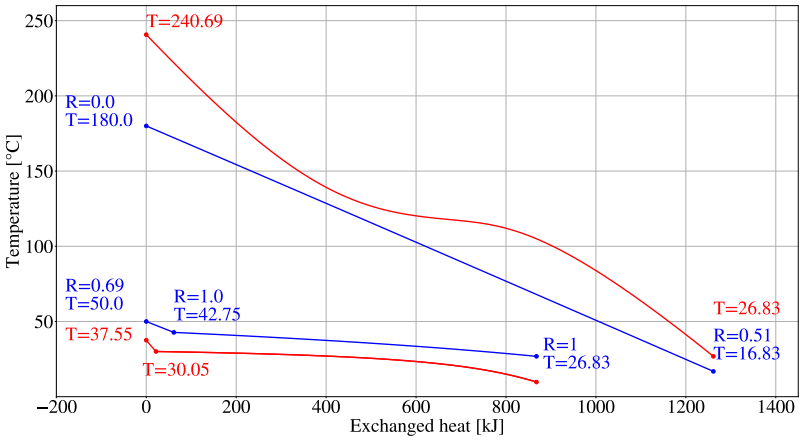

Figure C.2: T-Q diagram of the Ammonia mixture cycle for T_{A2} = 180 °C and T_{A3} = 50 °C with PPTD = 10 °C